The Effects of Multiple Fractures on the Performance of Gas Wells

by

Kissami Mimoune

A Thesis Presented to the

FACULTY OF THE COLLEGE OF GRADUATE STUDIES

KING FAHD UNIVERSITY OF PETROLEUM & MINERALS

DHAHRAN, SAUDI ARABIA

In Partial Fulfillment of the
Requirements for the Degree of

MASTER OF SCIENCE

In

PETROLEUM ENGINEERING

June, 1990

The Effect of Multiple Fractures on the Performance of Gas Wells

BY

KISSAMI MIMOUNE

A Thesis Presented to the

FACULTY OF THE COLLEGE OF GRADUATE STUDIES

KING FAHD UNIVERSITY OF PETROLEUM & MINERALS

DHAHRAN, SAUDI ARABIA

In Partial Fulfillment of the
Requirements for the Degree of

MASTER OF SCIENCE

In

PETROLEUM ENGINEERING

JUNE 1990

KING FAHD UNIVERSITY OF PETROLEUM AND MINERALS
DHAHRAN, SAUDI ARABIA

COLLEGE OF GRADUATE STUDIES

This thesis, written by Mr. Kissami Mimoune under the direction of his Thesis Advisor and approved by his Thesis Committee, has been presented to and accepted by the Dean of the College of Graduate Studies, in partial fulfillment of the requirements for the degree of MASTER OF SCIENCE in Petroleum Engineering.

Thesis Committee:

: Aug 22, 1990
Dr. Hasan S. Al-Hashim
Thesis Advisor

Dr. Hasan Y. Al-Yousef
Member

Dr. Mohamed A. Aggour
Member

11/11/90
Dr. Hamza K. Asar
Department Chairman

Dr. Ala H. Al-Rabeh
Dean, College of Graduate Studies

Date: 11/11/90

Dedicated to:

My parents and my wife.

ACKNOWLEDGEMENTS

Acknowledgement is due to King Fahd University of Petroleum and Minerals for providing financial support during the entire period of study .

I wish to express my deep appreciation to Dr. Hassan S. AL-Hashim whose effort, support, and guidance throughout this study made this research possible. I would also like to express my sincere appreciation to my thesis comitee members : Dr. Hassan Y. AL-Yousef and Dr. Mohamed A. Aggour for their guidance and valuable suggestions .

TABLE OF CONTENTS

LIST OF TABLES

LIST OF FIGURES

THESIS ABSTRACT

NAME OF STUDENT : KISSAMI MIMOUNE

TITLE OF STUDY : The Effect of Multiple Fractures on the Performance of Gas Wells .

MAJOR FIELD : Petroleum Engineering

DATE OF DEGREE : June, 1990

A single phase two-dimensional mathematical model was used to predict the performance of a gas well intersected by two perpendicular vertical fractures . The fractures half lengths (x_f and y_f) were assumed to extend equally on both sides of the wellbore . The fractures were assumed to have either infinite or finite conductivities . The analysis of the simulated drawdown tests at constant flow rate showed that the transient flow behavior of a gas well intersected by finite conductivities ($F_{CD} < 500$) perpendicular fractures does not exhibit neither the bilinear flow behavior nor the formation linear flow behavior when y_f / x_f is greater than zero . Instead it showed that the log-log plot of p_D versus t_{Dxf} presented slopes higher than the characteristic slopes of the bilinear and linear flow periods . On the other hand when the fractures conductivities were equal to or greater than 500, the formation linear flow period was observed . The square-root method was used to determine the fracture half length from the formation linear flow period and found to give a fracture half length that is equal to the sum of the fracture half lengths ($y_f + x_f$). At early times and for fracture conductivities up to 0.2π , the pressure drops, p_D , calculated for the cases where y_f / x_f are greater than zero were lower than those for single fracture ($y_f / x_f = 0.0$) . But , as the fracture conductivity increased the calculated pressure drops were found to increase to values higher than those for the single fracture cases after some time. This time was found to be a function of fracture conductivity where it decreased as the fracture conductivity increased . The results when plotted as a function of p_D versus $\log t_{Dxf}$ for both infinite and finite conductivities perpendicular vertical fractures gave , for large t_{Dxf} , a 1.151-slope straight line . Hence, semilogarithmic pressure analysis methods can be applied .

MASTER OF SCIENCE DEGREE

KING FAHD UNIVERSITY OF PETROLEUM AND MINERALS

Dhahran , Saudi Arabia

June 1990

إسم الطالب الكامل : قسامي ميمون
عنوان الدراســـة : تأثير التصدعات المتعددة على أداء آبار الغاز
التخصـــــص : هندسة البترول
تاريـــخ الشهادة : يونيو ١٩٩٠م

ملخص الرسالة

بإستخدام نموذج رياضي ثنائي الأبعاد أحادي الطور تم التنبوء بأداء بئر للغاز يقع عند تقاطع تصدعين رأسيين متعامدين . وقد افترض امتداد أنصاف أطوال التصدعات لمسافات متساوية على طرفي تجويف البئر لكل نسب أنصاف أطوال التصدعات التي تم بحثها . ولقد أعتبرت التصدعات محدودة الموصلية تارة وغير محدودة الموصلية تارة أخرى .ولقد أظهرت تحليل نتائج المحاكاه لاختبار السحب المنخفض عند معدل إنتاج ثابت أن السلوك المرحلي لانسياب بئر الغاز المقطوع بتصدعات متعامدة ذات موصليات محدودة (أقل من ٥٠٠) لم توضح أي من سلوكي الإنسياب الثنائي الخطي أو الانسياب الطبقي عندما تكون نسبة أنصاف الأطوال للتصدعات أكبر من الصفر . إلا أنها أظهرت أن الرسم اللوغريثمي للضغط اللابعدي والزمن اللابعدي أنتجت منحنيات أعلى من تلك التي تمتاز بها فترات الإنسياب الخطي والثنائي الخطي . غير أنه لوحظ وجود فترة انسياب خطي طبقي عندما تكون موصليات التصدعات مساوية أو أكبر من (٥٠٠) ، لذلك تم استخدام طريقة الجذر التربيعي لايجاد أنصاف أطوال التصدع من فترة الانسياب الخطي الطبقي ووجد أنه يساوي مجموع أنصاف طولي التصدع على المحورين . عند بدايات الزمن ، وعندما تكون نسب أنصاف أطوال التصدع أكبر من الصفر نجد أن إنخفاض الضغط يكون أقل عما يكون عليه عندما يكون هناك تصدع واحد (عمودي) ، ويستمر في الإنخفاض طول زمن البحث عندما تكون موصلية التصـــــدع تساوي ٢ر٠ ط (ط = ١٤١٥٩ر٣) ، ولكنه مع إزدياد موصلية التصدع يرتفع إنخفاض الضغط إلى قيم أكبر من تلك التي نحصل عليها من وجود تصدع واحد (عمودي) عند وقت معين . ووجد على أن هذا الوقت المعين يعتمد على موصلية التصدع بحيث يقل مع ازدياد موصلية التصدع . وعند رسم الضغط اللابعدي ولوغريثم الزمن اللابعدي لبئر غاز متقاطع بتصدعات رأسية متعامدة ذات موصليات محدودة وغير محدودة تعطي منحنى لخط مستقيم يساوي ١٥١ر١/على دورة لوغرتميه فعليه يمكن تطبيق طريقة تحليل الضغط الشبه اللوغريثمي .

Chapter One

CHAPTER 1

INTRODUCTION

Hydraulic fracturing is an effective technique for increasing the productivity of wells producing from low permeability formations . Considerable research has been conducted to determine the effect of hydraulic fractures on well performance and pressure transient behavior . The results have been used to improve the design of hydraulic fractures . [9 , 33 , 42]

The increasing use of hydraulic fracturing as a means of improving the productivity of oil and gas wells in low-permeability formations has resulted in many research efforts aimed at increasing fracturing capabilities as well as evaluating the characteristics of the fracture in the postfracturing period . [15]

With the advent of the massive hydraulic fracturing (MHF) treatment in recent years , it now appears that MHF is a proven technique for developing commercial wells in low-permeability or "tight" gas formations . The purpose of MHF is to expose a large surface area of the low-permeability formation (in-situ permeability of 0.1 md or less) to flow into the wellbore . [10]

Over the past few decades , techniques to improve the productivity of tight reservoirs have been mostly hydraulic fracturing and explosive shooting of wells. Recently an alternative to these two techniques , one that uses certain features of both but appears better for creating multiple fractures , is the technique known as Tailored-Pulse Loading. [27,40]

Many methods have been proposed to determine formation properties and fracture characteristics from pressure transient and flow rate data . These methods have been based on either analytical or numerical solutions of the transient flow of fluids toward fractured wells .

All the previous work presented in the literature has treated the transient of fluid (gas , oil) flow in hydraulically fractured wells but the study of the performance of a well intersected by multiple fractures resulting from pulse fracturing techniques has not been considered in the literature .

The purpose of this study is to investigate the effects of multiple vertical fractures , with different fracture lengths and conductivities , on the performance of gas wells. The applicability of the existing methods of analysis of a single vertical fracture system will be investigated . A fully implicit , finite difference numerical simulator based on non-Darcian flow will be used to investigate this study .

Chapter Two

CHAPTER 2

LITERATURE REVIEW

2.1 SINGLE VERTICAL FRACTURE

The evaluation of massive hydraulic fracture treatment performance with pressure transient tests has been of great interest to engineers for several years . Increased activities in developing tight gas sands through hydraulic fracturing have generated considerable interest in these evaluations . The existence of substantial quantities of natural gas in these unconventional, low permeability reservoirs has generated a considerable effort from researchers to develop numerical and analytical tools to evaluate fracture treatments and to predict future performance of such reservoirs. [32]

In 1961 , Prats [1] studied the production response and pressure behavior of a closed cylindrical reservoir producing an incompressible fluid through a single , vertical fracture located at the center of the cylinder . Prats' study considered the effect of fracture capacity and formation damage from fracture treatments , on the productive capacity of vertically fractured wells . In addition, the study gives the equivalent wellbore radius of a fracture having different lengths and capacities and , also , includes pressure distribution in and around the fracture . Prats concluded that the improvement in production rate due to a high capacity fracture is equal to the improvement in production rate due to an acid treatment which results in an effective well radius of one-fourth the fracture half length .

In 1964 , Russell and Truitt [2] investigated mathematically the pressure transient behavior of a well which produces a single compressible fluid through a single-plane vertical fracture . The fracture was assumed to possess infinite flow capacity , and to penetrate the producing formation completely in the vertical direction . Based on the results of their study , they concluded that the degree of inaccuracy involved in the analysis of transient flow in vertically fractured cases depends on the depth of penetration of the fracture into the formation . They also found that as fracture penetration increases , the formation capacity (kh) values calculated from pressure build-up and flow test curves become increasingly larger than the true values .

In 1968 , Millheim and Cichowicz [3] published a paper concerning the analysis of well pressure transient data for a hydraulically fractured gas well producing from a low permeability formation , including the effects of formation damage and turbulence . They indicated that a well test duration of at least 24 hours might be required in order to establish transient radial flow conditions .

In 1969 , Wattenbarger and Ramey [4] studied the effect of non-Darcy flow on the behavior of fractured gas wells . In their study it was assumed that non-Darcy flow occured in the formation only and the fracture has infinite conductivity. They found that turbulence effect did not stabilize during the linear flow period . It was also concluded that turbulence within the fracture itself could be more important than turbulence within the formation. They also showed that the formation capacity (kh) may be under estimated if observed pressure data are affected by non-Darcy flow .

In 1972 , Raghavan et al. [5] presented a detailed study of the method

proposed by Russell and Truitt [2] . Furthermore , the applications of Miller, Dyes ,and Hutchinson [46] , and type-curve matching methods to the analysis of pressure data for fractured wells were examined thoroughly .

In 1974 , Gringarten et al. [6] developed semi-analytical solutions for three special cases : infinite-conductivity vertical fracture , uniform flux vertical fracture , and horizontal fracture [7]. Their solutions were useful for type-curve analysis . But since not all systems behaved in this manner , the need for further solutions was warranted .

In 1976 , Holditch and Morse [8] investigated the effect of turbulent flow in a fracture and analyzed the transient behavior of specific conductivities (low, medium, and high), giving a qualitative approach to the solution. They stressed the need for greater detail on these solutions and showed that there was indeed a large reduction in the fracture conductivity when non-Darcy flow was included.

In 1978 , Cinco et al. [9] developed a mathematical model to study the transient behavior of a well with a finite-conductivity vertical fracture in an infinite slab reservoir. In their study they demonstrated that the assumption of infinite fracture conductivity is valid whenever the dimensionless fracture conductivity is greater than 300 ; all other cases , such as those represented by long or poorly conductive fractures , must be analyzed by considering a finite-conductivity fracture model . As a result of their study , the following conclusions were reached : (1) A decrease in the dimensionless fracture conductivity may be caused by a decrease in fracture permeability , an increase in fracture length or both; (2) The uniform flux , vertical fracture solution of

Gringarten [6] behaves like the infinite conductivity solution at small values of times ; at intermediate times , it follows a variable fracture conductivity solution. For large values of time , it follows a finite fracture conductivity of $F_{CD} = 4.4$ (3) The results when plotted as dimensionless wellbore pressure drop versus the logarithm of dimensionless time do follow (for large values of time) straight lines of slope equal to 1.151. Thus , semilogarithmic methods of analysis can be used ; and (4) The approximate start of the semilogarithmic straight line is a function of fracture conductivity. The dimensionless time for this point ranges from 2.5 to 5 for practical values of F_{CD} .

In 1979 , Agarwal et al. [10] presented a finite-difference model to study the transient behavior of finite conductivity vertically fractured gas wells , considering both the constant rate as well as the constant pressure cases . Based on the results of their study they concluded that the conventional pressure transient methods (both square-root time graph and type curve) , based on the concept of infinite conductivity are not adequate for evaluating massive hydraulic fractured wells with finite conductivity .

In 1981 , Cinco et al. [11] presented a new interpretation technique for early time pressure data for a well intersected by a finite-conductivity vertical fracture. This method was based on the bilinear flow theory , which considers transient linear flow in both fracture and formation . They also included the criteria to determine the end of wellbore storage effects .

In the same year , Evans and Caroll [12] presented a mathematical model which forms the basis for a reservoir simulator that can be used to assist in the interpretation and prediction of the performance of hydraulically fractured gas

wells completed in non continuous sand lense formations.

Allam [13] in 1981 , presented a three-dimensional finite difference fully implicit model to investigate the effect of fracture height on the performance of vertically fractured wells . The effects of layered media , turbulence , and closure pressure are also included in this work. As a result of his investigation, he concluded that : (1) the closure pressure stress decreases the productivity of fractured wells significantly in case of high production rates; (2) for all times, the behavior of two layers in the fractured system is similar to the single layer when the average parameters (k , h , φ) are used, and (3) the productivity of a fractured well is decreased with increasing the permeability ratio in stratified system with crossflow.

In 1982, AL-Hashim. [14] presented a two-dimensional fully implicit finite difference model to investigate the effects of turbulent flow and finite conductivity on the evaluation of formation and fracture characteristics . The effects of initial reservoir pressure , formation permeability and fracture half length were also investigated. Based on the results of his investigation, it was found that turbulent flow effect is most significant in the fracture, and for the range of kh investigated, a minimum of 96 hours flow period was required to get reliable estimates of kh from the build-up tests . He also recommended that hydraulic fracturing operations should be designed in such a way to obtain high permeability fractures and not necessarily very long fractures.

In their paper published in 1982 , Guppy et al. [15] developed a semi-analytical model to analyze the unsteady flow behavior of finite conductivity fractures producing at high flow rates. They presented a correlation that

provides a mean of determining the actual conductivity of a fracture where the effect of non-Darcy flow will not yield the actual conductivity using conventional methods .

One month later , Guppy et al. [16] presented a study concerning the analysis of pressure buildup data for finite conductivity fractures producing at high flow rates. A method was developed for analyzing buildup data in which non-Darcy effects are significant . As a result of their analysis, they concluded that the effect of non-Darcy flow on pressure build up analysis is to cause the fracture conductivity to be smaller than the true fracture conductivity . They stated that the difference could be as much as 85 percent .

In 1983 , Rubin [17] conducted a laboratory experiment to study hydraulic fracturing in an impermeable material . The borehole pressure , the pressure in the fracture at three locations , the fracture width at one location , and the fracture length were measured as functions of time during propagation of vertically contained hydraulic fracture . The experimental data were compared with the predictions of simple solutions and the results indicated that , when the finite width of the laboratory model is included in the analysis , the comparison between theory and experiment is quite good . The results also indicated that the assumption of uniform pressure distribution in the fracture is adequate to accurately predict the critical parameters .

In 1985 , Bennett et al. [18] derived new analytical solutions for the response at a well intersecting a layered reservoir , considering both the constant rate as well as the constant pressure cases . The main feature of their analytical solutions is that it can be used to study cases where the fracture extends above

and / or below the productive interval and cases where the conductivity of the fracture is a function of depth.

In 1986 , Bennett et al. [19] suggested methods to analyze well performance when the fracture conductivity is a function of fracture height and fracture length . They gave empirical guidelines for systematically choosing a grid system to obtain accurate solutions .

Tai Lee and Brockenbrough [20] presented an analytical solution , based on an approximate trilinear flow model , to study the transient behavior of a well intersected by a finite-conductivity vertical fracture . They presented early-time asymptotic solutions for both constant-pressure and constant-rate cases to illustrate the simultaneous influences of skin , wellbore storage and fracture storage at early testing times . Their solutions are reliable only for short time analysis (the time before semilog straight line behavior is reached) .

Kabir and Hassan [21] addressed the problem of treating the pressure sensitive viscosity - compressibility product while analyzing the prefracture test data in tight gas reservoirs . They concluded that for a gas well located in a very low-flow-capacity formation both drawdown and buildup tests respond to the viscosity-compressibility product variation in the same manner during either a constant-rate or constant-pressure testing in the infinite-acting flow regime.

In 1987 , Guppy [22] presented a method for analyzing late-time data for high flow rate wells that cause turbulent flow within the fracture . And he found that early-time correlations can not be used to correct the apparent values of fracture conductivity to obtain the true fracture conductivity .

In their paper , Holditch et al. [24] described the importance of collecting and analyzing data before , during and after hydraulic fracture treatment so that the three dimensional properties of both the formation and the fracture can be determined .

In 1988 , Guppy et al. [25] presented a technique for the analysis of buildup and drawdown data from wells produced at constant pressure with turbulent flow in the fracture . They concluded that : turbulent flow in the fracture reduces the true fracture conductivity ; the bilinear flow period can be detected in wells producing at high flow rates ; and the analysis of this period can be used to calculate the dimensionless apparent fracture conductivity .

In their paper published in 1988 , Tiab and Puthigai [26] developed a technique to calculate the fracture half length and formation permeability from pressure derivatives type curves . Based on the results of their study they concluded that the buildup type curves are identical to the drawdown type curves for uniform flux and infinite conductivity fractures .

In 1989 , Wilkinson [29] presented an analytical solution for pressure transient behavior of hydraulically fractured wells. His solution includes the effects of compressible flow in the fracture, storage in the fracture and wellbore storage. As a result of his study , he concluded that: infinite conductivity solution exhibits linear flow in the formation and radial flow at late time , and the finite conductivity solution exhibits linear fracture flow , bilinear and radial flows.

Okoye et al. [30] in 1989 , presented a mathematical model to describe pressure transient due to fluid flow in vertically fractured multi-layer double

porosity gas reservoirs . The analytical , semi-analytical and numerical solutions were presented. As a result of their study, they concluded that: the asymptotic analytical solutions can be used to analyze transient pressure data if the flow period can be identified, semi-analytical solution can be used to generate type curves for general purpose transient pressure data analysis of vertical fracture multi-layer reservoirs, and numerical solution can be used to verify the general semi-analytical solution.

In their paper published in 1989 , Olarewaju et al. [32] presented a new analytical solution for the pressure response of a well intersecting a finite conductivity fracture in a finite rectangular reservoir . Their model includes the effects of wellbore storage , fracture height , drainage boundary size and phase segregation on the pressure response of such wells . Based on the results of their study , they concluded that : a model that accounts for both finite conductivity and wellbore storage should be used to estimate the fracture half length in wells with finite conductivity fractures when build-up tests with wellbore storage distortion are analyzed ; and the more conductive a fracture is , the less severe will be the effects of wellbore storage and phase segregation .

2.2 MULTIPLE FRACTURES

Controlled Pulse Fracturing (CPF) is an emerging technology for stimulation of oil and gas producing formations. The CPF process uses an electrically ignited tool containing a solid propellant charge placed in the wellbore adjacent the zone requiring stimulation. Upon ignition, the CPF tool rapidly generates a high pressure gas pulse. This pulse of gas causes the rock to fracture and generates multiple, short fractures, radiating from the wellbore.[31]

Many papers [31,36,40] have dealt with the applications of CPF technique, but no investigation has been made to study the performance of a well intersected by multiple fractures which is the goal of this study.

In 1979 , Warpanski et al. [37] and Schmidt et al. [38] have demonstrated that propellants can create multiple fractures in a field environment without damaging the wellbore region . Based on the results of their study , they concluded that : the long loading duration of the pulse allows greater fracture extension and thus affords a better opportunity for connecting a wellbore to the natural fracture system of the reservoir .

In 1980 , a laboratory experiment was devised by Swift and Kusubov [39] to provide controlled pressurization of the borehole of rock samples at intermediate loading rates . Their experiment provides a way to establish the susceptibility of specific rock types to multiple fracturing .

In the same year , Schmidt et al. [41] conducted a series of five full-scale tests performed to evaluate various multiple fracture concepts . The results of their tests suggest that a multiple fracture criterion be based on borehole pressure-loading rate , and peak pressure conditions may not be important if loading rate requirements are adequate .

In 1982 , Swift and Kusubov [40] developed a laboratory experiment to study the effects of pressurizing boreholes of rock samples with tailored pulses at intermediate loading rates . Their experiment focused on ascertaining the loading conditions needed to initiate multiple-fracture growth from a borehole . As a result of their investigation multiple radial fractures were observed without damaging the wellbore as can be seen from figure 2.1 .

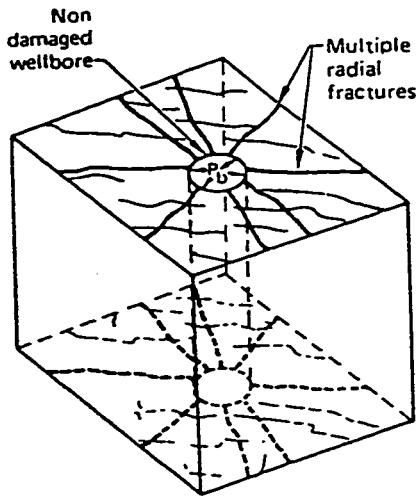

c. Tailored-pulse,
$\dot{P} \approx 10^2 \sim 10^6$ MPa/s, $P_b \geq P_{in\ situ}$

Figure 2.1 : Multiple radial fractures resulting from tailored pulse technique . [ref. 40]

In 1986 , Cuderman and Northrop [36] conducted a series of experiments for specifying the pressure pulse required for producing multiple fractures and for choosing propellants to achieve the desired pressure pulse . Based on the results of their investigation they concluded that : multiple fractures occur when the rise time (which is function of Raleigh surface wave velocity and the borehole diameter) approaches the multiple-explosive boundary , and as the multiple-explosive boundary is approached , the shear fractures occur first at 30° to the maximum principal stress plane and finally at 45° for rise times near the multiple explosive boundary as can be seen from figure 2.2 .

In 1988 , Soliman et al. [28] concluded in their study of completion and stimulation of horizontal wells that, if a horizontal well is drilled parallel to the minimum horizontal stress , multiple fractures may be created . And they also concluded that if high or essentially infinite conductivity is feasible , an optimum number of fractures may be obtained . This optimum number depends on formation and fluid properties and the presence of natural fractures.

In 1989 , Hunt and Shu [31] described the basis of the Controlled Pulse Fracturing (CPF) stimulation technique , which causes the rock to fracture and generates multiple fractures radiating from the wellbore . Laboratory results and field evidence were presented to validate their theory . As a result of their study they concluded that: the CPF is a developing technology which can be used to create multiple near-wellbore fractures without casing damage, and further development of CPF will depend on a better understanding of the exact pressure-time response of various commercial tools coupled with engineering models for design of specific stimulation jobs.

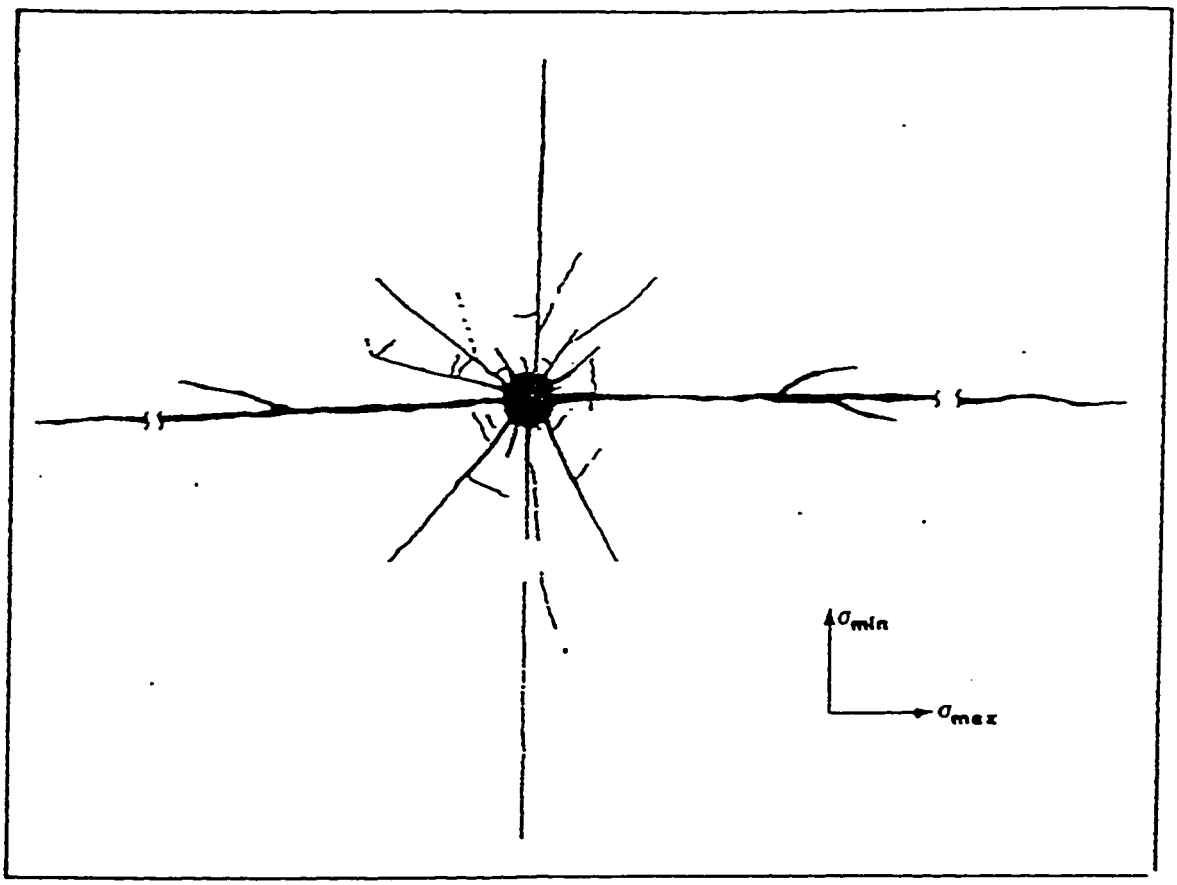

Figure 2.2 : Schematic of typical multiple fracture pattern resulting from tailored pulse technique . [ref. 36]

2.3 PROPOSED RESEARCH

All of the previous work has increased significantly the understanding of transient fluid flow in hydraulically fractured wells . In recent years , Controlled Pulse Fracturing was introduced to economically exploit low-permeability oil and gas reservoirs . An illustration of fracture patterns resulting from such technique are shown in figures 2.1 and 2.2 . Although a considerable amount of fractured gas well test theory has been developed , no investigation has been made to study the behavior of gas wells intersected by multiple fractures resulting from pulse fracturing technique.

The objective of this study is to investigate the effects of induced vertical fractures of different fracture length ratios (y_f / x_f) , and conductivities on well performance and pressure transient behavior . In addition , the applicability of the existing methods of analysis of a single vertical fracture to the multiple fractures will be investigated .

The investigation will be conducted for a well intersected by two perpendicular vertical fractures in the center of a square reservoir and producing at constant flow rate under unsteady-state condition. The reservoir is assumed to be homogeneous with sealed upper and lower boundaries and no flow across the outer boundaries. Each fracture extends an equal distances on both sides of the wellbore (figure 2.3). A fully implicit finite difference numerical simulator will be used to investigate this problem.

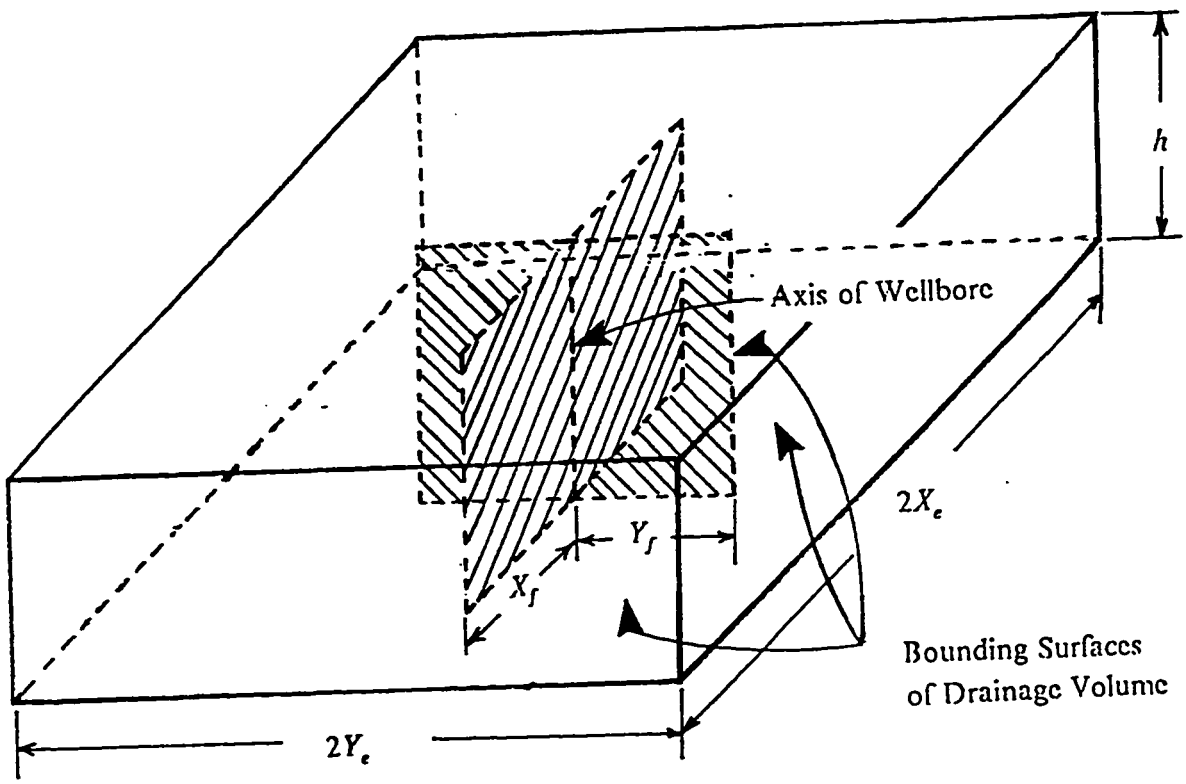

Figure 2.3 : Schematic diagram showing the model used in this study .

Chapter Three

CHAPTER 3

MATHEMATICAL MODEL

The mathematical model used in this investigation was developed to study the performance of hydraulically fractured gas wells [14]. The model is a single-phase two-dimensional model .

3.1 THE MODEL FLOW EQUATION

The forthcoming development of the equations describing the flow of natural gas in porous media is based upon the following assumptions :

1. Isothermal horizontal flow , no gravity effects ;
2. Real gas of constant composition ;
3. No Klinkenberg effect , gas saturation equals to 100% ;
4. The reservoir has uniform thickness ; isotropic porous media ;

The fundamental equation governing the flow of real gases in porous media was derived using the principle of conservation of mass , Darcy's law modified to include turbulence , and the equation of state as follows :

$$-\frac{\partial(\rho v_x)}{\partial x}-\frac{\partial(\rho v_y)}{\partial y}+q_m^{\bullet}=\frac{\partial(\rho\varphi)}{\partial t} \qquad (3.1)$$

$$v_x=-|\delta_x|\frac{k_x}{\mu}\frac{dp}{dx} \qquad (3.2)$$

$$v_y=-|\delta_y|\frac{k_y}{\mu}\frac{dp}{dy} \qquad (3.3)$$

$$\rho = \frac{p\,M}{z\,R\,T} \qquad (3.4)$$

Substituting equations (3.2) through (3.4) in equation (3.1) and utilizing the pseudo-pressure function :

$$m(p) = \int_{p1}^{p2} \frac{p}{\mu z} dp \qquad (3.5)$$

The following equation was obtained :

$$\frac{\partial}{\partial x}(|\delta_x| k_x \frac{\partial m}{\partial x}) + \frac{\partial}{\partial y}(|\delta_y| k_y \frac{\partial m}{\partial y}) + q_m^{\bullet} = \varphi \mu c_g \frac{\partial m}{\partial t} \qquad (3.6)$$

Equation (3.6) represents the flow of gas in the formation and fracture at any point in the reservoir for any instant . It is a partial differential equation similar to the diffusivity equation obtained in the case of slightly compressible fluid . It differs by being written in terms of m rather than p , and having coefficients which depend on pressure and pressure gradient [13,14,34] .

3.2 THE NUMERICAL MODEL

Numerical simulators have been used extensively to model complex patterns of reservoir behavior . In some cases , the analytical tools are difficult or impossible to use because of the complexity of the problem . However using a numerical model to study such difficult systems is essential [45] .

The mathematical model used in this study is a single phase two dimensional, fully implicit model developed for simulating gas wells intersected by either a finite or infinite conductivity vertical fractures. The model has the feature of accounting for turbulent flow in the fracture , the formation or both .

3.2.1 Finite Difference Equation

Equation (3.6) governs the fluid flow in the formation and fractures . To solve this equation , the Newtonian iterative procedure was followed . The Newtonian method requires that equation (3.6) be written in a finite difference form and then put in a residual form as follows :

$$R(m^{n+1})_{i,j} = A_{i,j}\delta^{n}_{x_{i+1/2,j}} m^{n+1}_{i+1,j} - \left(A_{i,j}\delta^{n}_{x_{i+1/2,j}} + B_{i,j}\delta^{n}_{x_{i-1/2,j}}\right)m^{n+1}_{i,j}$$
$$+ B_{i,j}\delta^{n}_{x_{i-1/2,j}} m^{n+1}_{i-1,j} + C_{i,j}\delta^{n}_{y_{i,j+1/2}} m^{n+1}_{i,j+1} - \left(C_{i,j}\delta^{n}_{y_{i,j+1/2}} + D_{i,j}\delta^{n}_{y_{i,j-1/2}}\right)m^{n+1}_{i,j}$$
$$+ D_{i,j}\delta^{n}_{y_{i,j-1/2}} m^{n+1}_{i,j-1} + q^{*}_{m} - F_{i,j}\left(\frac{1}{\Delta t}\right)(\mu c_g)^{n+1}_{i,j}\left(m^{n+1}_{i,j} - m^{n}_{i,j}\right) \approx 0 \quad (3.7)$$

Where ;

$A_{i,j} = 0.006328\ h\ \Delta y_j k_{x_{i+1/2,j}} / (x_{i+1} - x_i)$

$B_{i,j} = 0.006328\ h\ \Delta y_j k_{x_{i-1/2,j}} / (x_i - x_{i-1})$

$C_{i,j} = 0.006328\ h\ \Delta x_i k_{y_{i,j+1/2}} / (y_{j+1} - y_j)$

$D_{i,j} = 0.006328\ h\ \Delta x_i k_{y_{i,j-1/2}} / (y_j - y_{j-1})$

$F_{i,j} = V_{p_{i,j}}$

$q^{*}_{m} = \frac{RT}{M}\rho_{sc}\, q_{sc}$

$$k_{x_{i+1/2,j}} = [(x_{i+1} - x_i)\, k_{x_{i,j}} k_{x_{i+1,j}}] / [(x_{i+1} - x_{i+1/2})\, k_{x_{i,j}} + (x_{i+1/2} - x_i)\, k_{x_{i+1,j}}]$$
$$k_{x_{i-1/2,j}} = [(x_i - x_{i-1})\, k_{x_{i,j}} k_{x_{i-1,j}}] / [(x_i - x_{i-1/2})\, k_{x_{i-1,j}} + (x_{i-1/2} - x_{i-1})\, k_{x_{i,j}}]$$
$$k_{y_{i,j+1/2}} = [(y_{i+1} - y_i)\, k_{y_{i,j}} k_{y_{i,j+1}}] / [(y_{j+1} - y_{j+1/2})\, k_{y_{i,j}} + (y_{j+1/2} - y_j)\, k_{y_{i,j+1}}]$$
$$k_{y_{i,j-1/2}} = [(y_j - y_{j-1})\, k_{y_{i,j}} k_{y_{i,j-1}}] / [(y_j - y_{j-1/2})\, k_{y_{i,j-1}} + (y_{j-1/2} - y_{j-1})\, k_{y_{i,j}}]$$

Several points should be noted in formulating the equivalent finite difference, Eq. (3.7) :

a- An irregular grid is used .

b- As fluid and reservoir properties are only defined at grid points , some techniques must be used for approximating interblock flow coefficients based on values at the grid points . At the fractures faces , permeability changes rapidly from grid block to another ; these sharp changes in permeability could cause a significant difficulty . For these reasons , the harmonic mean of the values of permeabilities at the adjacent grid points was used in evaluating permeability at the block face .

c- The dependent pseudo-pressure function is calculated at the center of each block .

3.2.2 Method of Solution

The matrix resulting from equation (3.7) is a band matrix with two diagonals separated from the main diagonal and two diagonals adjacent to the main diagonal . The construction of this matrix requires that the derivatives of the residual function , equation (3.7) , be evaluated at each node with respect to itself and to the surrounding nodes . The system of equations was then solved by a solver using a D4 ordering scheme .

3.2.3 Computer Program

The computer program consists of a main program and several subroutines for calculating the gas properties , the permeability for gas between cells in x and y directions , gas velocity and turbulent coefficient . Also, it includes a solver subroutine which uses either standard ordering or D4 ordering scheme .

The main program is used for all input , output , and controlling parameters . Appendix A shows a flow chart of the computer program used in this study.

3.3 TESTING OF THE SIMULATOR

Since there is no published solutions in the literature for the transient pressure behavior of a well (gas , oil) intersected by multiple fractures to compare with , the simulator was checked considering single vertical fracture , and the model results were compared to the analytical and semianalytical solutions for a single vertical fracture having infinite and finite conductivities presented by Gringarten et al. [6] and Cinco et al. [9] respectively. Some points of interest should be mentioned before any discusions of results . First : the wellbore size is determined by the width of the fractures. Second : a finer grid near the well and near the fractures tips was used . Third : a comprehensive investigation was carried out to eliminate the effect of grid sizes and grid distributions , and to determine time step sizes that give stable and reliable solutions .

3.3.1 Infinite Conductivity Case

Several runs were made with different number of grids and grid sizes to test the sensitivity of the solution to the grid system . As a result of this investigation a minimum of (28×26) grids were found to be necessary to reproduce the analytical solution . Table 3.1 gives the reservoir data , fracture data and the grid system used for this comparison and Table 3.2 presents the computer solution for this run .

A second run was done with the same conditions as in the previous one ,

TABLE 3.1

Input Data used for Comparison between Numerical Solution and Analytical Solution [6].

Reservoir Data

$p_i = 5000\ psia$
$k\,h = 1\ md\text{-}ft$
$x_e = 4000\ ft$
$y_e = 4000\ ft$
$T = 200\ °F$
$\varphi = 0.14$ *(fraction of pore volume)*
$T_{sc} = 60\ °F$
$p_{sc} = 14.7\ psia$

Fracture Data

$x_f = 100\ ft$
$w = 0.5\ in$
$k_f = 1.0 \times 10^6\ md$
$\varphi_f = 0.5$

TABLE 3.1 (CONT)

Model Grid Block Centers and Block Boundaries

Block-Bound. x-Direct. ft	Block-Center x-Direct. ft
1.00000000	0.50000000
3.00000000	2.00000000
7.00000000	5.00000000
15.0000000	11.0000000
28.0000000	21.5000000
43.0000000	35.5000000
58.0000000	50.5000000
73.0000000	65.5000000
88.0000000	80.5000000
95.5000000	91.7500000
98.5000000	97.0000000
100.000000	99.2500000
101.500000	100.750000
104.500000	103.000000
110.500000	107.500000
122.500000	116.500000
137.500000	130.000000
152.500000	145.000000
182.500000	167.500000
242.500000	212.500000
362.500000	302.500000
560.000000	461.250000
800.000000	680.000000
1280.00000	1040.00000
1960.00000	1620.00000
2640.00000	2300.00000
3320.00000	2980.00000
4000.00000	3660.00000

TABLE 3.1 (CONT)

Model Grid Block Centers and Block Boundaries

Block-Bound. y-Direct. ft	Block-Center y-Direct. ft
0.249999985E-01	0.124999993E-01
0.499999970E-01	0.374999940E-01
0.749999881E-01	0.624999702E-01
0.999999642E-01	0.874999762E-01
0.149999917	0.124999940
0.249999940	0.199999928
0.449999928	0.349999905
0.849999905	0.649999619
1.64999962	1.24999905
3.25000000	2.44999981
6.44999981	4.84999943
12.8499994	9.64999390
25.6499939	19.2499847
45.6499939	35.6499939
65.6499939	55.6499939
85.6499939	75.6499939
105.649994	95.6499939
145.649994	125.649994
225.649994	185.649902
385.649902	305.649902
705.649902	545.649902
1320.00000	1012.82495
1960.00000	1640.00000
2640.00000	2300.00000
3320.00000	2980.00000
4000.00000	3660.00000

TABLE 3.2

Simulator Results for Infinite Conductivity
($F_{CD} = 500$)

t_{Dxf}	p_D	t_{Dxf}	p_D
0.59997E-05	0.46472E-02	0.35981E-01	0.31543E+00
0.11999E-04	0.66097E-02	0.47981E-01	0.35853E+00
0.17999E-04	0.80679E-02	0.59981E-01	0.39605E+00
0.29999E-04	0.10270E-01	0.83982E-01	0.45765E+00
0.41999E-04	0.12096E-01	0.10798E+00	0.50995E+00
0.66000E-04	0.15000E-01	0.13198E+00	0.55567E+00
0.90000E-04	0.17460E-01	0.15598E+00	0.59645E+00
0.11400E-03	0.19624E-01	0.17998E+00	0.63336E+00
0.13800E-03	0.21575E-01	0.23998E+00	0.71047E+00
0.16200E-03	0.23364E-01	0.29998E+00	0.77630E+00
0.22200E-03	0.27193E-01	0.35997E+00	0.83396E+00
0.28199E-03	0.30576E-01	0.47997E+00	0.92900E+00
0.34199E-03	0.33632E-01	0.59997E+00	0.10090E+01
0.46199E-03	0.38900E-01	0.83998E+00	0.11350E+01
0.58199E-03	0.43577E-01	0.10800E+01	0.12371E+01
0.82200E-03	0.51475E-01	0.13200E+01	0.13229E+01
0.10620E-02	0.58383E-01	0.15600E+01	0.13968E+01
0.13020E-02	0.64576E-01	0.18000E+01	0.14618E+01
0.15420E-02	0.70227E-01	0.23978E+01	0.15907E+01
0.17820E-02	0.75453E-01	0.29957E+01	0.16947E+01
0.23820E-02	0.86763E-01	0.35935E+01	0.17820E+01
0.29819E-02	0.96813E-01	0.41914E+01	0.18570E+01
0.35819E-02	0.10592E+00	0.47892E+01	0.19226E+01
0.47819E-02	0.12162E+00	0.53871E+01	0.19810E+01
0.59819E-02	0.13555E+00	0.59850E+01	0.20334E+01
0.83820E-02	0.15900E+00	0.65828E+01	0.20811E+01
0.10782E-01	0.17941E+00	0.71807E+01	0.21246E+01
0.13182E-01	0.19762E+00	0.77785E+01	0.21648E+01
0.15582E-01	0.21413E+00	0.83764E+01	0.22020E+01
0.17982E-01	0.22929E+00	0.89742E+01	0.22367E+01
0.23982E-01	0.26166E+00	0.95720E+01	0.22692E+01
0.29981E-01	0.29003E+00	0.10170E+02	0.22997E+01

but in this case the grid system was constructed based on the fracture width in the other direction (the first cell is equal to the fracture width). It was found that a minimum of (29 × 29) grids are necessary to reproduce the analytical solution . Table 3.3 gives the reservoir data , fracture data and the grid system used in this case, and Table 3.4 presents computer solution for this comparison .

Figures 3.1 and 3.2 show the comparison between the computer solution for the two cases and Gringarten et al's analytical solution . As it can be seen from these figures an excellent agreement between the two sets of results and Gringarten et al. analytical solution is obtained .

3.3.2 Finite Conductivity Case

To check the validity of the numerical model against Cinco et al.[9] semianalytical solution for finite conductivity , three sets of computer runs were made using the finite difference simulator for dimensionless fracture conductivities (F_{CD}) having values of 0.2 π , π and 10 π with (29 × 29) grid system .

Table 3.5 gives the reservoir data , fracture data and grid system used in cases of 0.2 π , π and 10 π dimensionless fracture conductivities and Tables 3.6 , 3.7 and 3.8 present computer solution for these cases . Figures 3.3 and 3.4 show an excellent agreement between the numerical solution and Cinco et al's semianalytical solution for all cases considered .

It should be noted that , the model was also checked in the other direction and found to give the same solution for both infinite and finite conductivity cases .

As a result of testing the model the following observations were noted :

1. Although Newton's method is stable at large time steps and converges in one to three iterations , a small time step (10^{-6} day) at the start was necessary for the system investigated .
2. The accuracy of the solution is dependent upon the appropriate choice of the number of segments in the fracture and in the formation , and on the time steps used.
3. A (29 × 29) grid system was found to be appropriate for accurate results for both infinite and finite conductivity vertical fracture which was developed based on the guidelines suggested by Bennett et al. [19] .
4. D4 ordering is superior to Gauss elimination procedure for solving large matrix .

In summary figures 3.1 , 3.2 , 3.3 and 3.4 show that for practical purposes , the numerical model solution (for both infinite and finite conductivity vertical fracture) matches the semianalytical solution . This gives a sufficiently accurate representation of a converged numerical solution , and also gives confidence in the computer program and in the method of solution .

TABLE 3.3

Input Data used for Comparison between Numerical Solution and Analytical Solution [6].

Reservoir Data

$p_i = 5000\ psia$
$k\,h = 1\ md\text{-}ft$
$x_e = 3000\ ft$
$y_e = 3000\ ft$
$T = 200\ °F$
$\varphi = 0.14$ *(fraction of pore volume)*
$T_{sc} = 60\ °F$
$p_{sc} = 14.7\ psia$

Fracture Data

$x_f = 100\ ft$
$w = 0.5\ in$
$k_f = 2.400 \times 10^6\ md$
$\varphi_f = 0.5$

TABLE 3.3 (CON'T)

Model Grid Block Centers and Block Boundaries

Block-Bound. x-Direct. ft	Block-Center x-Direct. ft	Block-Bound. y-Direct. ft	Block-Center y-Direct. ft
0.0208	0.0104	0.0208	0.0104
0.0624	0.0416	0.0624	0.0416
0.1456	0.1040	0.1456	0.1040
0.3120	0.2288	0.3120	0.2288
0.6448	0.4784	0.6448	0.4784
1.1135	0.8792	1.1135	0.8792
2.0510	1.5823	2.0510	1.5823
3.9260	2.9885	3.9260	2.9885
7.6760	5.8010	7.6760	5.8010
15.1760	11.4260	15.1760	11.4260
30.1760	22.6760	23.1760	19.1760
48.2570	39.2165	33.9792	28.5776
66.3380	57.2975	44.9999	39.4896
84.4190	75.3785	59.9999	52.4999
98.5000	91.4595	79.9999	69.9999
100.0000	99.2500	99.9999	89.9999
101.5000	100.7500	139.9999	119.9999
104.5000	103.0000	199.9999	169.9999
110.5000	107.5000	279.9998	239.9998
122.5000	116.5000	379.9998	329.9998
137.5000	130.0000	499.9998	439.9998
167.5000	152.5000	639.9998	569.9998
227.5000	197.5000	799.9998	719.9998
347.5000	287.5000	979.9998	889.9998
587.5000	467.5000	1339.9990	1159.9990
1067.5000	827.5000	1739.9990	1539.9990
1577.5000	1322.5000	2139.9990	1939.9990
2288.7500	1933.1250	2539.9990	2339.9980
3000.0000	2644.3750	2999.9990	2769.9980

TABLE 3.4

Simulator Results for Infinite Conductivity
($F_{CD} = 500$)

t_{Dxf}	p_D	t_{Dxf}	p_D
0.59997E-05	0.52644E-02	0.35981E-01	0.31729E+00
0.11999E-04	0.72904E-02	0.47981E-01	0.36266E+00
0.17999E-04	0.87657E-02	0.59981E-01	0.40086E+00
0.29999E-04	0.10970E-01	0.83982E-01	0.46798E+00
0.41999E-04	0.12786E-01	0.10798E+00	0.52195E+00
0.66000E-04	0.15684E-01	0.13198E+00	0.56874E+00
0.90000E-04	0.18137E-01	0.15598E+00	0.61028E+00
0.11400E-03	0.20296E-01	0.17998E+00	0.64777E+00
0.13800E-03	0.22243E-01	0.23998E+00	0.73735E+00
0.16200E-03	0.24030E-01	0.29998E+00	0.80536E+00
0.22200E-03	0.27875E-01	0.35997E+00	0.86421E+00
0.28199E-03	0.31265E-01	0.47997E+00	0.97739E+00
0.34199E-03	0.34325E-01	0.59997E+00	0.10576E+01
0.46199E-03	0.39627E-01	0.83998E+00	0.12178E+01
0.58199E-03	0.44315E-01	0.10800E+01	0.13118E+01
0.82200E-03	0.52287E-01	0.13200E+01	0.13956E+01
0.10620E-02	0.59230E-01	0.15600E+01	0.14655E+01
0.13020E-02	0.65450E-01	0.18000E+01	0.15267E+01
0.15420E-02	0.71121E-01	0.23978E+01	0.17243E+01
0.17820E-02	0.76360E-01	0.29957E+01	0.17796E+01
0.23820E-02	0.87843E-01	0.35935E+01	0.18806E+01
0.29819E-02	0.97959E-01	0.41914E+01	0.19365E+01
0.35819E-02	0.10710E+00	0.47892E+01	0.20021E+01
0.47819E-02	0.12307E+00	0.53871E+01	0.20513E+01
0.59819E-02	0.13701E+00	0.59850E+01	0.21006E+01
0.83820E-02	0.16077E+00	0.65828E+01	0.21427E+01
0.10782E-01	0.18103E+00	0.71807E+01	0.21829E+01
0.13182E-01	0.19897E+00	0.77785E+01	0.22192E+01
0.15582E-01	0.21520E+00	0.83764E+01	0.22533E+01
0.17982E-01	0.23011E+00	0.89742E+01	0.22850E+01
0.23982E-01	0.26342E+00	0.95720E+01	0.23148E+01
0.29981E-01	0.29189E+00	0.10170E+02	0.23429E+01

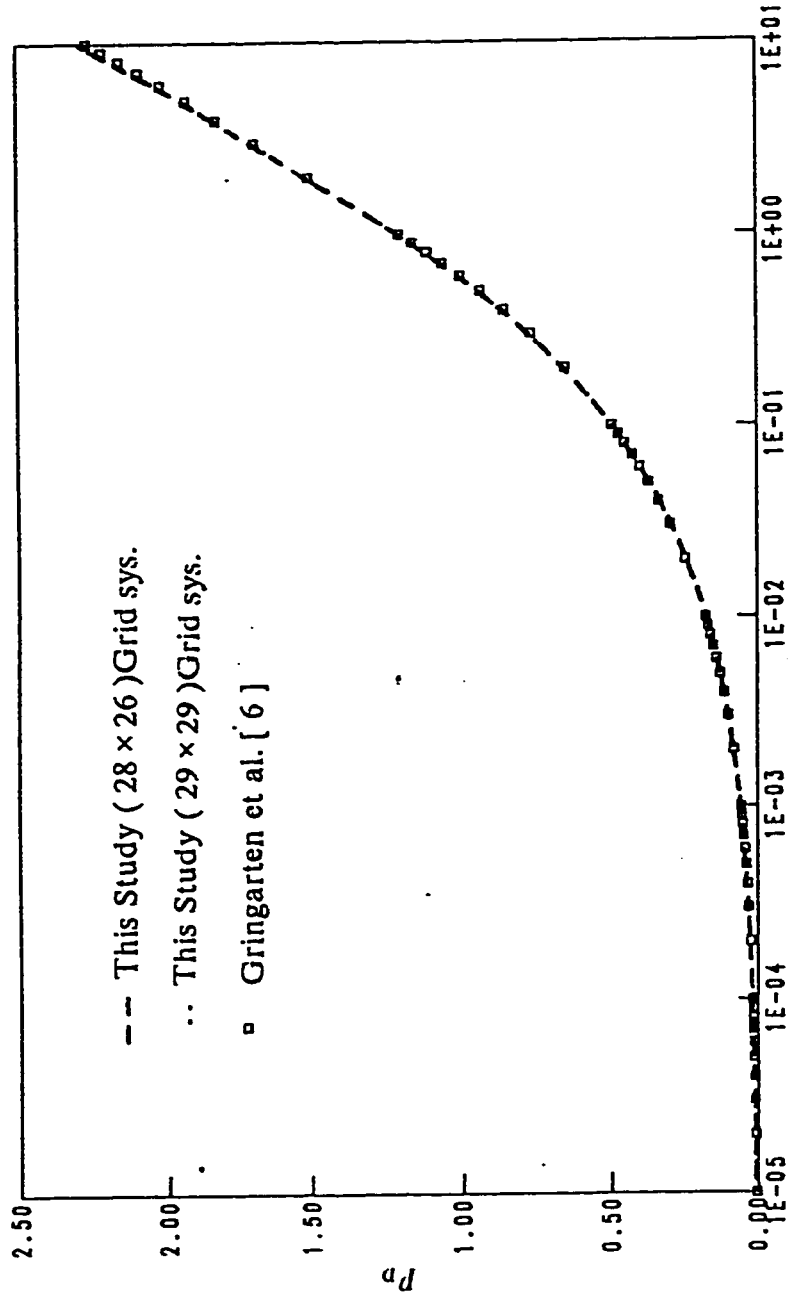

Figure 3.1 : Comparison between numerical solution and analytical solution for infinite conductivity vertical fracture .

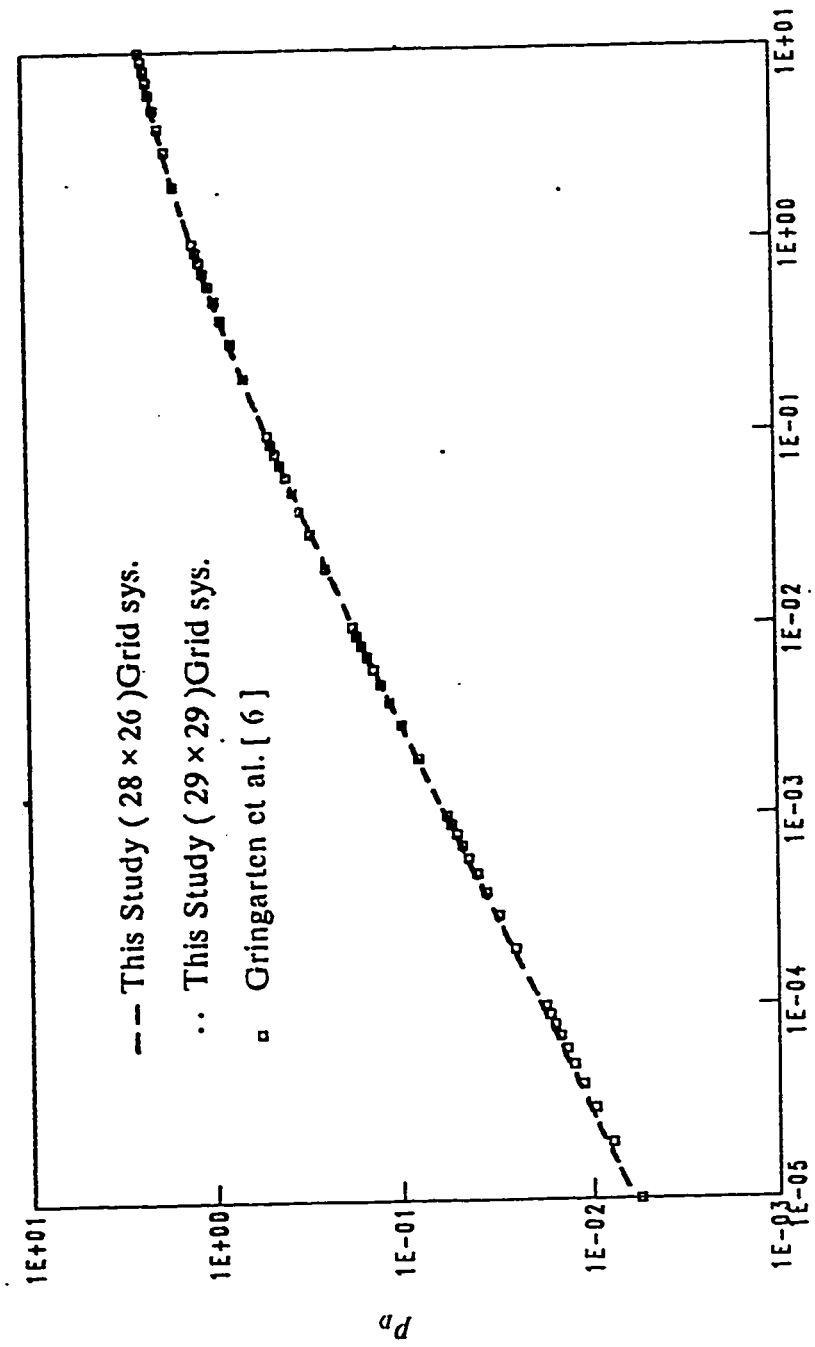

Figure 3.2 : Comparison between numerical solution and analytical solution for infinite conductivity vertical fracture .

TABLE 3.5

Input Data used for Comparison between Numerical Solution and Analytical Solution [9].

Reservoir Data

$p_i = 5000\ psia$
$k\,h = 1\ md\text{-}ft$
$x_e = 3000\ ft$
$y_e = 3000\ ft$
$T = 200\ °F$
$\varphi = 0.14\ (fraction\ of\ pore\text{-}volume)$
$T_{sc} = 60\ °F$
$p_{sc} = 14.7\ psia$

Fracture Data

$x_f = 100\ ft$
$w = 0.5\ in$
$k_f = 1.5080 \times 10^3\ md$
$k_f = 7.5400 \times 10^3\ md$
$k_f = 7.5398 \times 10^4\ md$
$\varphi_f = 0.5\ (fraction\ of\ porevolume)$

TABLE 3.5 (CONT)

Model Grid Block Centers and Block Boundaries

Block-Bound. x-Direct. ft	Block-Center x-Direct. ft	Block-Bound. y-Direct. ft	Block-Center y-Direct. ft
0.0416	0.0208	0.0208	0.0104
0.1248	0.0832	0.0624	0.0416
0.2912	0.2080	0.1456	0.1040
0.6240	0.4576	0.3120	0.2288
1.2896	0.9567	0.6448	0.4784
2.6207	1.9551	1.1135	0.8792
5.2832	3.9520	2.0510	1.5823
10.6079	7.9455	3.9260	2.9885
25.6079	18.1079	7.6760	5.8010
40.6079	33.1079	15.1760	11.4260
55.6079	48.1079	23.1760	19.1760
70.6079	63.1079	33.9792	28.5776
85.6079	78.1079	44.9999	39.4896
96.2575	90.9327	59.9999	52.4999
98.4999	97.3787	79.9999	69.9999
99.9999	99.2499	99.9999	89.9999
101.4999	100.7499	139.9999	119.9999
104.4999	102.9999	199.9999	169.9999
110.4999	107.4999	279.9998	239.9998
122.4999	116.4999	379.9998	329.9998
146.4999	134.4998	499.9998	439.9998
194.4999	170.4998	639.9998	569.9998
290.4997	242.4977	799.9998	719.9998
482.4997	386.4997	979.9998	889.9998
866.4997	674.4997	1339.9990	1159.9990
1399.8740	1133.1870	1739.9990	1539.9990
1933.2490	1666.5620	2139.9990	1939.9990
2466.6250	2199.9350	2539.9990	2339.9980
2999.9990	2733.3110	2999.9990	2769.9980

TABLE 3.6

Simulator Results for Finite Conductivity
($F_{CD} = 0.2\,\pi$)

t_{Dxf}	p_D	t_{Dxf}	p_D
0.59997E-05	0.12441E+00	0.49140E+02	0.43031E+01
0.90000E-04	0.29571E+00	0.50265E+02	0.43140E+01
0.82200E-03	0.52634E+00	0.51015E+02	0.43212E+01
0.83820E-02	0.90693E+00	0.52140E+02	0.43317E+01
0.83982E-01	0.14759E+01	0.53265E+02	0.43420E+01
0.98999E+00	0.24114E+01	0.54015E+02	0.43487E+01
0.10650E+01	0.24452E+01	0.55140E+02	0.43587E+01
0.30150E+01	0.29336E+01	0.56265E+02	0.43684E+01
0.41400E+01	0.30875E+01	0.57015E+02	0.43748E+01
0.52650E+01	0.32055E+01	0.58140E+02	0.43842E+01
0.60150E+01	0.32711E+01	0.59265E+02	0.43934E+01
0.71400E+01	0.33559E+01	0.60015E+02	0.43994E+01
0.82651E+01	0.34283E+01	0.61140E+02	0.44084E+01
0.90151E+01	0.34713E+01	0.62265E+02	0.44171E+01
0.10140E+02	0.35296E+01	0.63015E+02	0.44229E+01
0.11265E+02	0.35817E+01	0.64140E+02	0.44314E+01
0.12015E+02	0.36137E+01	0.64890E+02	0.44369E+01
0.13140E+02	0.36580E+01	0.65265E+02	0.44397E+01
0.14265E+02	0.36986E+01	0.66015E+02	0.44452E+01
0.15015E+02	0.37239E+01	0.67140E+02	0.44533E+01
0.16140E+02	0.37596E+01	0.68265E+02	0.44613E+01
0.17265E+02	0.37928E+01	0.69015E+02	0.44665E+01
0.18015E+02	0.38138E+01	0.70140E+02	0.44742E+01
0.19140E+02	0.38436E+01	0.71265E+02	0.44819E+01
0.20265E+02	0.38716E+01	0.72015E+02	0.44869E+01
0.21015E+02	0.38895E+01	0.73140E+02	0.44943E+01
0.22140E+02	0.39151E+01	0.74265E+02	0.45016E+01
0.23265E+02	0.39394E+01	0.75015E+02	0.45064E+01
0.24015E+02	0.39549E+01	0.76140E+02	0.45135E+01
0.25140E+02	0.39773E+01	0.77265E+02	0.45205E+01
0.26265E+02	0.39987E+01	0.78015E+02	0.45252E+01
0.27015E+02	0.40125E+01	0.79140E+02	0.45320E+01
0.28140E+02	0.40324E+01	0.80265E+02	0.45387E+01

TABLE 3.6 (CON'T)

Simulator Results for Finite Conductivity
($F_{CD} = 0.2\,\pi$)

t_{Dxf}	p_D	t_{Dxf}	p_D
0.29265E+02	0.40515E+01	0.81015E+02	0.45432E+01
0.30015E+02	0.40639E+01	0.82140E+02	0.45498E+01
0.31140E+02	0.40818E+01	0.83265E+02	0.45563E+01
0.32265E+02	0.40991E+01	0.84015E+02	0.45605E+01
0.33015E+02	0.41103E+01	0.85140E+02	0.45669E+01
0.34140E+02	0.41266E+01	0.86265E+02	0.45732E+01
0.35265E+02	0.41423E+01	0.87015E+02	0.45773E+01
0.36015E+02	0.41526E+01	0.88140E+02	0.45834E+01
0.37140E+02	0.41675E+01	0.89265E+02	0.45895E+01
0.38265E+02	0.41820E+01	0.90015E+02	0.45935E+01
0.39015E+02	0.41914E+01	0.91140E+02	0.45994E+01
0.40140E+02	0.42052E+01	0.92265E+02	0.46052E+01
0.41265E+02	0.42186E+01	0.93015E+02	0.46091E+01
0.42015E+02	0.42273E+01	0.94140E+02	0.46148E+01
0.43140E+02	0.42401E+01	0.95265E+02	0.46205E+01
0.44265E+02	0.42526E+01	0.96015E+02	0.46242E+01
0.45015E+02	0.42607E+01	0.97140E+02	0.46297E+01
0.46140E+02	0.42727E+01	0.98265E+02	0.46352E+01
0.47265E+02	0.42843E+01	0.99390E+02	0.46407E+01
0.48015E+02	0.42919E+01	0.10014E+03	0.46442E+01

TABLE 3.7

Simulator Results for Finite Conductivity
($F_{CD} = \pi$)

t_{Dxf}	p_D	t_{Dxf}	p_D
0.59997E-05	0.56735E-01	0.41115E+02	0.33573E+01
0.90000E-04	0.13424E+00	0.42240E+02	0.33705E+01
0.11400E-03	0.14311E+00	0.43365E+02	0.33833E+01
0.10620E-02	0.25127E+00	0.44115E+02	0.33917E+01
0.10782E-01	0.44475E+00	0.45240E+02	0.34040E+01
0.10798E+00	0.82822E+00	0.46365E+02	0.34159E+01
0.20998E+00	0.10097E+01	0.47115E+02	0.34238E+01
0.32998E+00	0.11538E+01	0.48240E+02	0.34352E+01
0.50998E+00	0.13063E+01	0.49365E+02	0.34465E+01
0.62998E+00	0.13865E+01	0.50115E+02	0.34538E+01
0.74998E+00	0.14560E+01	0.51240E+02	0.34646E+01
0.86998E+00	0.15172E+01	0.52365E+02	0.34751E+01
0.98999E+00	0.15720E+01	0.53115E+02	0.34821E+01
0.12900E+01	0.16828E+01	0.54240E+02	0.34922E+01
0.21900E+01	0.19214E+01	0.55365E+02	0.35022E+01
0.30900E+01	0.20848E+01	0.56115E+02	0.35087E+01
0.43650E+01	0.22521E+01	0.57240E+02	0.35184E+01
0.51150E+01	0.23294E+01	0.58365E+02	0.35278E+01
0.62401E+01	0.24269E+01	0.59115E+02	0.35340E+01
0.73651E+01	0.25086E+01	0.60240E+02	0.35431E+01
0.81151E+01	0.25565E+01	0.61365E+02	0.35521E+01
0.92401E+01	0.26208E+01	0.62115E+02	0.35580E+01
0.10365E+02	0.26778E+01	0.63240E+02	0.35667E+01
0.11115E+02	0.27125E+01	0.64365E+02	0.35752E+01
0.12240E+02	0.27603E+01	0.65115E+02	0.35808E+01
0.13365E+02	0.28039E+01	0.66240E+02	0.35891E+01
0.14115E+02	0.28310E+01	0.67365E+02	0.35972E+01
0.15240E+02	0.28690E+01	0.68115E+02	0.36026E+01
0.16365E+02	0.29043E+01	0.69240E+02	0.36105E+01
0.17115E+02	0.29265E+01	0.70365E+02	0.36183E+01
0.18240E+02	0.29580E+01	0.71115E+02	0.36234E+01
0.19365E+02	0.29876E+01	0.72240E+02	0.36310E+01
0.20115E+02	0.30063E+01	0.73365E+02	0.36384E+01

TABLE 3.7 (CON'T)

Simulator Results for Finite Conductivity
($F_{CD} = \pi$)

t_{Dxf}	p_D	t_{Dxf}	p_D
0.21240E+02	0.30332E+01	0.74115E+02	0.36433E+01
0.22365E+02	0.30586E+01	0.75240E+02	0.36506E+01
0.23115E+02	0.30749E+01	0.76365E+02	0.36577E+01
0.24240E+02	0.30983E+01	0.77115E+02	0.36625E+01
0.25365E+02	0.31206E+01	0.78240E+02	0.36694E+01
0.26115E+02	0.31350E+01	0.79365E+02	0.36763E+01
0.27240E+02	0.31557E+01	0.80115E+02	0.36808E+01
0.28365E+02	0.31756E+01	0.81240E+02	0.36876E+01
0.29115E+02	0.31884E+01	0.82365E+02	0.36942E+01
0.30240E+02	0.32070E+01	0.83115E+02	0.36985E+01
0.31365E+02	0.32249E+01	0.84240E+02	0.37050E+01
0.32115E+02	0.32365E+01	0.85365E+02	0.37114E+01
0.33240E+02	0.32534E+01	0.86115E+02	0.37156E+01
0.34365E+02	0.32697E+01	0.87240E+02	0.37218E+01
0.35115E+02	0.32802E+01	0.88365E+02	0.37280E+01
0.36240E+02	0.32957E+01	0.89490E+02	0.37341E+01
0.37365E+02	0.33106E+01	0.90240E+02	0.37381E+01
0.38115E+02	0.33203E+01	0.91365E+02	0.37441E+01
0.39240E+02	0.33345E+01	0.92115E+02	0.37480E+01
0.40365E+02	0.33483E+01	0.93240E+02	0.37538E+01

TABLE 3.8

Simulator Results for Finite Conductivity
(F_{CD} = 10 π)

t_{Dxf}	p_D	t_{Dxf}	p_D
0.59997E-05	0.17914E-01	0.49140E+02	0.31106E+01
0.11999E-04	0.23285E-01	0.50265E+02	0.31217E+01
0.11400E-03	0.44584E-01	0.51015E+02	0.31289E+01
0.10620E-02	0.87941E-01	0.52140E+02	0.31395E+01
0.10782E-01	0.21055E+00	0.53265E+02	0.31499E+01
0.10798E+00	0.54227E+00	0.54015E+02	0.31567E+01
0.20998E+00	0.71052E+00	0.55140E+02	0.31667E+01
0.32998E+00	0.84674E+00	0.56265E+02	0.31765E+01
0.50998E+00	0.99323E+00	0.57015E+02	0.31830E+01
0.62998E+00	0.10706E+01	0.58140E+02	0.31925E+01
0.74998E+00	0.11377E+01	0.59265E+02	0.32018E+01
0.86998E+00	0.11971E+01	0.60015E+02	0.32079E+01
0.98999E+00	0.12502E+01	0.61140E+02	0.32169E+01
0.10650E+01	0.12809E+01	0.62265E+02	0.32257E+01
0.21150E+01	0.15819E+01	0.63015E+02	0.32315E+01
0.30150E+01	0.17457E+01	0.64140E+02	0.32401E+01
0.41400E+01	0.18962E+01	0.65265E+02	0.32486E+01
0.52650E+01	0.20122E+01	0.66015E+02	0.32541E+01
0.60150E+01	0.20771E+01	0.67140E+02	0.32623E+01
0.71400E+01	0.21610E+01	0.68265E+02	0.32703E+01
0.82651E+01	0.22329E+01	0.69015E+02	0.32756E+01
0.90151E+01	0.22757E+01	0.70140E+02	0.32834E+01
0.10140E+02	0.23338E+01	0.71265E+02	0.32911E+01
0.11265E+02	0.23858E+01	0.72015E+02	0.32962E+01
0.12015E+02	0.24177E+01	0.73140E+02	0.33037E+01
0.13140E+02	0.24620E+01	0.74265E+02	0.33111E+01
0.14265E+02	0.25026E+01	0.75015E+02	0.33159E+01
0.15015E+02	0.25280E+01	0.76140E+02	0.33231E+01
0.25890E+02	0.27968E+01	0.77265E+02	0.33302E+01
0.26265E+02	0.28039E+01	0.78015E+02	0.33349E+01
0.27015E+02	0.28177E+01	0.79140E+02	0.33418E+01

TABLE 3.8 (CON'T)

Simulator Results for Finite Conductivity
(F_{CD} = 10 π)

t_{Dxf}	p_D	t_{Dxf}	p_D
0.28140E+02	0.28378E+01	0.80265E+02	0.33486E+01
0.29265E+02	0.28570E+01	0.81015E+02	0.33531E+01
0.30015E+02	0.28695E+01	0.82140E+02	0.33598E+01
0.31140E+02	0.28875E+01	0.83265E+02	0.33663E+01
0.32265E+02	0.29049E+01	0.84015E+02	0.33706E+01
0.33765E+02	0.29272E+01	0.85140E+02	0.33771E+01
0.34140E+02	0.29326E+01	0.86265E+02	0.33834E+01
0.35265E+02	0.29485E+01	0.87015E+02	0.33876E+01
0.36015E+02	0.29588E+01	0.88140E+02	0.33938E+01
0.37140E+02	0.29739E+01	0.89265E+02	0.33999E+01
0.38265E+02	0.29885E+01	0.90015E+02	0.34039E+01
0.39015E+02	0.29980E+01	0.91140E+02	0.34099E+01
0.40140E+02	0.30119E+01	0.92265E+02	0.34158E+01
0.41265E+02	0.30254E+01	0.93015E+02	0.34197E+01
0.42015E+02	0.30342E+01	0.94140E+02	0.34255E+01
0.43140E+02	0.30471E+01	0.95265E+02	0.34312E+01
0.44265E+02	0.30597E+01	0.96015E+02	0.34350E+01
0.45015E+02	0.30679E+01	0.97140E+02	0.34406E+01
0.46140E+02	0.30799E+01	0.98265E+02	0.34461E+01
0.47265E+02	0.30917E+01	0.99390E+02	0.34516E+01
0.48015E+02	0.30994E+01	0.10014E+03	0.34552E+01

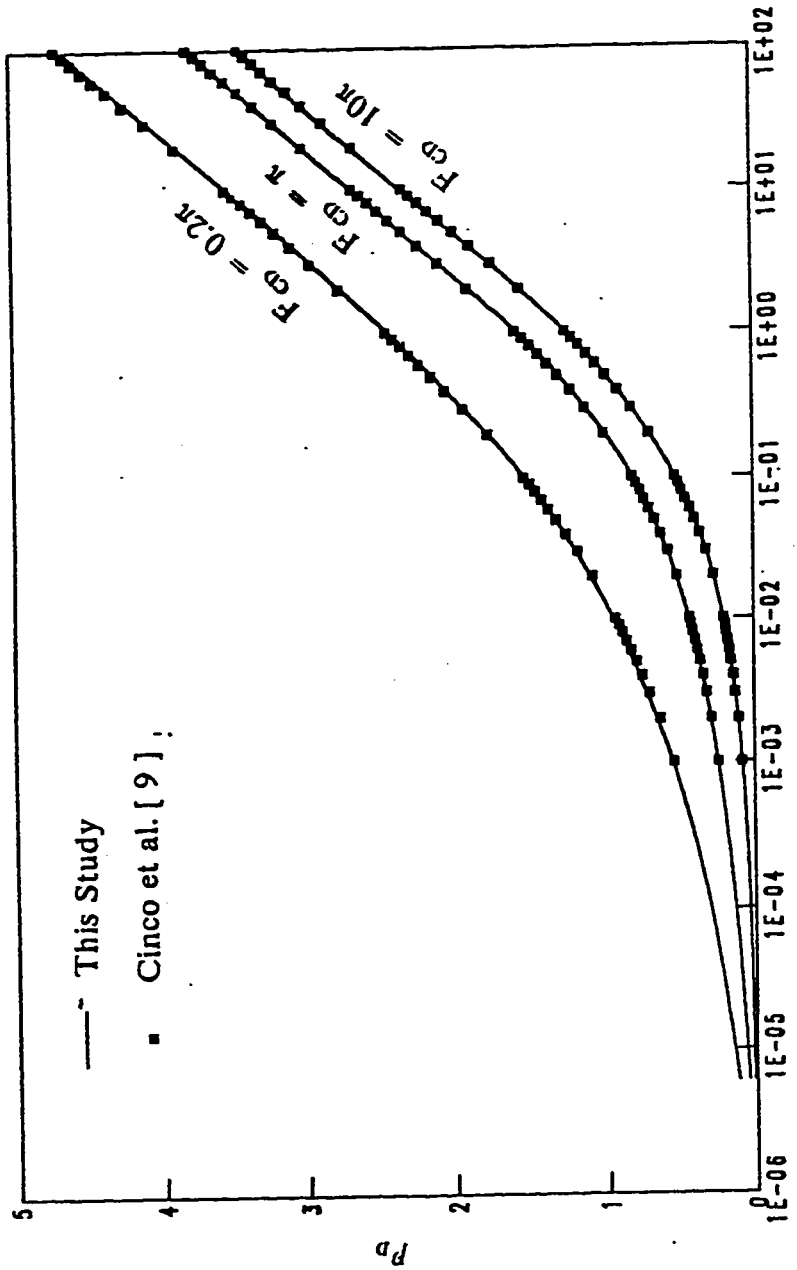

Figure 3.3 : Comparison between numerical solution and semianalytical solution for finite conductivity vertical fracture .

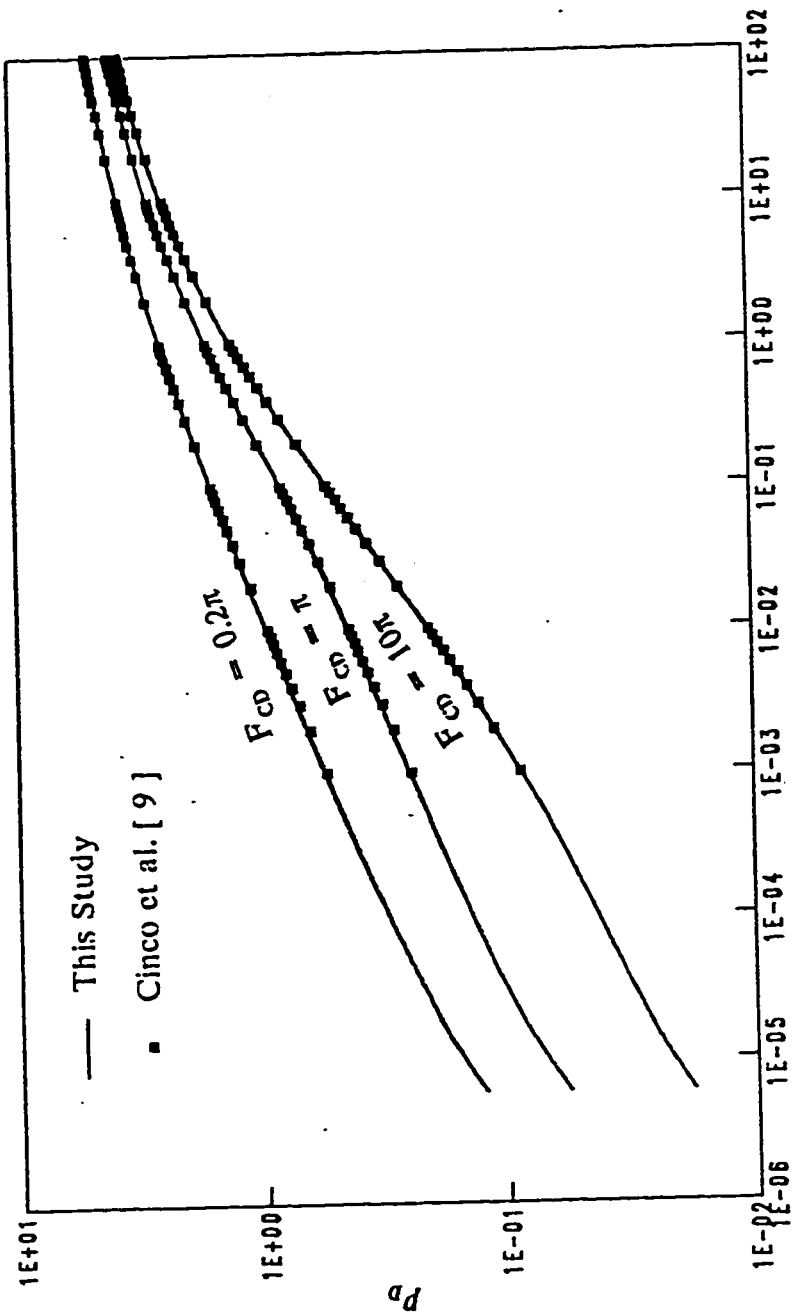

Figure 3.4 : Comparison between numerical solution and semianalytical solution for finite conductivity vertical fracture .

Chapter Four

CHAPTER 4

RESULTS AND DISCUSSION

INTRODUCTION

All studies on fractured wells with infinite and finite conductivity fracture are based on the assumption that one vertical fracture of large horizontal extension is induced . Although this assumption might be correct in many cases of MHF, multiple short radial fractures could also be created as a result of Tailored Pulse Loading Technique . This technique , which uses a full wellbore charge of propellant , is tailored to produce pressurization in the borehole that avoids crushing yet produces multiple fractures radiating from the wellbore . These fractures provide a number of conduits for natural gas to flow into the well [36,41] .

In this study the pressure transient behavior of a gas well intersected by two perpendicular fractures with infinite and finite conductivities will be investigated. Figure 4.1 presents schematic representation of the two fractures considered in this study and figure 4.2 shows the grid system used for modeling this system of fractures .

Since the fracture length is one of the most important parameters to be considered in any fracturing job , several drawdown runs were made for single ($y_f / x_f = 0.0$) and two fractures ($y_f / x_f \neq 0.0$) to study the pressure transient behavior of a gas well intersected by two perpendicular fractures. For the case of two fractures , different ratios of the fractures half lengths were tested to

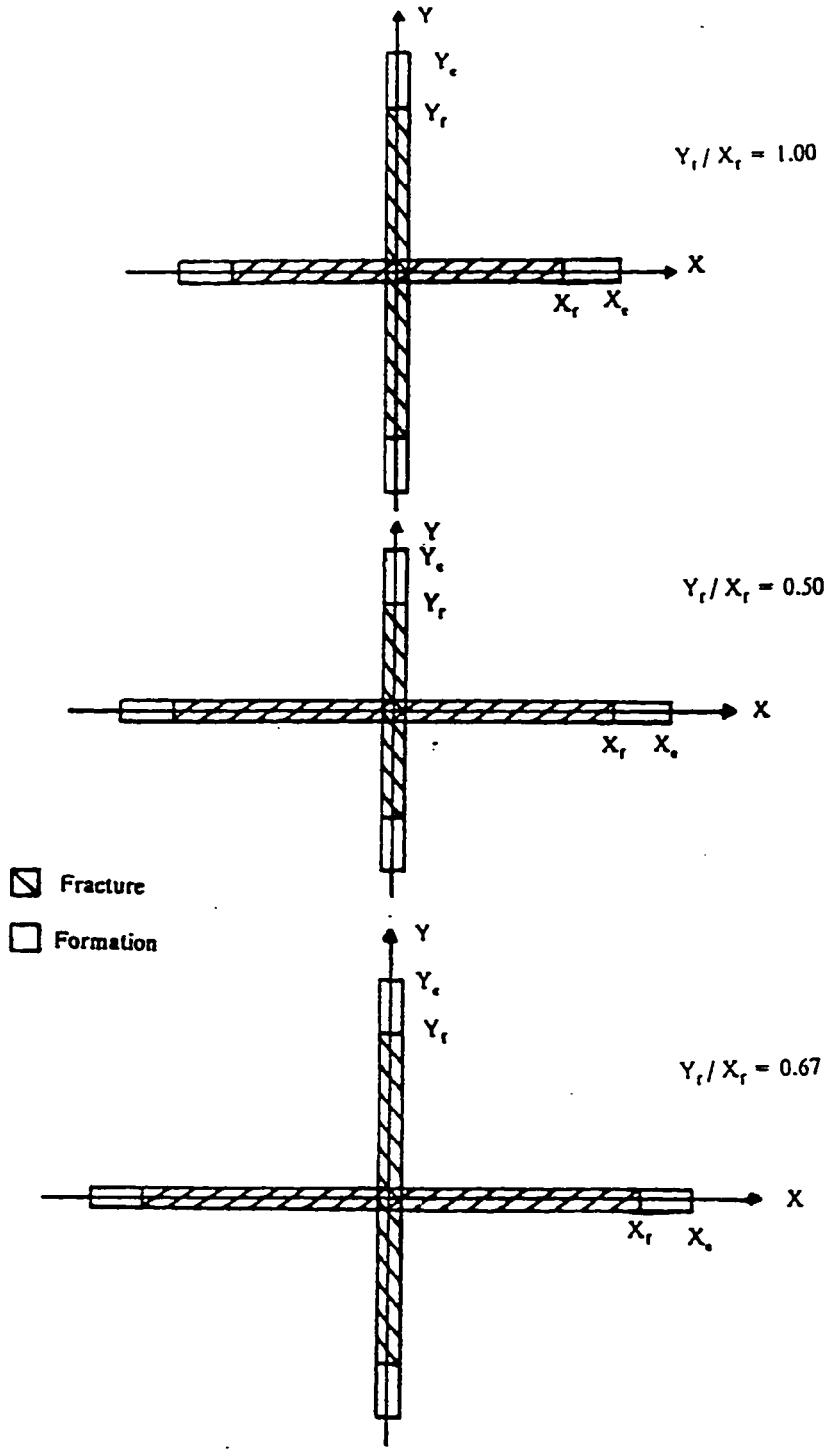

Figure 4.1 : Schematic representation of the two fractures considered in this study .

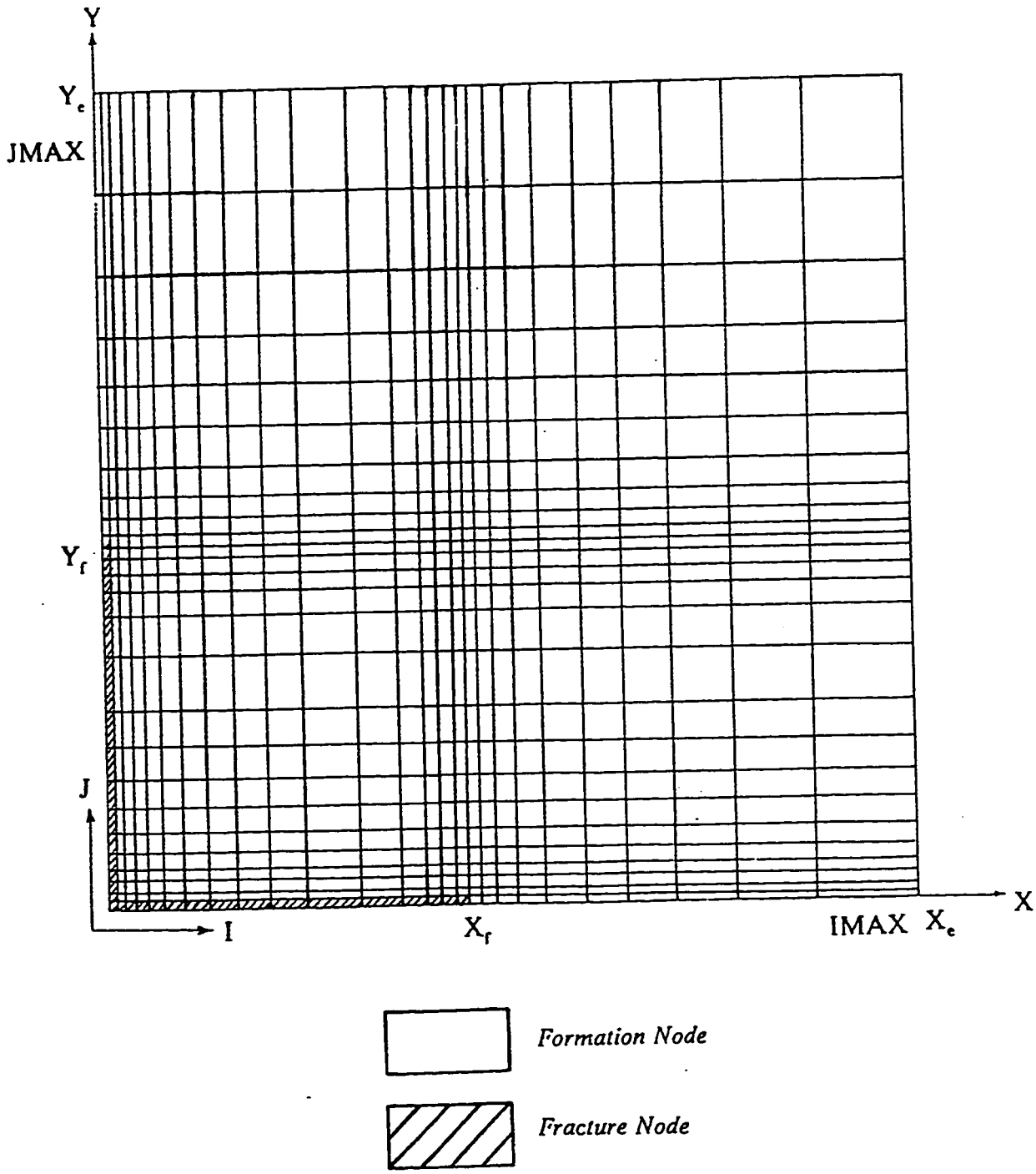

Figure 4.2 : Grid pattern used for modeling the two vertical fractures .

study the effect of y_f / x_f on the performance of gas wells. The drawdown runs were made under constant flow rate for all cases. Model parameters common to all runs are listed in Table 4.1. The grid system used in each case was constructed according to the empirical guidelines suggested by Bennett et al.[19] The determination of the fractures half lengths and formation flow capacities from the proper flow period will be investigated using the methods suggested for the analysis of single vertical fracture . These methods are presented and discussed in the following sections .

4.1 INFINITE CONDUCTIVITY

In a vertically fractured well , the fracture conductivity is defined as :

$$F_{CD} = \frac{k_f w}{k x_f} \tag{4.1}$$

A fracture is said to have an infinite flow conductivity when there is negligible or no pressure drop inside the fracture . Cinco et al. [9] demonstrated that the assumption of infinite fracture conductivity is valid whenever $F_{CD} \geq 300$. The transient flow behavior of a well intersected by an infinite conductivity vertical fracture includes three flow periods [11,14,29]. Initially , there is a fracture linear flow period; after a transition flow period , a formation linear flow occurs; and finally the system reaches a pseudo radial flow period .

4.1.1 Fracture linear flow period

Fracture linear flow behavior occurs at very small values of dimensionless time. During this flow period , most of the fluid entering the wellbore comes from the expansion of the fluid within the fracture and the flow is essentially

TABLE 4.1

Reservoir and Fluid Property Data Common to All Runs.

x_e	3000.0 feet
y_e	3000.0 feet
Flow rate	0.01 MMSCFD
Formation capacity	1.0 md-ft
Gas gravity	0.70 (air = 1.0)
Initial pressure	5000 psia
Reservoir temperature	660°R
Standard temperature	520°R
Standard pressure	14.7 psia
Formation porosity	0.14
Fracture porosity	0.5
Fracture width	0.5 inches
β	0.0

linear [11] . The dimensionless pressure response at the wellbore during this period is given by [11] :

$$p_D = \frac{2}{F_{CD}} \sqrt{\eta_{fD}\, t_{Dxf}} \tag{4.2}$$

This equation indicates that a log-log graph of p_D versus t_{Dxf} yields a straight line whose slope is equal to one half . The end of this flow period has been found to be equal to [11] :

$$t_{Dxf} = \frac{0.01\ F_{CD}^2}{\eta_{fD}^2} \tag{4.3}$$

where ; η_{fD} is the dimensionless fracture hydraulic diffusivity ,

$$\eta_{fD} = \frac{k_f \varphi\, c_t}{k\, \varphi_f\, c_{ft}} \tag{4.4}$$

In this study , this flow period was observed in both single vertical fracture and two fractures systems , but it occurs at a time too small to be of practical use .

4.1.2- Formation linear flow period

In a hydraulically fractured well , where fracture conductivity is high and wellbore storage and damage effects are minimal , early time flow from the formation into the fracture is characterized by a linear flow , and early time pressure data plotted as a function of square root of time fall on a straight line [10, 11] . Millheim and Cicowicz showed that when linear flow dominates in a drawdown test , the pressure time behavior of a gas well is modeled by [3] :

$$m(P_{wf}) = m(P_i) - \frac{40.93\, q_{sc}\, T}{2h\sqrt{\varphi}} \sqrt{1/k\, x_f^2} \sqrt{t_f / \mu c_g} \tag{4.5}$$

During this flow period the dimensionless pressure drop at the well is given by [6,7] :

$$p_D = \sqrt{\pi\, t_{Dxf}} \tag{4.6}$$

Equation (4.6) indicates that a log-log plot of p_D as a function of t_{Dxf} during the formation linear flow period will result in a straight line with a slope equals to one half . Agarwal et al. [10] investigated the applicability of equation (4.5) to MHF wells using two dimensional , single phase (Darcy) finite difference model . As a result of their investigation the following were observed :

1. Early time pressure data for high fracture conductivities ($F_{CD} > 500$) fall on a straight line when plotted as $\Delta(p^2)$ versus $\sqrt{t_f}$
2. The early portion of the log-log plot of $\Delta(p^2)$ versus $\sqrt{t_f}$ revealed a straight line with a slope of one half for infinite conductivity fractures .
3. Early-time data of cartesian plot of p_{WD} versus t_{Dxf} for infinite conductivity fall on straight line passing through the origin , with a slope equals to $\sqrt{\pi}$ or 1.772.

Figures 4.3 through 4.7 present log-log plots of p_D versus t_{Dxf} for different values of y_f / x_f. It should be noted from these figures that the early portion of all the cases presented display the characteristic straight line with a slope of one-half , which is a characteristic feature of formation linear flow period for high fracture conductivity . Figure 4.3 represents the case with $y_f / x_f = 0.0$ (single vertical fracture) . As it can be seen from this case that the duration of the linear flow period agree with Cinco et al's solutions [11] .

It should also be noted from figures 4.3 through 4.7 and Table 4.2 that the

TABLE 4.2

Simulator Results for Infinite Conductivity Linear Flow Period
(F_{CD} = 500)

y_f / x_f	t_{Dblf}	t_{Delf}
0.00	3.46e-4	1.56e-2
0.25	1.62e-4	1.89e-1
0.50	1.62e-4	4.00e-1
0.80	1.62e-4	4.50e-1
1.00	1.62e-4	5.00e-1

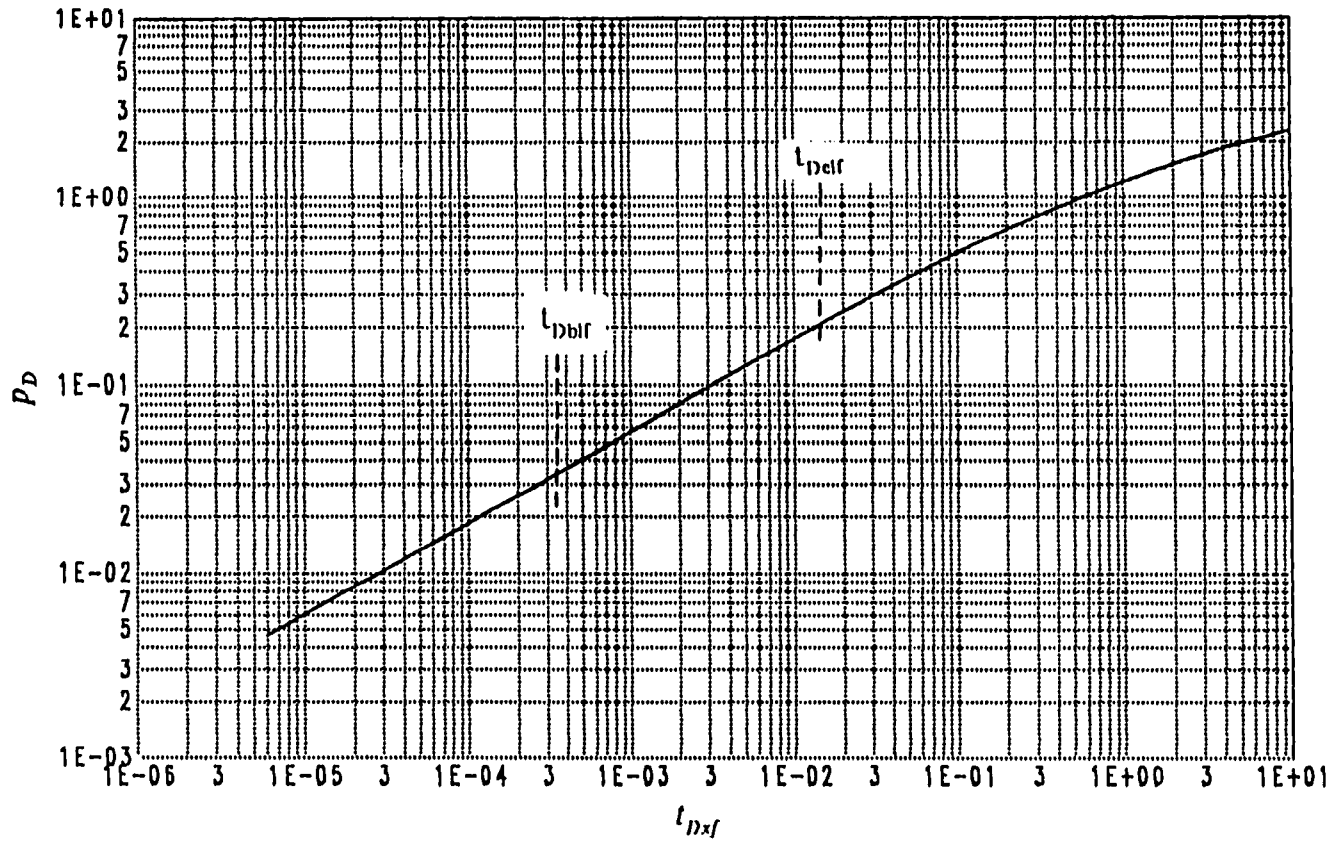

Figure 4.3 : Effect of $y_f / x_f = 0.0$ on the linear flow period ; for a well with infinite conductivity vertical fracture ($F_{CD} = 500$) .

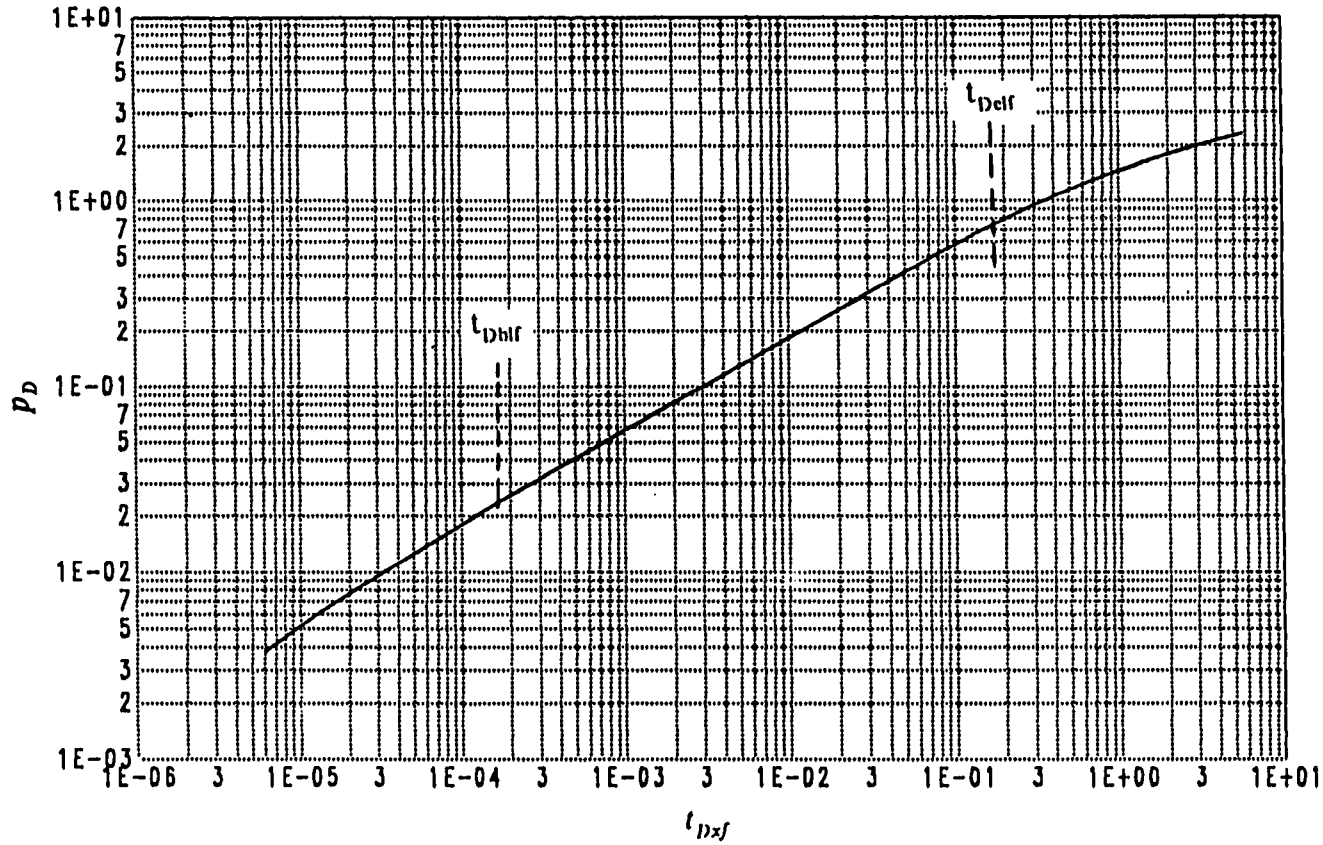

Figure 4.4 : Effect of $y_f / x_f = 0.25$ on the linear flow period ; for a well with infinite conductivities perpendicular fractures ($F_{CD} = 500$) .

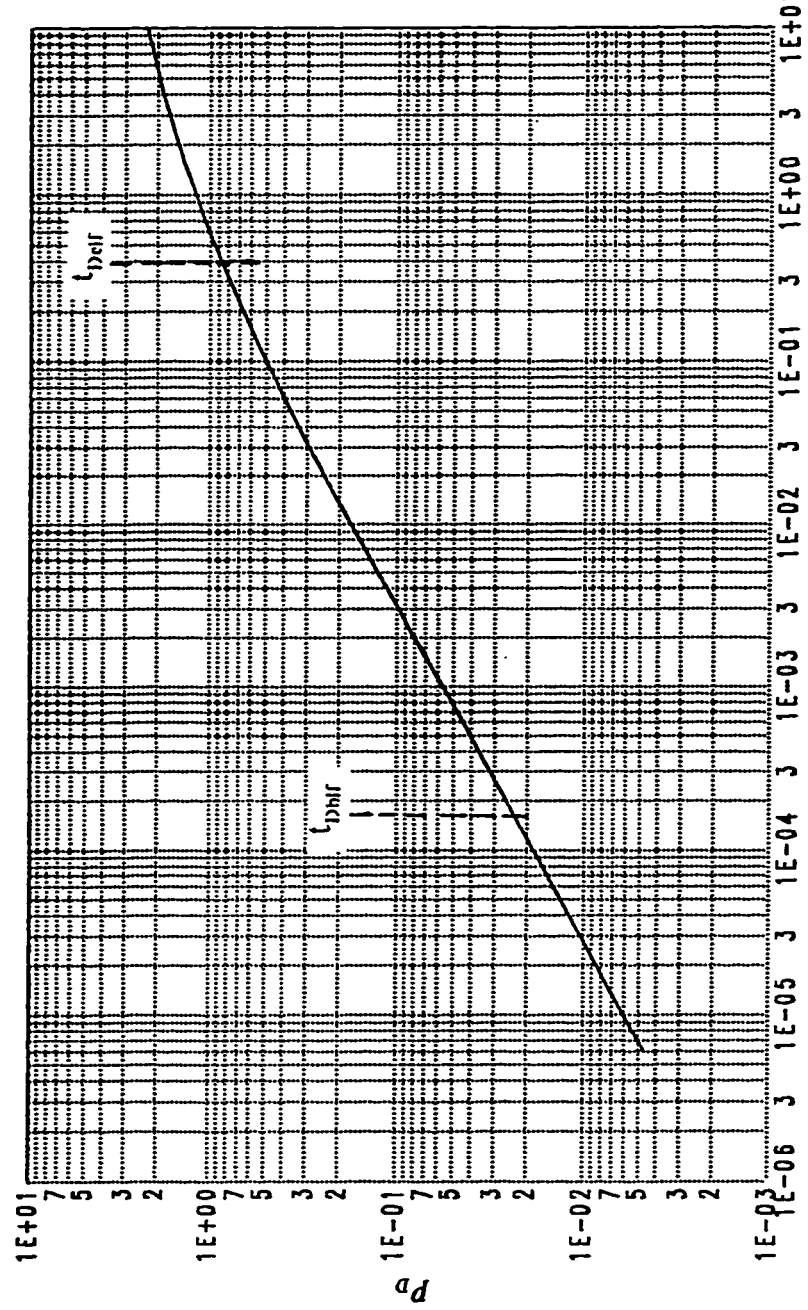

Figure 4.5 : Effect of $y_f / x_f = 0.50$ on the linear flow period ; for a well with infinite conductivities perpendicular fractures ($F_{CD} = 500$) .

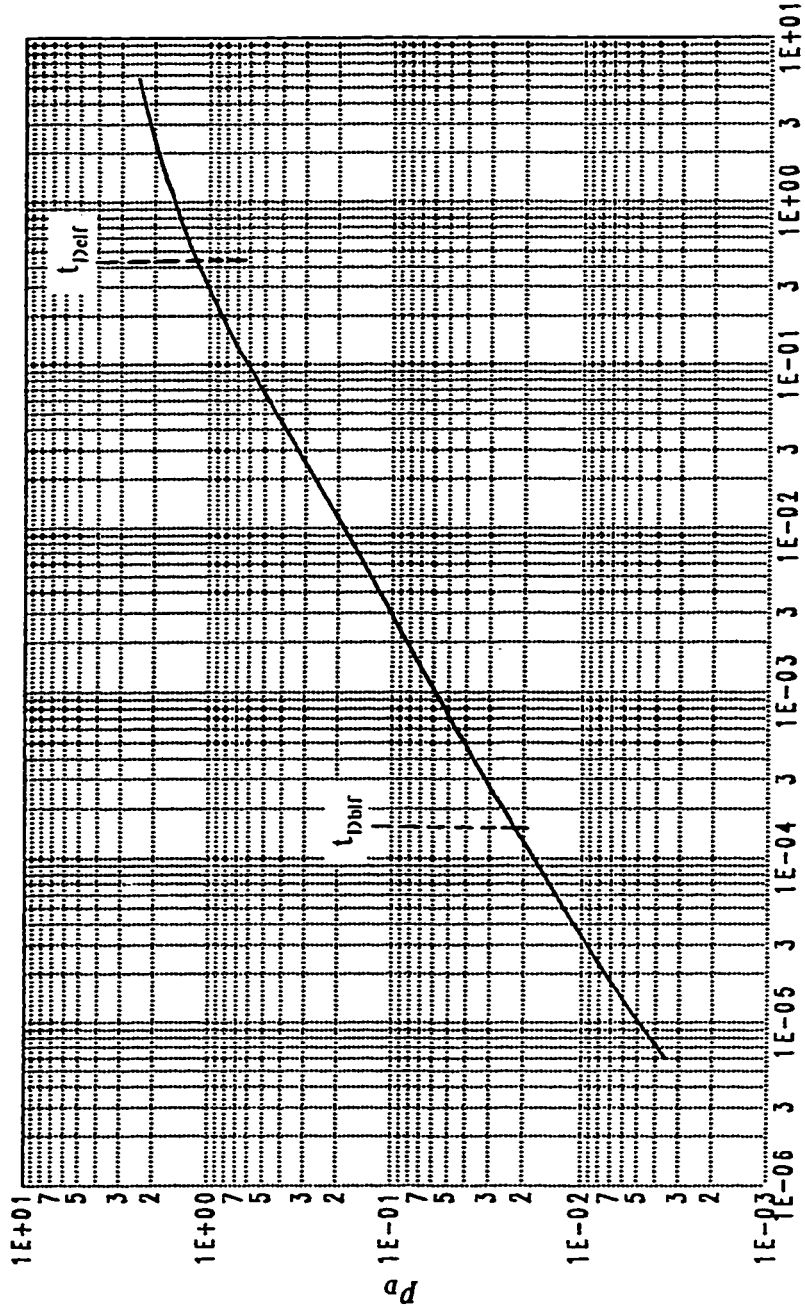

Figure 4.6 : Effect of $y_f / x_f = 0.80$ on the linear flow period ; for a well with infinite conductivities perpendicular fractures ($F_{cD} = 500$) .

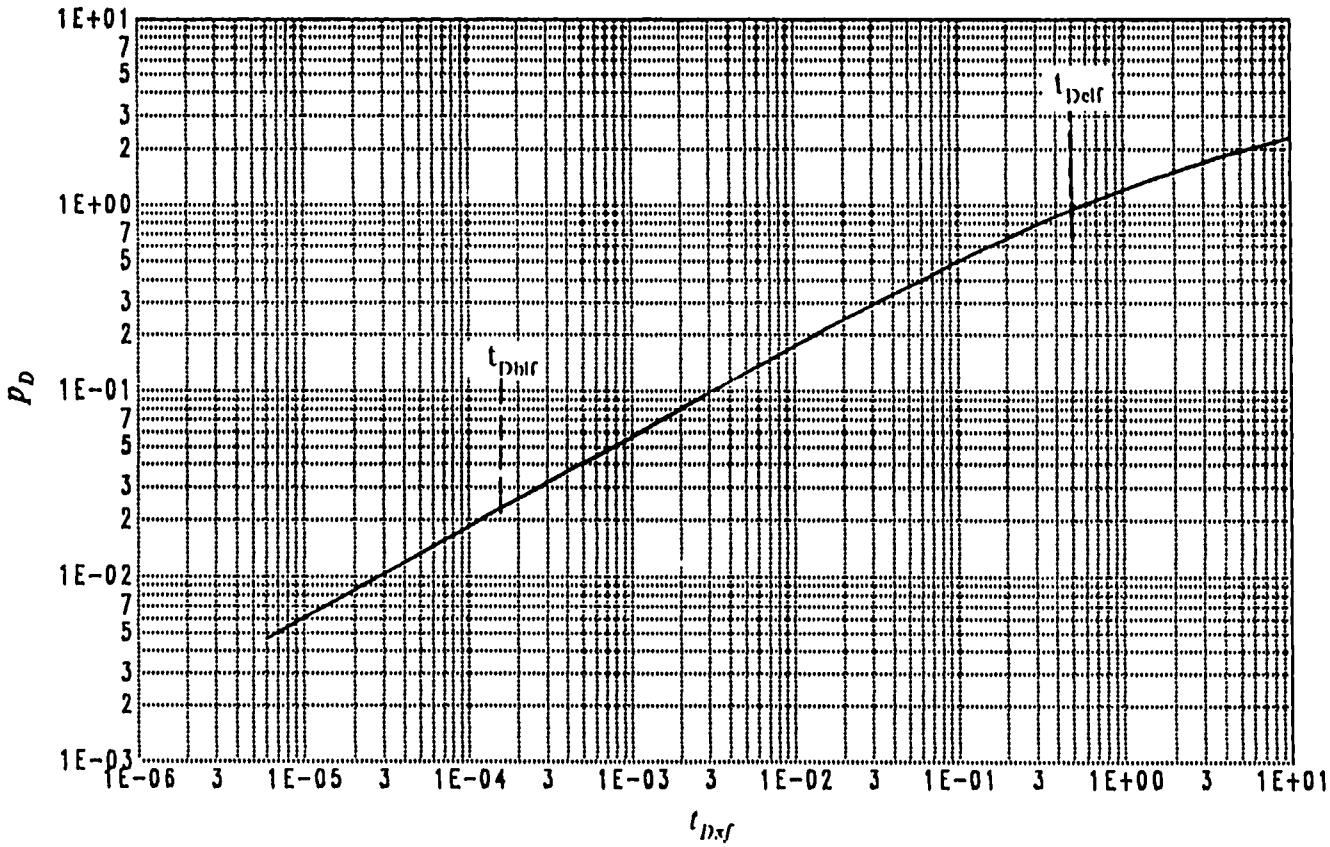

Figure 4.7 : Effect of $y_f / x_f = 1.00$ on the linear flow period ; for a well with infinite conductivities perpendicular fractures ($F_{CD} = 500$) .

duration of the linear flow period increases as the y_f / x_f ratio increases . This is because for highly conductive fractures ($F_{CD} > 500$) the flux density is high at the portions of the fractures away from the wellbore , and approximately two thirds of the total flow entering the wellbore comes from the farthest half of the fractures from the wellbore . As y_f / x_f ratio decrease the effect of the contribution of the fracture in y -direction on the formation linear flow decreases, and the duration of this flow period decreases. The effect of increasing y_f / x_f on the formation linear flow period is similar to the effect of increasing fracture half length (x_f) in case of a single vertical fracture , which was demonstrated by Russell and Truitt [2] . It is interesting to note that the beginning of the formation linear flow period for y_f / x_f ratios greater than zero is the same for all ratios and smaller than that of the single fracture ($y_f / x_f = 0.0$). Figures 4.8 through 4.12 present the dimensionless pressure drop as a function of square root of dimensionless time for the same cases presented in figures 4.3 through 4.7 . It is noted from these figures that the slope of the early time data fall on straight line with a slope of 1.772 , which reflects the linear flow period as indicated by Agarwal et al. [10] and AL-Hashim [14] .

Since the formation linear flow region was defined from log-log plot , the square-root time graph was applied and the fracture half length was evaluated for each y_f / x_f ratio . As a result of this analysis the fracture half length for each case was found to be close to 100 feet (input value). These investigations show that the fracture half length calculated in each case is the sum of the fractures half lengths ($x_f + y_f$) . This indicates that the slope of 1.772 is an indication of formation linear flow in the case of two infinite conductivities perpendicular

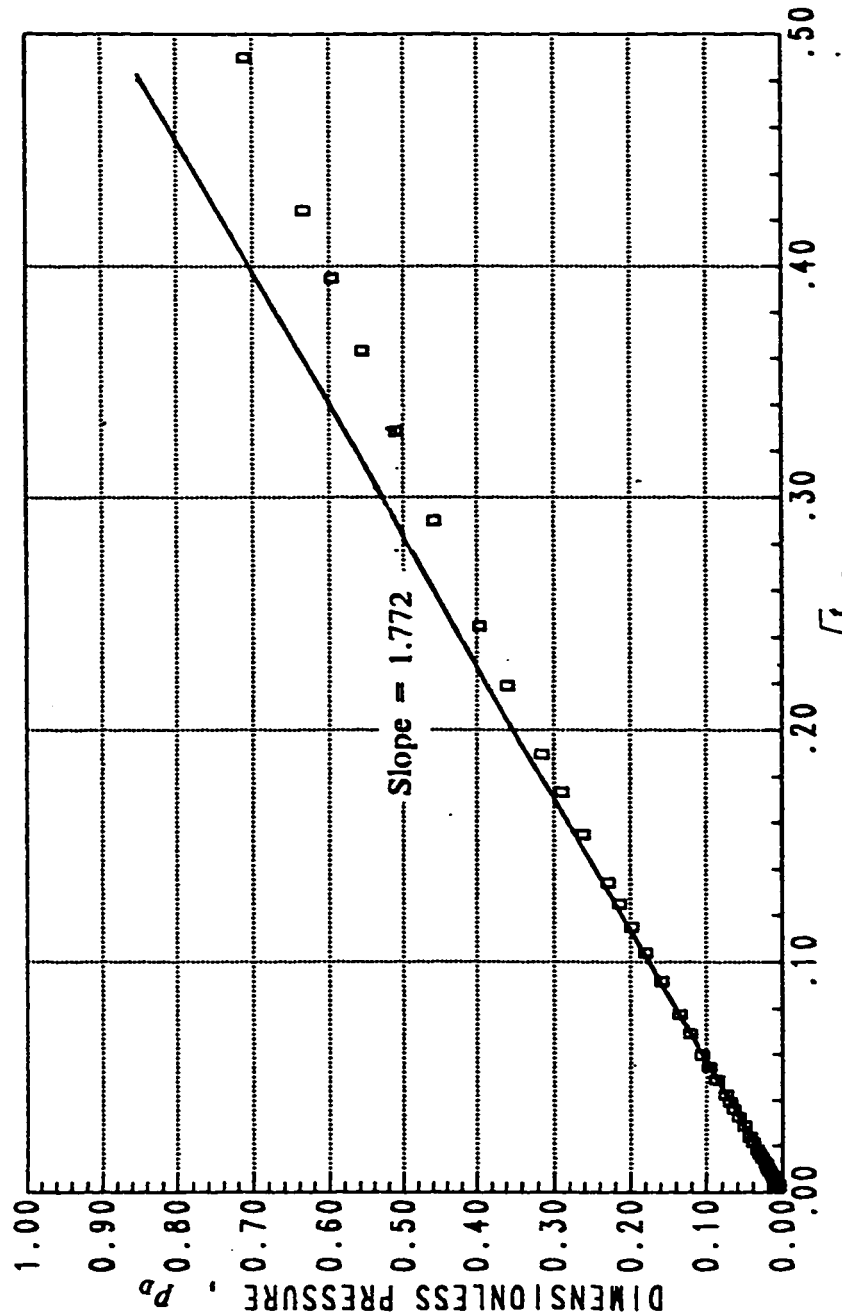

Figure 4.8 : Early time data showing the slope of 1.772 for $y_f / x_f = 0.0$; infinite conductivity case ($F_{cD} = 500$) .

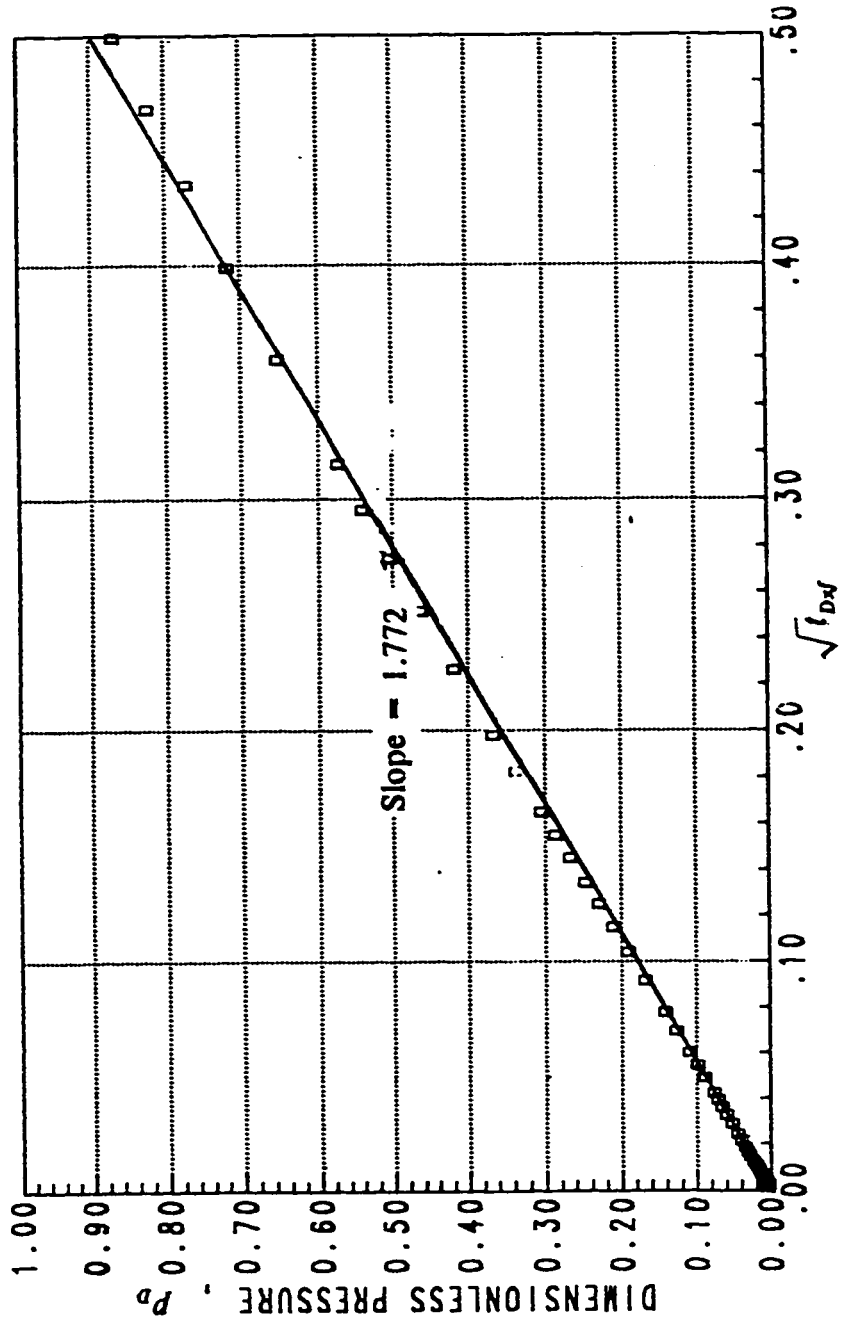

Figure 4.9 : Early time data showing the slope of 1.772 for $y_f / x_f = 0.25$; infinite conductivity case ($F_{cD} = 500$) .

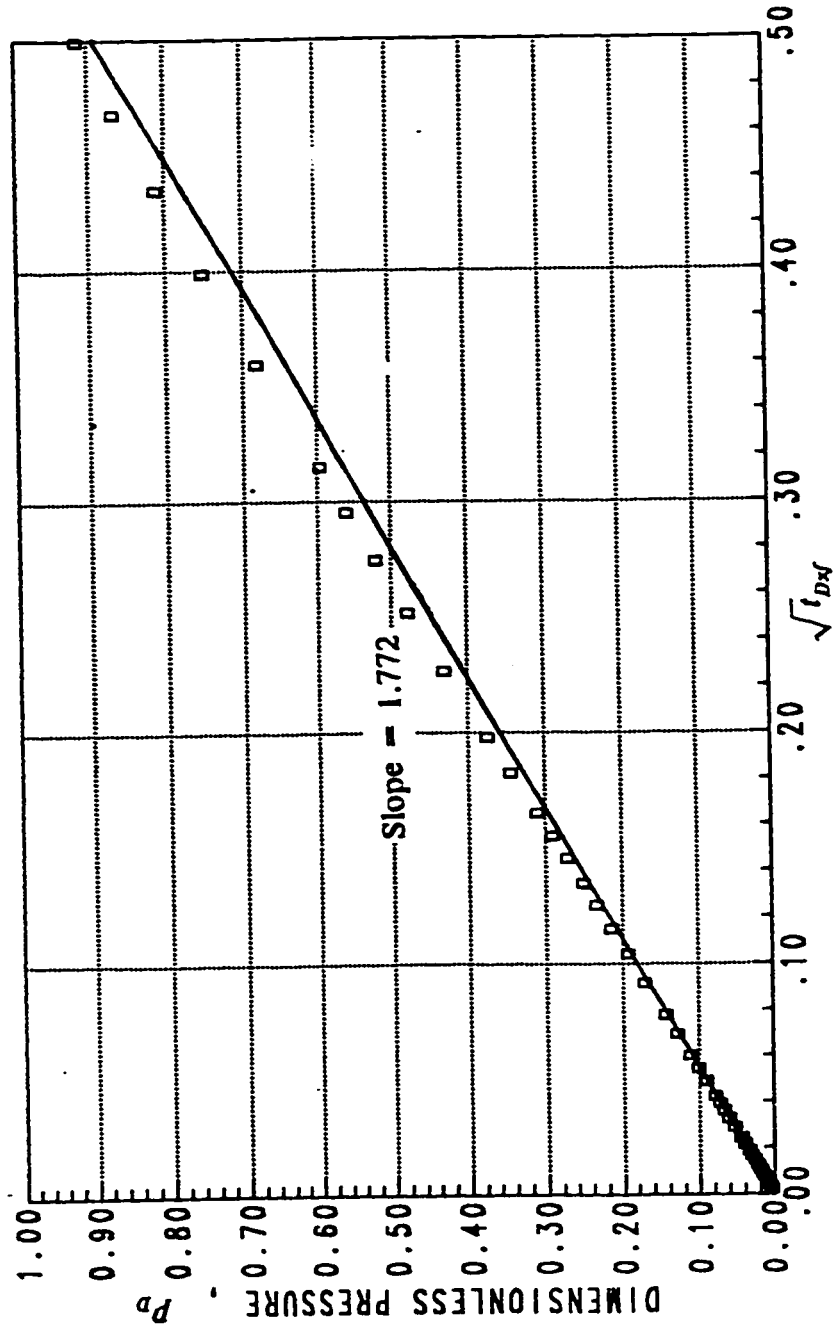

Figure 4.10 : Early time data showing the slope of 1.772 for $y_f / x_f = 0.50$; infinite conductivity case ($F_{CD} = 500$) .

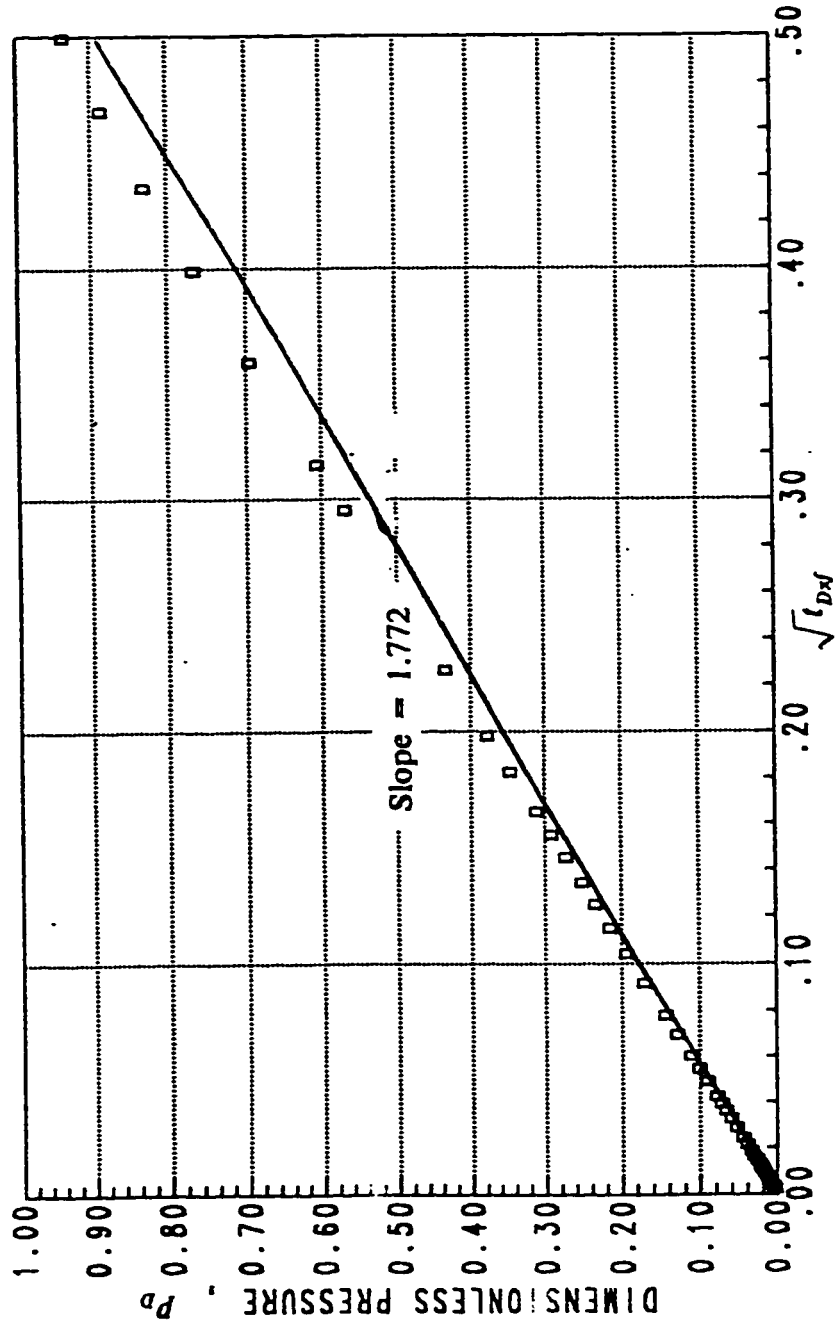

Figure 4.11 : Early time data showing the slope of 1.772 for $y_f / x_f = 0.80$; infinite conductivity case ($F_{CD} = 500$) .

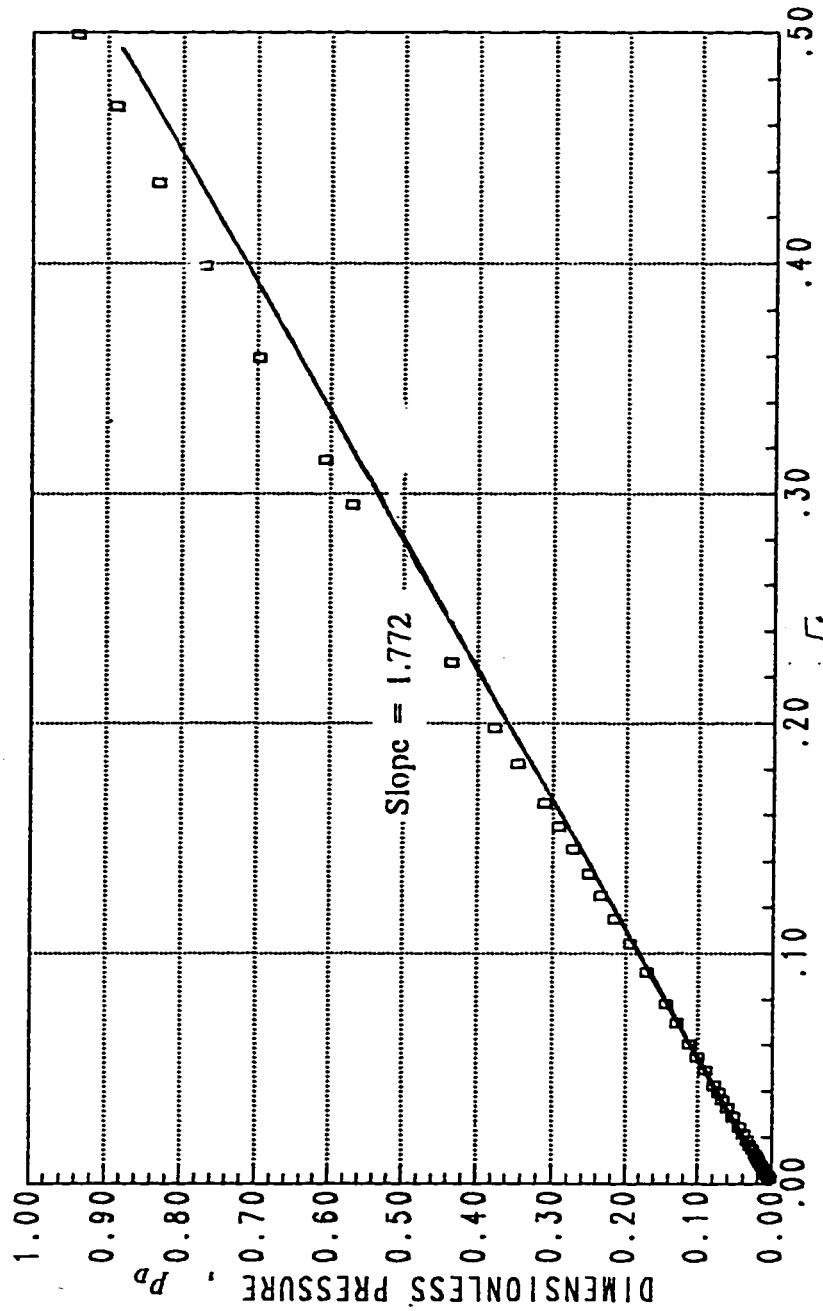

Figure 4.12 : Early time data showing the slope of 1.772 for $y_f / x_f = 1.00$; infinite conductivity case ($F_{cD} = 500$) .

fractures. It should also be noted that the dimensionless time used for the two fractures cases is based on the total half fracture lengths ($x_f + y_f$) .

4.1.3- Pseudoradial flow period

Regardless of the fracture conductivity , a fractured well will reach the pseudoradial flow period eventually provided that the boundary effects do not become significant . This period is recognized by the 1.151/log cycle slope on a semilog graph of dimensionless wellbore pressure drop versus dimensionless time [2] . Cinco et al. [9] observed that this flow period occurs at about $t_{Dxf} \geq 2.5$. Figures 4.13 through 4.17 , and Table 4.3 show that for all y_f / x_f ratios the pseudoradial flow period (1.151/log cycle slope) was developed .

Figure 4.13 presents a case where $y_f / x_f = 0.0$, and the time required for the pseudoradial flow behavior to develop in this case is within the range ($t_{Dxf} = 2.5$ to 5.0) observed by Cinco et al. [9] for infinite conductivity vertical fracture . It is noted from figures 4.13 through 4.18 and Table 4.3 that the time required for the pseudoradial flow behavior to develop decreases as the y_f / x_f ratio increases , and after $y_f / x_f = 0.8$ the starting point for radial flow period is the same as that of $y_f / x_f = 1.0$. It should also be noted that the effect of increasing y_f / x_f ratio on the beginning of pseudoradial flow is similar to that of small fracture penetration x_f / x_e discussed by Russell and Truitt [2] for infinite conductivity vertical fracture .

Figures 4.18 and 4.19 show that as the y_f / x_f ratio increases, the dimensionless pressure drop, at any dimmensionless time greater than

TABLE 4.3

Simulator Results for Infinite Conductivity Pseudoradial Flow Period
(F_{CD} = 500)

y_f / x_f	t_{Dbssl}	t_{fbssl}
0.00	4.191	123.72
0.25	1.036	29.520
0.50	0.900	26.570
0.80	0.700	20.665
1.00	0.700	20.665

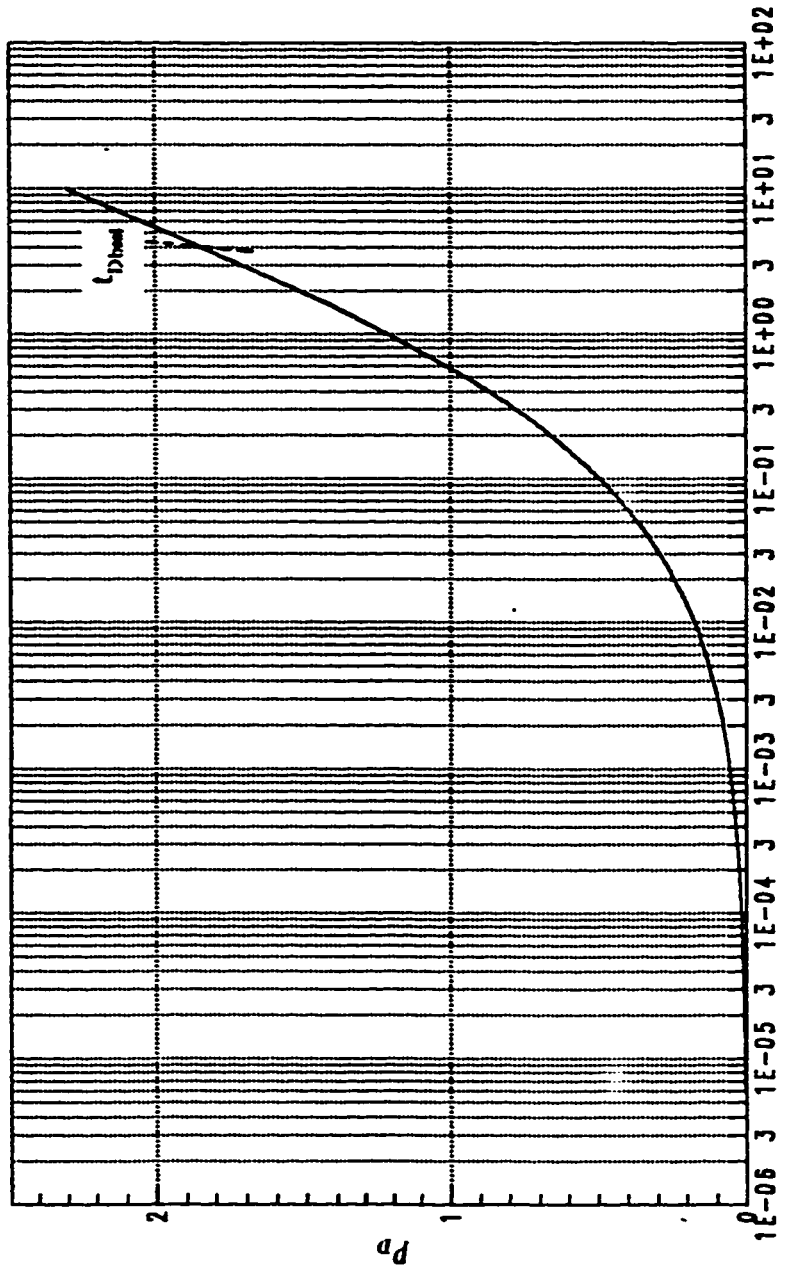

Figure 4.13 : Effect of y_f / x_f = 0.0 on drawdown of real gas ; infinite conductivity case (F_{cD} = 500) .

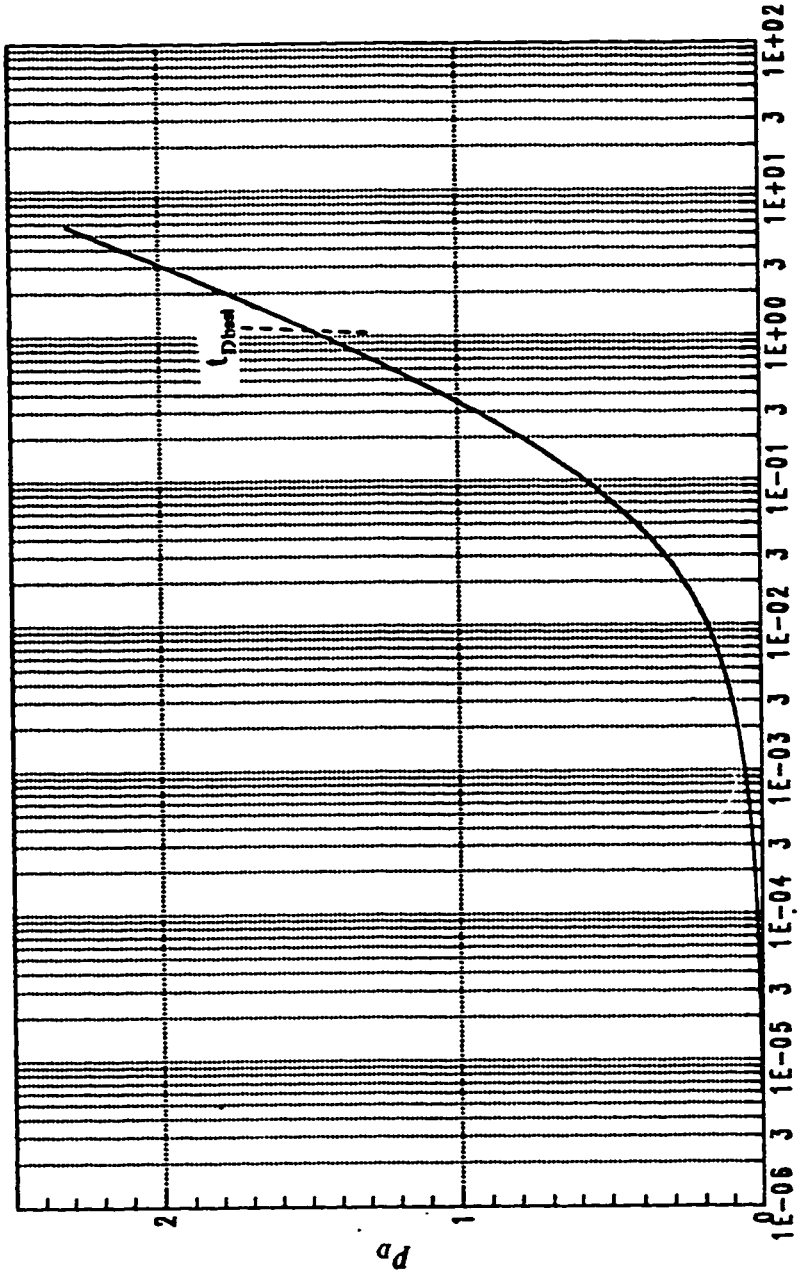

Figure 4.14 : Effect of y_f / x_f = 0.25 on drawdown of real gas ; infinite conductivity case (F_{CD} = 500) .

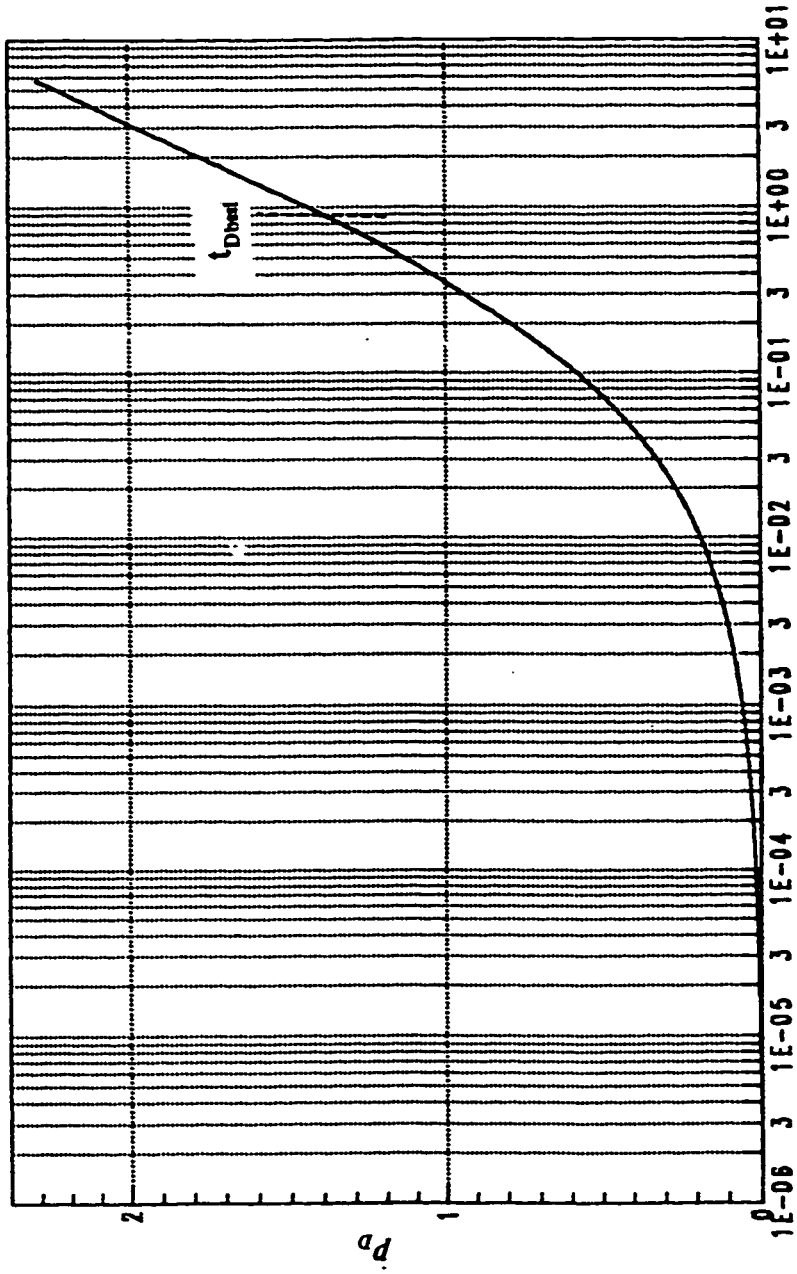

Figure 4.15 : Effect of $y_f / x_f = 0.50$ on drawdown of real gas ; infinite conductivity case ($F_{CD} = 500$) .

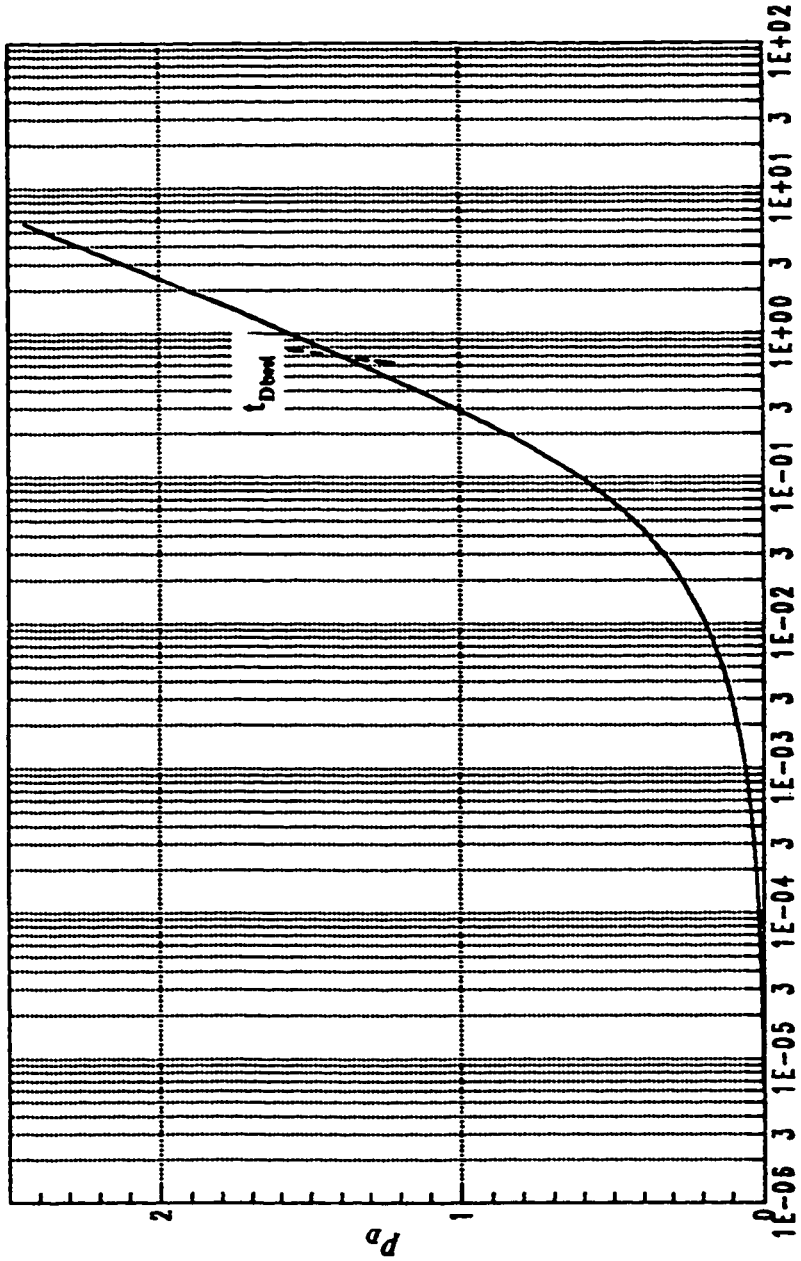

Figure 4.16 : Effect of $y_f / x_f = 0.80$ on drawdown of real gas , infinite conductivity case ($F_{CD} = 500$) .

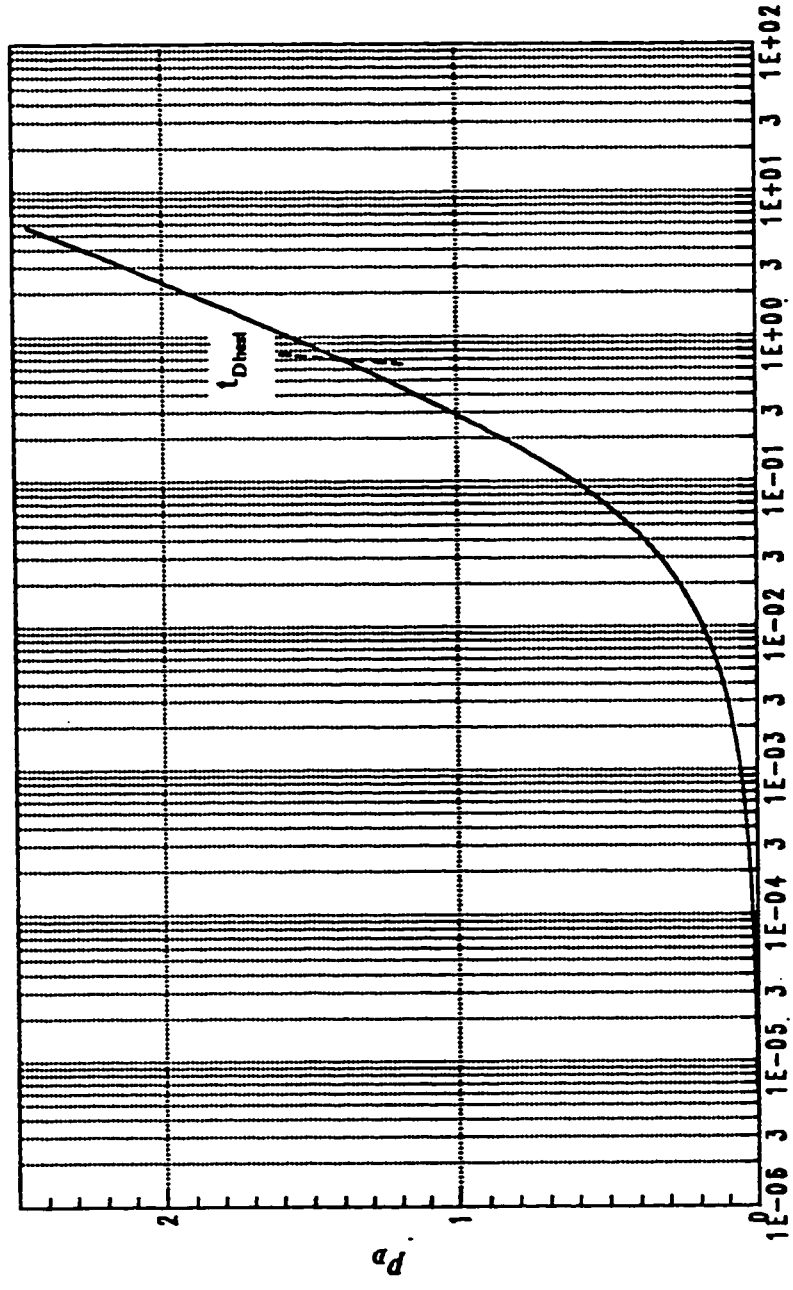

Figure 4.17 : Effect of $y_f / x_f = 1.00$ on drawdown of real gas ; infinite conductivity case ($F_{CD} = 500$) .

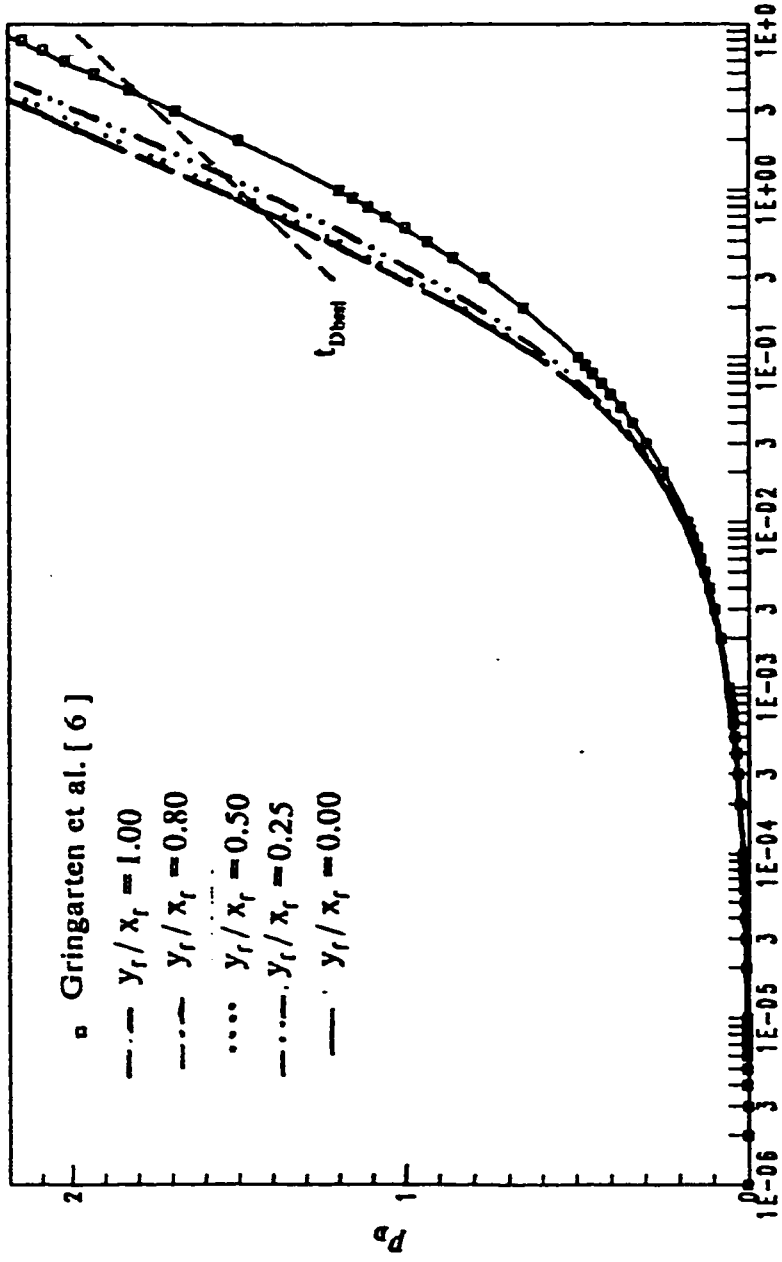

Figure 4.18 : p_D vs. t_{Dxf} showing the effect of y_f / x_f ratios on drawdown of real gas ; infinite conductivity case ($F_{CD} = 500$) .

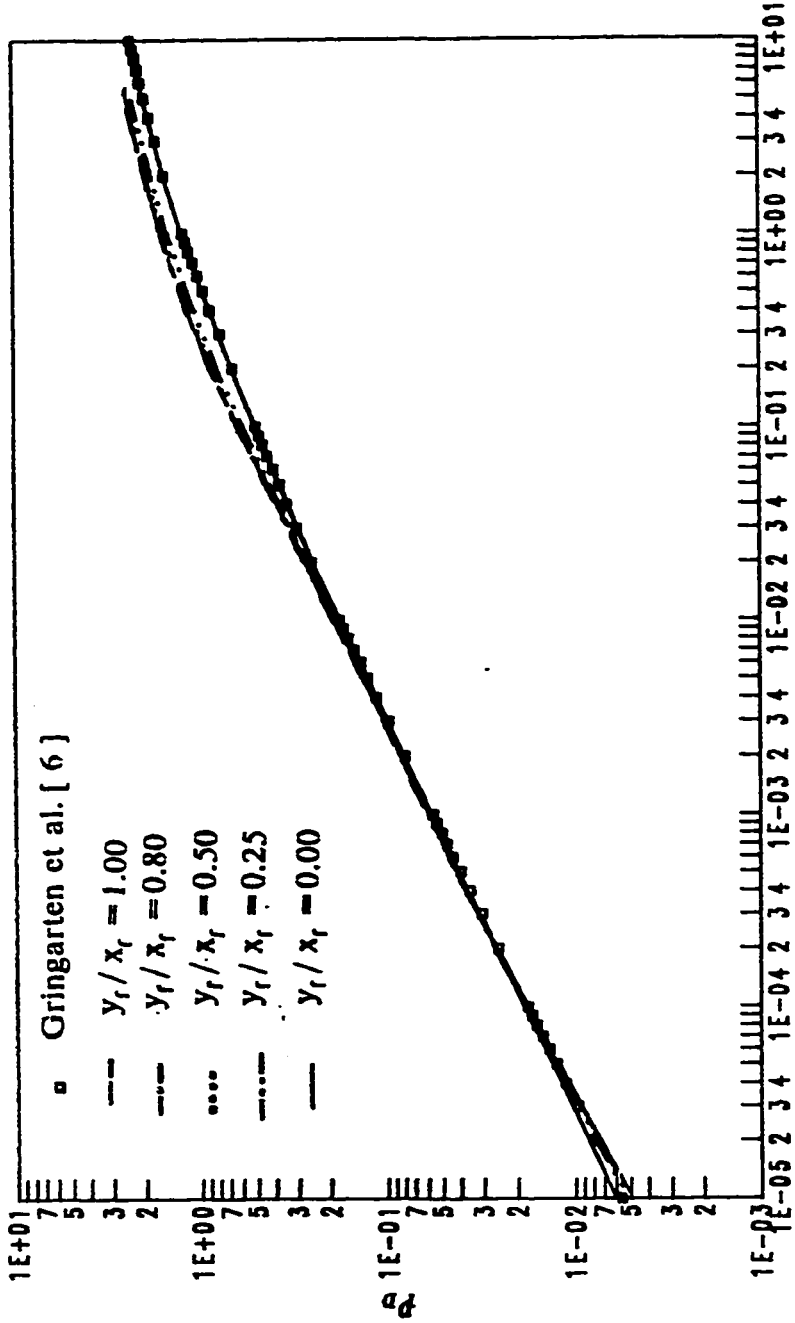

Figure 4.19 : p_D vs. t_{Dxf} showing the effect of y_f / x_f ratios on drawdown of real gas ; infinite conductivity case ($F_{cD} = 500$) .

1.0×10^{-3} , is getting higher and higher, and the highest was observed when $y_f / x_f = 1.0$. This indicates that the productivity of the well intersected by multiple fractures will be less than that of the same well if it is intersected by a single vertical fracture in the case of infinite conductivity fractures.

4.2 FINITE CONDUCTIVITY

Cinco et al. [9] demonstrated that the assumption of infinite fracture conductivity is valid whenever the dimensionless fracture conductivity (F_{CD}) is greater than or equal to 100π . All other cases, such as those represented by long or poorly conductive fractures, should be analyzed by considering a finite conductivity fracture. [11] A fracture is said to have a finite conductivity when there is a significant pressure drop along its axis [10] . In the case of finite conductivity fracture ($F_{CD} < 500$) , it has been found that the pressure transient behavior of such a well exhibits early time linear flow in the fracture , intermediate time bilinear flow and late time pseudoradial flow periods [11,19,29] .

For the finite conductivity case , several sets of computer runs were made for different y_f / x_f ratios (using data of Table 4.1 with $F_{CD} = 0.2\pi$) . As a result of this investigation , it was found that for $y_f / x_f = 0.5$ and 0.8 , the results were the same as those for $y_f / x_f = 1.0$. Using $F_{CD} = \pi$ and 10π , it was found that $y_f / x_f = 0.1$ and $y_f / x_f = 0.25$ essentially produced the same results ; and for $y_f / x_f = 0.50$, 0.8 and 1.0 the results were also essentially identical .

4.2.1 Fracture linear flow period

This behavior occurs at very small values of dimensionless time , and it is exhibited by finite and infinite conductivity vertical fractures . Wilkinson [29] showed that the dimensionless pressure response at the wellbore during the linear flow period inside the fracture is given by :

$$p_{wD} = 2 \sqrt{\eta_{fD} t_{Dxf} / \pi} \tag{4.7}$$

In theory , this flow period exists , regardless of the value of η_{Df}, though in practice its duration is very short and its effect will be masked by wellbore storage [11,29]. In this study (in case of finite conductivity), for $y_f / x_f = 0.0$ this behavior observed at very small time to be of practical use and will not be investigated .

4.2.2 Bilinear flow period

Bilinear flow is defined as the period where two linear flows occur simultaneously . One flow is a linear incompressible flow within the fracture and the other is a linear compressible flow in the formation . A bilinear flow exists , whenever most of the fluid entering the wellbore comes from the formation and fracture tip effects have not yet affected the well behavior [11] . The dimensionless wellbore pressure for the bilinear flow period is given by [11,29] :

$$p_{wD} = \frac{2.45}{\sqrt{F_{CD}}} t_{Dxf}^{1/4} \tag{4.8}$$

This equation indicates that a graph of p_{wD} versus $t_{Dxf}^{1/4}$ produces a straight line whose slope is $2.45 / \sqrt{F_{CD}}$, passing through the origin from which the fracture conductivity can be estimated . It also indicates that a log-log graph of p_{wD}

versus t_{Dxf} yields a straight line with a slope of 0.25 that can be used as diagnostic tool for bilinear flow identification .

The end of the bilinear flow depends on the fracture conductivity and may be expressed by [11]:

$$t_{Debf} \approx \frac{0.1}{F_{cD}^2} \quad , \text{for} \quad F_{CD} \geq 3 \tag{4.9}$$

$$t_{Debf} \approx 0.0205\{(F_{CD}) - 1.5\}^{-1.53} \quad , \text{for} \quad 1.6 \leq F_{CD} \leq 3 \tag{4.10}$$

and

$$t_{Debf} \approx \{\frac{4.55}{\sqrt{F_{CD}}} - 2.5\}^{-4} \quad , \text{for} \quad F_{CD} \leq 1.6 \tag{4.11}$$

4.2.3 Pseudoradial flow period

The pseudoradial flow period is characterized by a semilog relationship between the dimensionless wellbore pressure and dimensionless time , which can be expressed as [22,29]:

$$p_D = \frac{1}{2}[\ln(t_{Dxf}) + 4\ln(2) + \gamma] \tag{4.12}$$

Equation 4.12 indicates that if p_D is plotted versus log t_{Dxf}, then a slope of 1.151/log cycle will be visible .

Figures 4.20 to 4.22 present log-log plot of p_D versus t_{Dxf} for different cases having different conductivities and y_f / x_f ratios, and figures 4.23 to 4.25 show the semilog plot of p_D versus t_{Dxf} for the same cases presented in figures 4.20 to 4.22. Cinco solution for the single fracture ($y_f / x_f = 0.0$) is also presented in the above figures for comparison purposes.

Several remarks are to be noted from these figures :

1. At early times, the pressure drops, p_D, calculated for the cases where y_f / x_f are greater than zero were lower than those for single fracture ($y_f / x_f = 0.0$) as can be seen from figures 4.20 to 4.22, and the slopes observed during this time are higher than the characteristic slope of the bilinear flow period for finite conductivity fractures (0.25 slope). This indicates that the bilinear flow period will not be observed in the case of finite conductivity multiple fracture system, and that, the technique presented to analyze data for vertically fractured well in the bilinear flow period can not be used for the two fractures system.
2. The pressure drop continued to be lower than that of the single fracture for the time investigated when the fracture conductivity is equal to 0.2π as can be seen from figures 4.20 and 4.23. This indicates that very low conductivity multiple fractures are better than one single fracture of the same conductivity and total length.
3. When the fracture conductivity increased from 0.2π to π and then to 10π the calculated pressure drop were found to increase to values higher than the single fracture cases after some time. This time was found to be a function of fracture conductivity where it decreases as the fracture conductivity increases as can be seen from figures 4.21 , 4.22 , 4.24 and 4.25.
4. When the system reaches the pseudoradial flow behavior all cases showed a constant slope of 1.151 / log cycle with a shift in the level of pressure drop during this period as can be noted from figures 4.23 to 4.25. This indicates that as the fracture conductivity increases, the pressure drops at the well intersected by the multiple fractures will be higher in short time and

consequently the productivity of the well will decrease. This behavior can be explained by the fact that most of the fluid produced through the well comes from the furthest half of the fracture when the fracture conductivity is high. On the other hand when the fracture conductivity is low the fluid comes from the closest half of the fracture and as a result of this a fluid competion takes place causing the pressure drop to be lower than that entering the wellbore through the first half of a single fracture.

5. Figures 4.23 through 4.25 present drawdown cases to show the effect of fractures half lengths ratio , on the evaluation of the formation flow capacity $k\,h$. As it can be seen from these figures and Tables 4.4 and 4.5 that the pseudoradial flow period was developed in all cases , so that the formation flow capacity calculated in each case using semilogarithmic pressure analysis method was essentially equal to 1.0 (the input value) . This indicates that the slope of 1.151/log cycle is a characteristic slope of the pseudoradial flow period for the different y_f / x_f ratios considered . It is also noted that from all the cases presented in figures 4.23 through 4.25 that , if the well had not been produced for more than t_{Dbssl} (beginning of semilog straight line) given in Tables 4.4 and 4.5 an erroneous value of the slope will be used , and an optimistic value of formation permeability will be computed.

Figures 4.26 and 4.27 present log-log plot of p_D versus t_{Dxf} for $y_f / x_f = 0.25$ and 1.0 , for different fractures conductivities. Figures 4.28 and 4.29 show the semilog plot of p_D versus t_{Dxf} for the same cases presented in figures 4.26 and 4.27. From these figures the following remarks are to be noted:

1. The one quarter slope does not exist in all cases presented, and at small values of dimensionless time the curves have a distinct form for different

values of F_{CD} , as it can be seen from figures 4.26 and 4.27 .

2. As the fracture conductivity increases for a given y_f / x_f ratio, the system behaves as the single fracture system showing a decrease in the pressure drop as can be seen from figures 4.26 and 4.27. It should also be noted that, the effect of increasing fracture conductivity at a given y_f / x_f ratio on the transient behavior of gas well is similar to the effect of increasing fracture conductivity on the transient behavior of vertically fractured wells.
3. Figures 4.28 and 4.29 show the effect of varying the conductivity on the pressure performance of the gas well for y_f / x_f ratios of 0.25 and 1.0 respectively. From these figures , it can be seen that the time required for the pseudoradial flow period to develop increases with increasing the fractures conductivities and it is maximum for F_{CD} = 500 (infinite conductivity) . These results are consistent with Cinco et al. [9] conclusion for hydraulically fractured wells . They pointed out that the approximate start of the semilogarithmic straight line is a function of F_{CD}, as the fracture conductivity increases the time required for the pseudoradial flow to develop increases .

TABLE 4.4

Simulator Results for Finite Conductivity Pseudoradial Flow Period
($F_{CD} = 0.2\pi$)

y_f / x_f	t_{Dbssl}	t_{fbssl}
0.00	2.700	79.710
0.10	2.000	59.043
0.25	0.750	22.141
1.00	0.550	16.240

TABLE 4.5

Simulator Results for Finite Conductivity Pseudoradial Flow Period
($F_{CD} = \pi , 10\pi$)

y_f / x_f	$t_{Dbssl}(F_{CD}=\pi)$	$t_{fbssl}(F_{CD}=\pi)$	$t_{Dbssl}(F_{CD}=10\pi)$	$t_{fbssl}(F_{CD}=10\pi)$
0.00	2.900	85.612	3.000	88.565
0.25	0.950	28.045	1.000	29.512
1.00	0.650	19.189	0.700	20.665

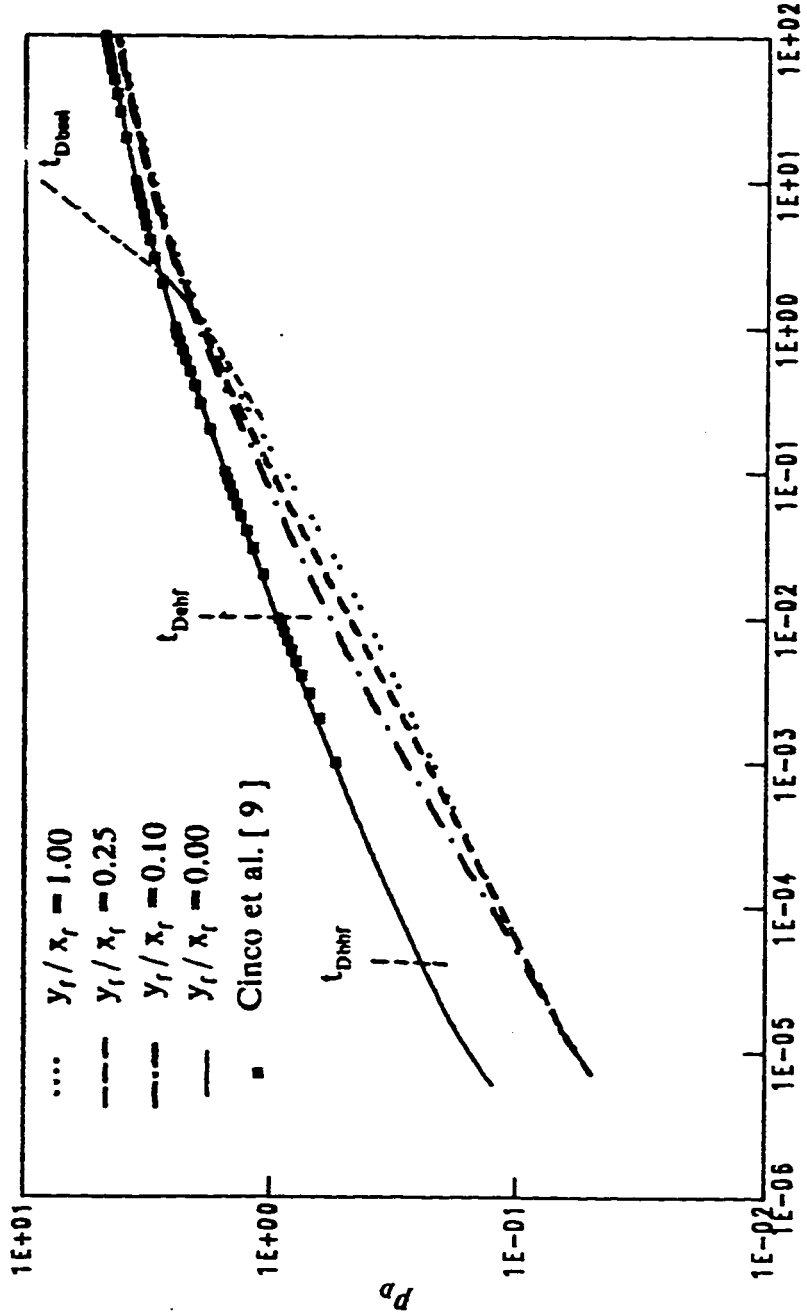

Figure 4.20 : Log-Log graph showing the effect of y_f / x_f ratios on drawdown of real gas ; finite conductivity case ($F_{CD} = 0.2\,\pi$).

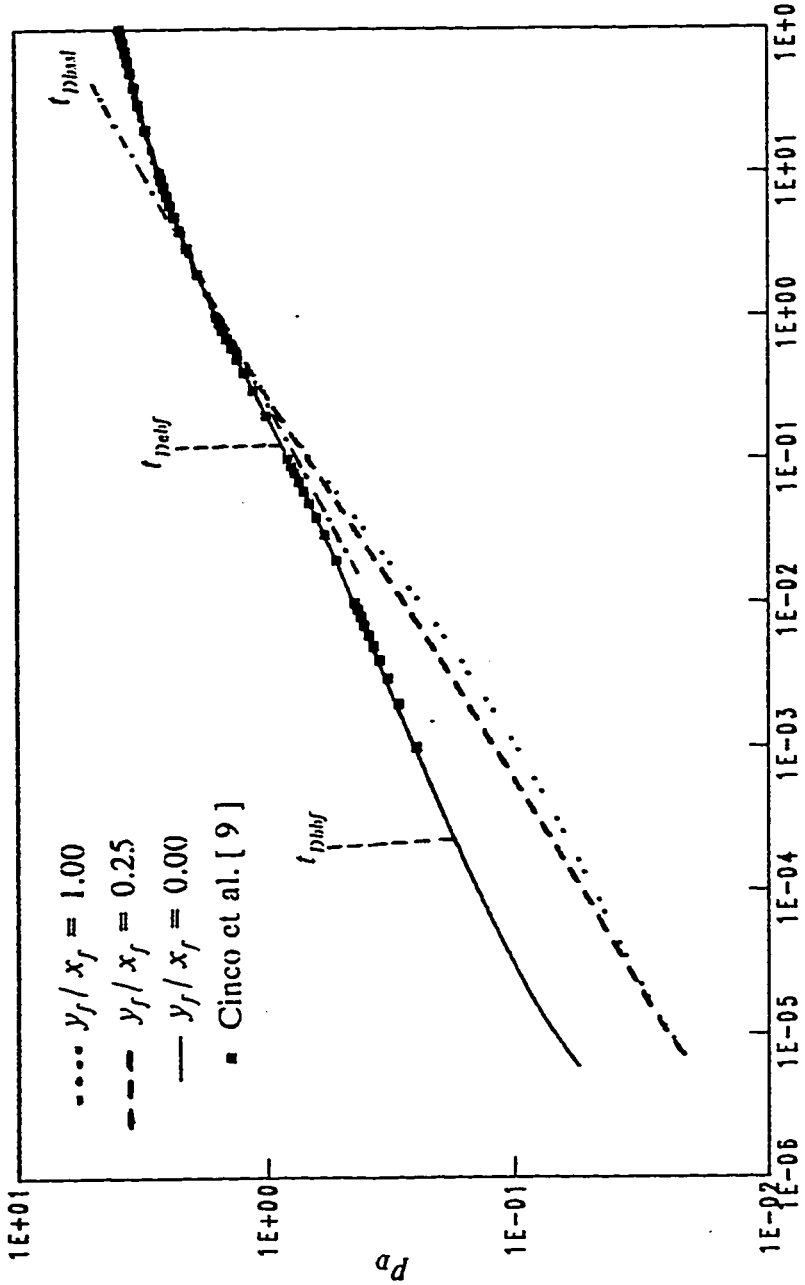

Figure 4.21 : Log-Log graph showing the effect of y_f / x_f ratios on drawdown of real gas ; finite conductivity case ($F_{cD} = \pi$) .

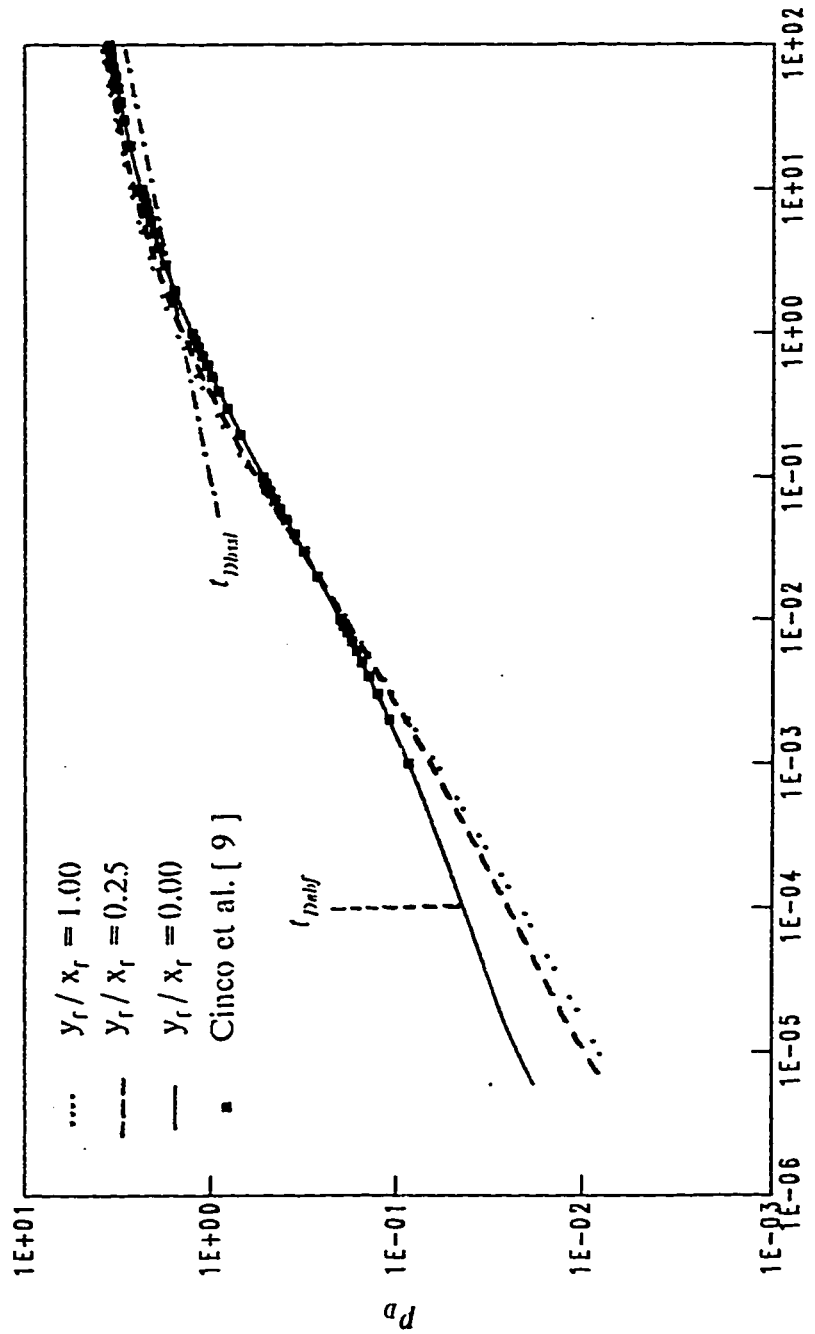

Figure 4.22 : Log-Log graph showing the effect of y_f / x_f ratios on drawdown of real gas ; finite conductivity case (F_{CD} = 10.0 π) .

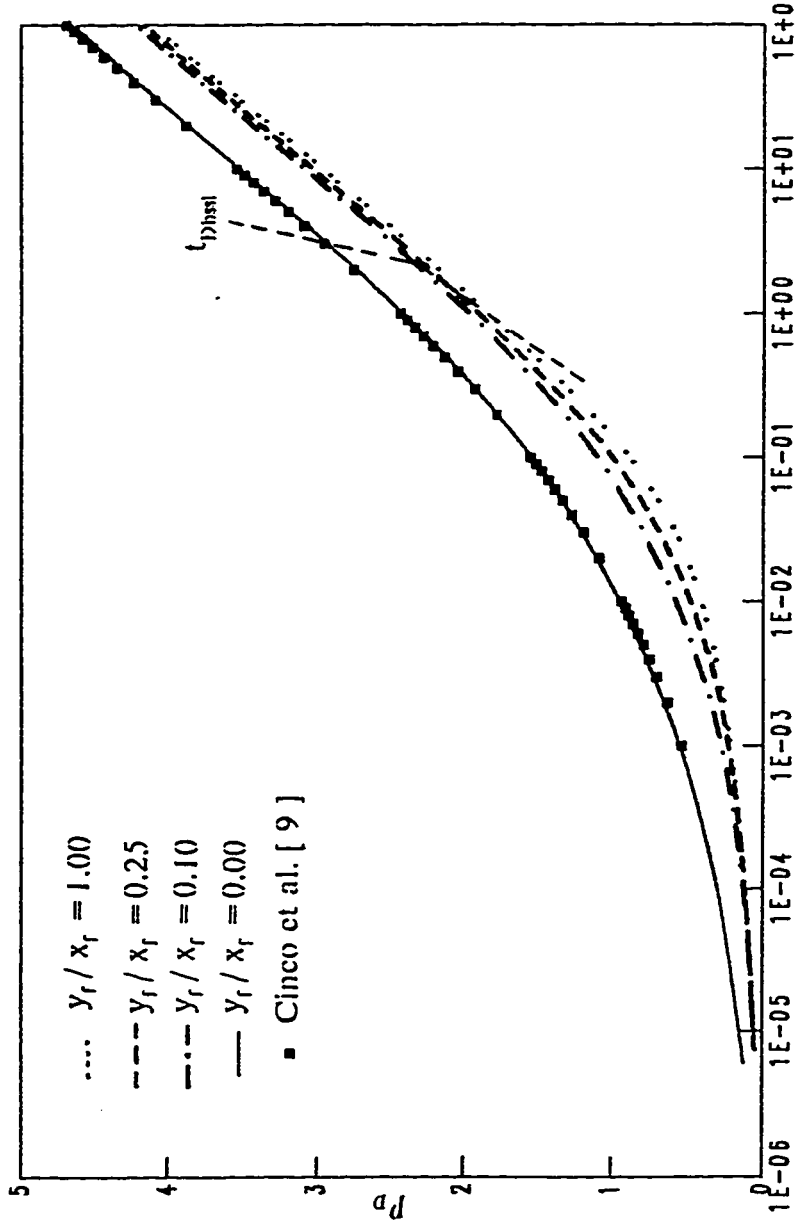

Figure 4.23 : p_D vs. t_{Dxf} showing the effect of y_f / x_f ratios on drawdown of real gas ; finite conductivity case ($F_{cD} = 0.20\ \pi$) .

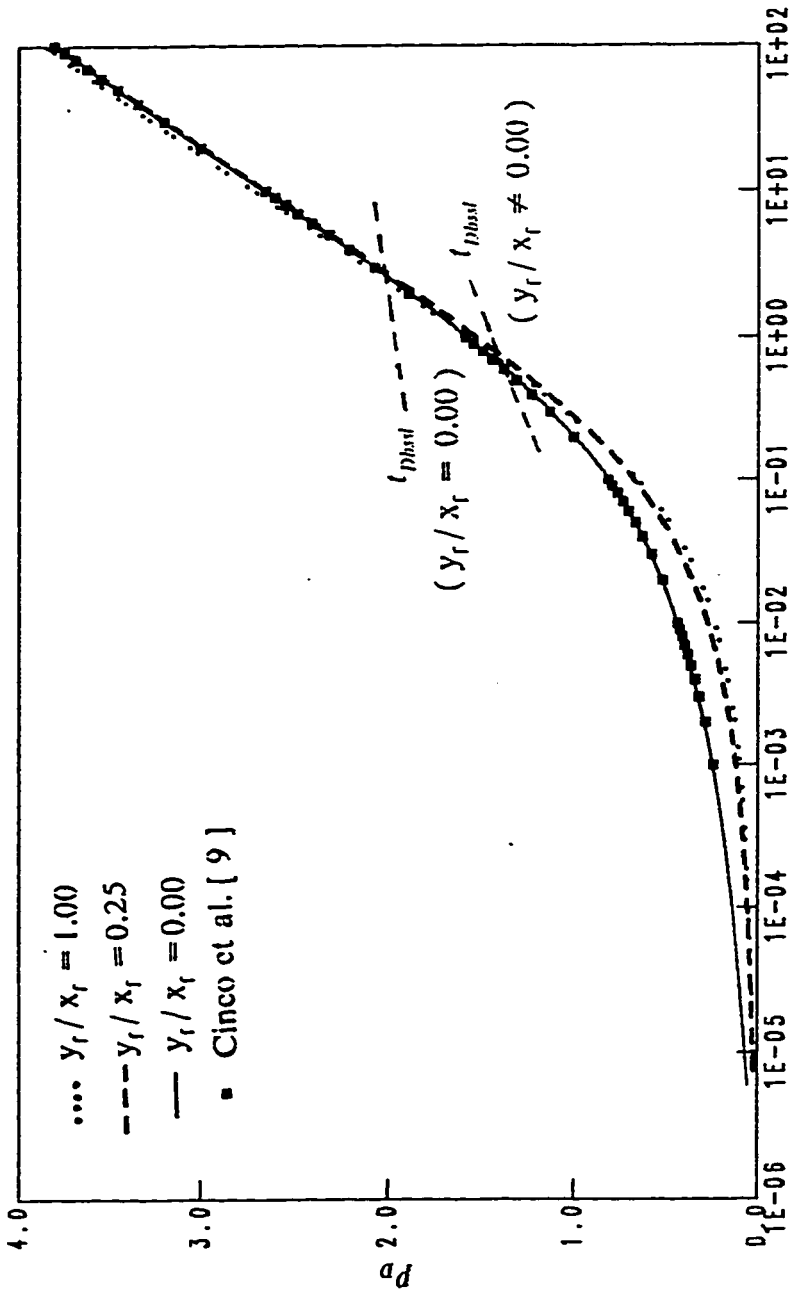

Figure 4.24 : p_D vs. t_{Dxf} showing the effect of y_f / x_f ratios on drawdown of real gas ; finite conductivity case ($F_{CD} = \pi$).

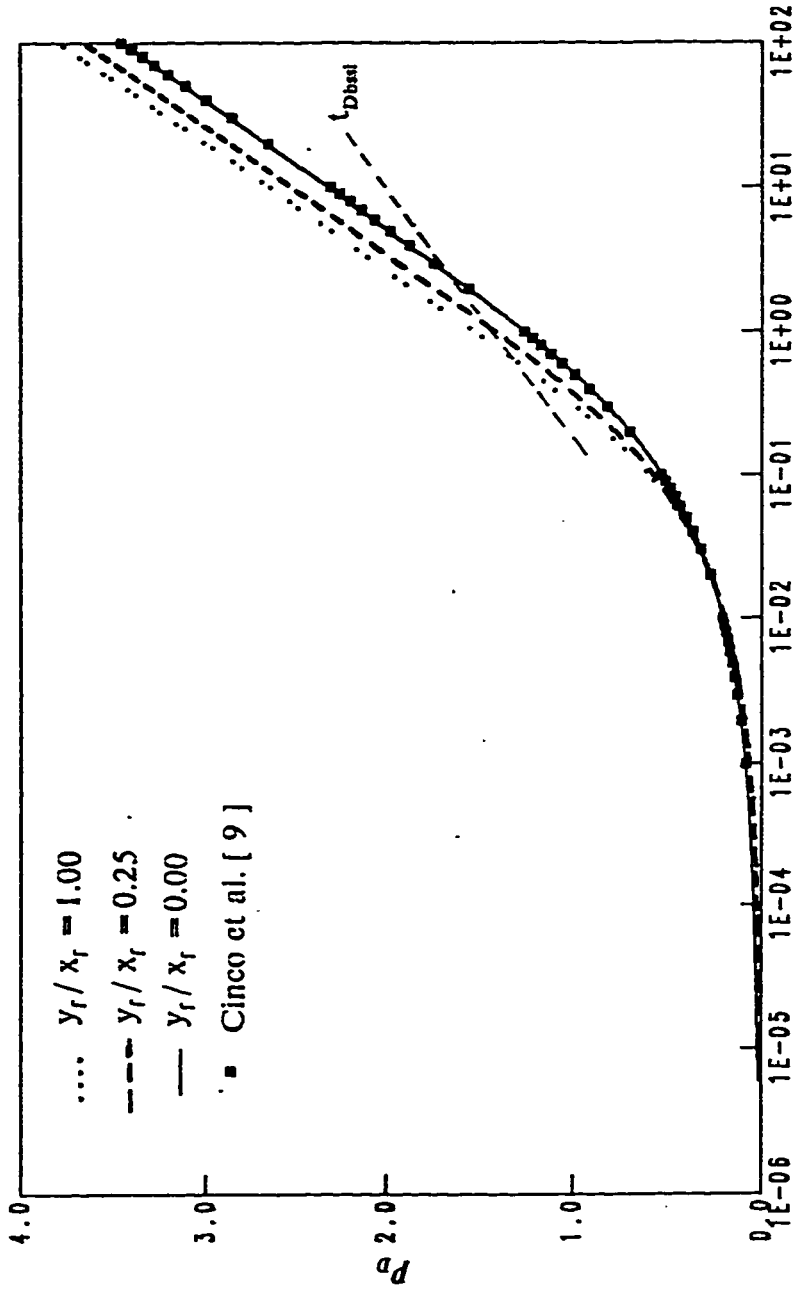

Figure 4.25 : p_D vs. t_{Dxf} showing the effect of y_f / x_f ratios on drawdown of real gas ; finite conductivity case ($F_{CD} = 10.0\ \pi$) .

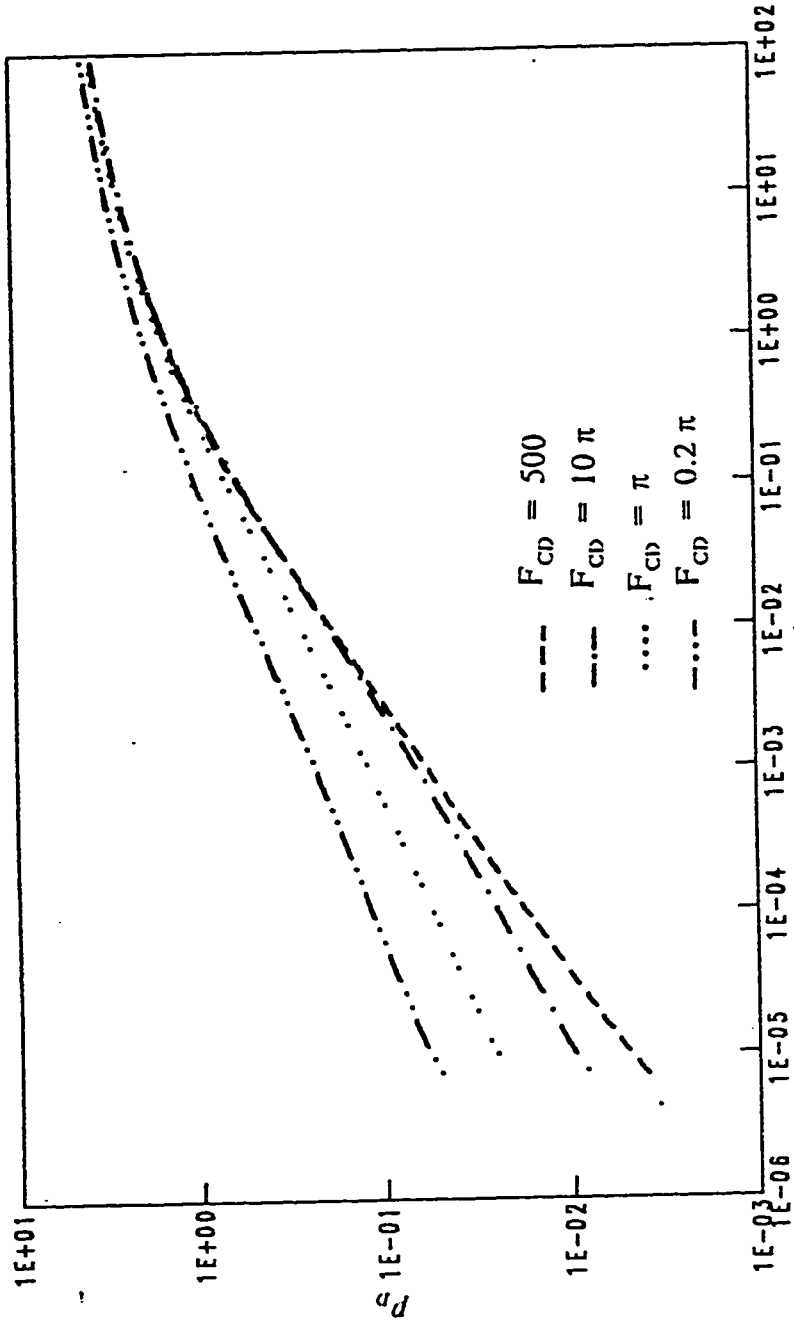

Figure 4.26 : Log-Log graph showing the effect of fracture conductivities on drawdown of real gas ; for $y_f / x_f = 0.25$.

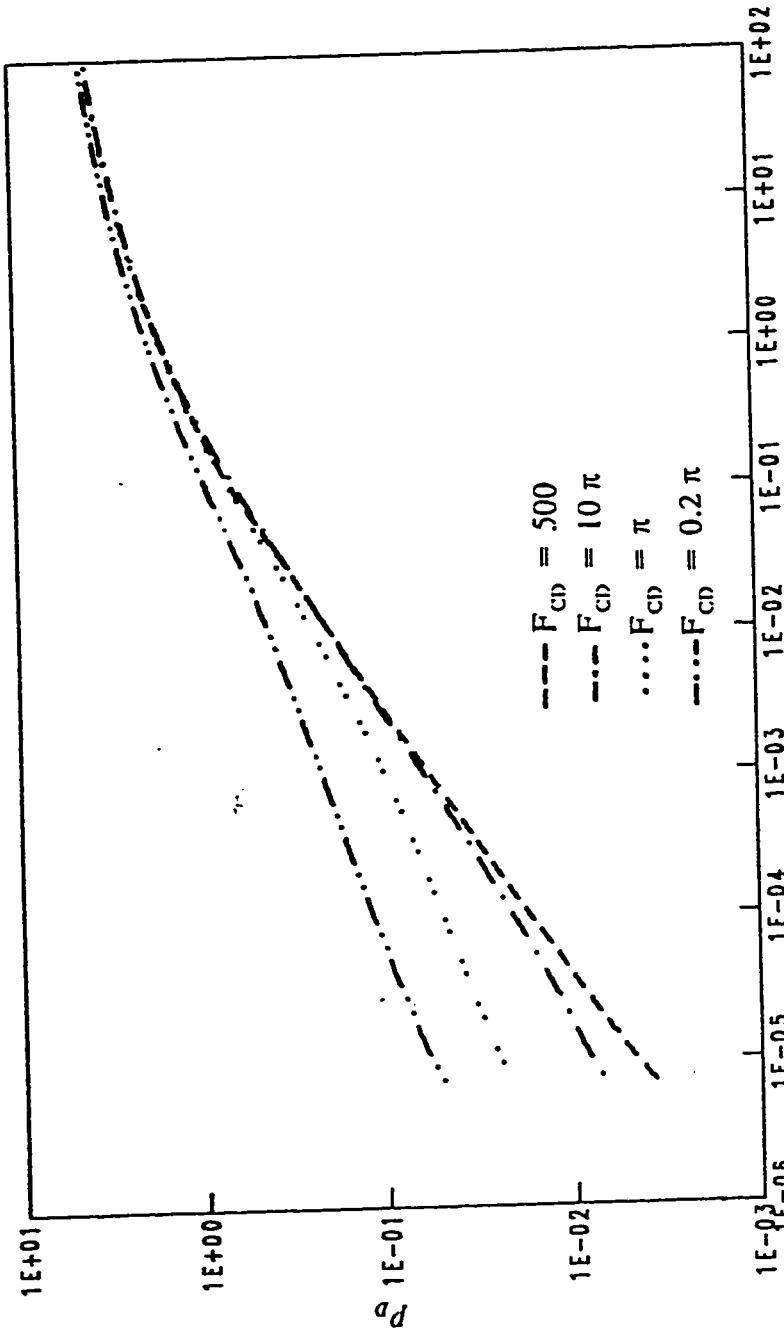

Figure 4.27 : Log-Log graph showing the effect of fracture conductivities on drawdown of real gas ; for $y_f / x_f = 1.00$.

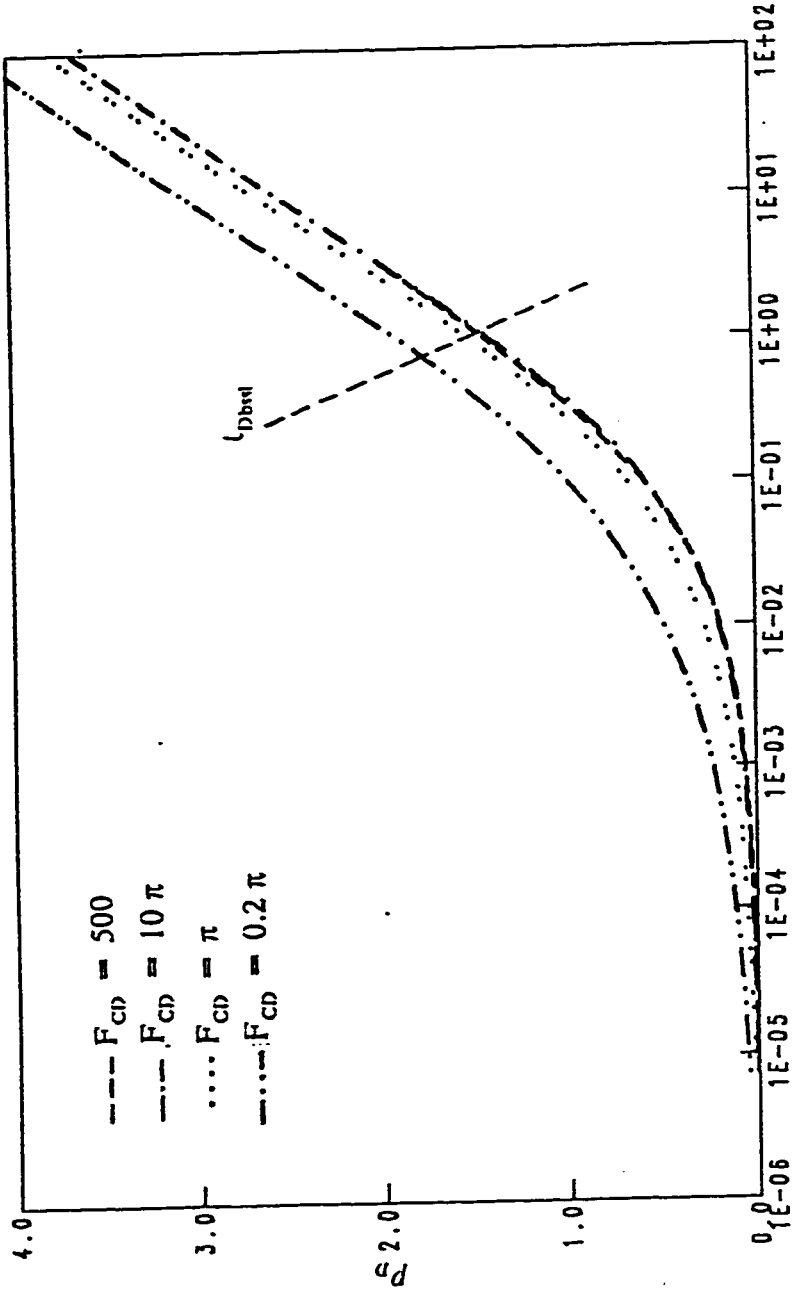

Figure 4.28 : p_D vs. t_{Dxf} showing the effect of fracture conductivities on drawdown of real gas ; for $y_f / x_f = 0.25$.

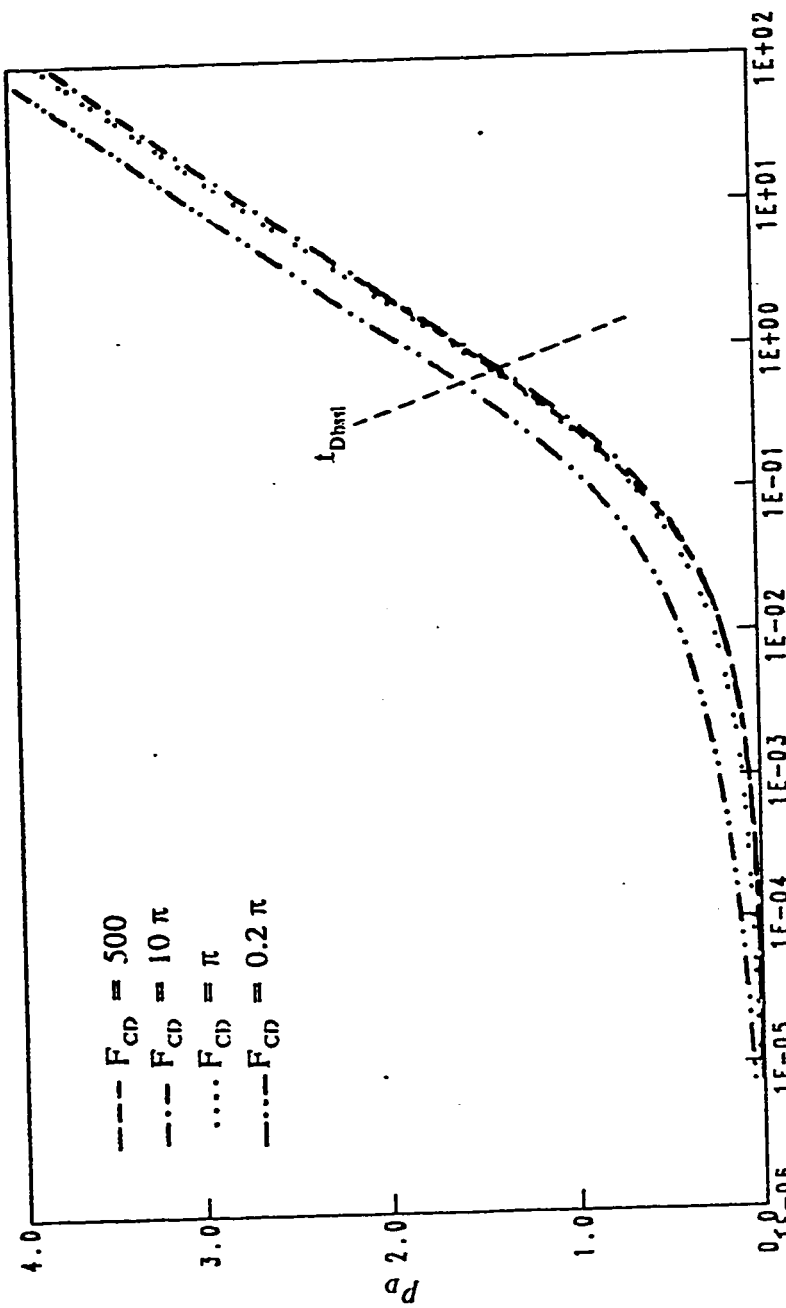

Figure 4.29 : p_D vs. t_{Dxf} showing the effect of fracture conductivities on drawdown of real gas ; for $y_f / x_f = 1.00$.

Chapter Five

CHAPTER 5

CONCLUSIONS AND RECOMMENDATIONS

Based on the work carried out in the present study concerning evaluation and prediction of the performance of gas wells in low permeability reservoirs intersected by two perpendicular fractures , the following conclusions and recommendations are made .

A. Conclusions :

1. The transient flow behavior of a gas well intersected by finite conductivities perpendicular fractures does not exhibit neither the bilinear flow solution (one-fourth slope on $\log p_D$ versus $\log t_{Dxf}$) , nor the formation linear flow solution (one-half slope on $\log p_D$ versus $\log t_{Dxf}$) for all y_f / x_f ratios .
2. Formation linear flow period was observed at early times for all y_f / x_f ratios when the fracture conductivity is infinite .
3. The fracture half lengths calculated from the formation linear flow periods are found to be the sum of the fractures half lengths ($y_f + x_f$) when the fracture conductivity is infinite ($F_{CD} \geq 500$) .
4. The start of the formation linear flow period ($t_{Dxf} = 1.62 \times 10^{-4}$ which is lower than that of single vertical fracture $t_{Dxf} = 4.0 \times 10^{-4}$) is the same for all y_f / x_f ratios greater than zero , but , the duration of this period

increases as y_f / x_f ratio increases .

5. The time at which the pseudoradial flow behavior starts decreases with :

   (a) increasing y_f / x_f ratio ;

   (b) decreasing fractures conductivities .

6. As the fracture conductivity increases , the pressure drop at the well will be higher in the case of multiple fractures than that of the single fracture after some time . This time was found to be a function of the fracture conductivity where it decreases as the fracture conductivity increases .

B. Recommendations :

1. The transient behavior of a gas well intersected by two perpendicular fractures should be investigated considering the following :

   (a) Infinite and finite conductivity fractures with turbulent flow into and / or around the fractures ;

   (b) One fracture with a finite conductivity and the other with infinite conductivity .

2. There are many factors , such as wellbore storage , fractures storage , closure pressure , and reservoir heterogeneity that complicate the analysis . These factors have not been considered in this study and deserve further investigation .

NOMENCLATURE

$A_{i,j}$ $= 0.006328\, h\, \Delta y_j k_{x_{i+1/2,j}} / (x_{i+1} - x_i)$

$B_{i,j}$ $= 0.006328\, h\, \Delta y_j k_{x_{i-1/2,j}} / (x_i - x_{i-1})$

b Slope

$C_{i,j}$ $= 0.006328\, h\, \Delta x_i k_{y_{i,j+1/2}} / (y_{j+1} - y_j)$

c_g Gas compressibility

c_{ft} Fracture storage capacity

c_t Total compressibility

$D_{i,j}$ $= 0.006328\, h\, \Delta x_i k_{y_{i,j-1/2}} / (y_j - y_{j-1})$

D Non-Darcy flow constant

$F_{i,j}$ $= V_{p_{i,j}}$

F_{CD} $= k_f w / k x_f$

H,h Reservoir thickness

k Permeability

k_x Permeability in the x-direction

k_y Permeability in the y-direction

M Gas molecular weight

$m, m(p)$ Real-gas pseudo-pressure

p Pressure

p_{sc} Pressure at standard condition (14.7 psia)

p_D Dimensionless pressure $= 1.987328 \times 10^{-5} T_{sc} k[m(p_i) - m(p_{wf})] / 0.5 p_{sc} q_{sc} T$

p_i Initial reservoir pressure

q_{sc} Volumetric flow rate at standard condition

$q_m^{\bullet}$	Source term $= \frac{RT}{M}\rho_{sc}\, q_{sc}$
R	Universal gas constant = 10.73
$R(m)_{i,j}$	Residual function
r_w	Wellbore Radius
T	Reservoir temperature
t_{Dxf}	Dimensionless time $= 2.64 \times 10^{-4} kT / \varphi\mu c_g x_f^2$
T_{sc}	Temperature at standard condition
t_f	Flow time
t_{Dbbf}	Beginning of bilinear flow (dimensionless)
t_{Debf}	End of bilinear flow (dimensionless)
t_{Dblf}	Beginning of formation linear flow (dimensionless)
t_{Delf}	End of formation linear flow (dimensionless)
t_{Dbssl}	Beginning of semilog straight line (dimensionless)
t_{fbssl}	Beginning of semilog straight line (real time)
t	Time
V_p	Pore volume
v	Velocity
w	Fracture width
x, y	Cartesian space coordinates
x_f	Fracture half length in x-direction
x_e	Distance from well to drainage boundary
Δx	Finite-difference increment in x-direction
y_f	Fracture half length in y-direction
y_e	Distance from well to drainage boundary

Δy	Finite-difference increment in y-direction
z	Gas deviation factor
β	Beta factor
δ	Turbulent coefficient $= 1 / (1 + 1.8295 \times 10^{-16} \frac{\beta \rho k}{\mu} v)$
δ_x	Turbulent coefficient in x-direction
δ_y	Turbulent coefficient in y-direction
∂	Partial derivative
φ	Porosity
φ_f	Fracture porosity
μ	Viscosity
η_{fD}	Fracture hydraulic diffusivity
γ_g	Gas gravity
γ	Euler constant = 0.577215
ρ	Gas density
ρ_{sc}	Gas density at standard condition

Subscripts and Superscripts

bbf	Beginning of bilinear flow
blf	Beginning of linear flow
bssl	Beginning of semilog straight line
CD	Conductivity
D	Dimensionless
e	External
ebf	End of bilinear flow
elf	End of linear flow

f	Fracture , Flowing
g	Gas
i	Discrete index in x-direction ; initial
$i \pm 1/2, j$	Representative value between blocks i, j and $i \pm 1, j$
$IMAX$	Index number of last mesh-point of x-direction
j	Discrete index in y-direction
$i, j \pm 1/2$	Representative value between blocks i, j and $i, j \pm 1$
$JMAX$	Index number of last mesh-point of y-direction
n	Discrete index of time-step level
sc	Standard condition
w	Wellbore
x , y	Direction in cartesian coordinate

REFERENCES

[1] Prats, M. : *" Effect of Vertical Fractures on Reservoir Behavior Incompressible Fluid case ,"* Soc. Pet. Eng. J. (June 1961) 105-118 .

[2] Russell, D.G., and Truitt, N.E. : *" Transient Pressure Behavior in Vertically Fractured Reservoirs "* J . Pet. Tech. (October 1964) 1159-1170 .

[3] Millheim, K.K., and Cichowicz, L. : *" Testing and Analyzing Low-Permeability Fractured Gas Wells ,"* J . Pet. Tech. (February 1968) 193-198 .

[4] Wattenbarger, R.A and Ramey ,H.J.Jr. : *" Well Test Interpretation of vertically Fractured Gas Wells, "* J . Pet. Tech. (May 1969) 625-632 .

[5] Raghavan R., Cady, C.V., and Ramey ,H.J.Jr. : *" Well-Test Analysis for Vertically Fractured Wells ,"* J . Pet. Tech. (August 1972) 1014-1020 .

[6] Gringarten ,A.C., Ramey ,H.J.Jr. and Raghavan ,R. : *" Unsteady State Pressure Distributions Created by a Well With a Single Infinite Conductivity Vertical Fracture ,"* Soc. Pet. Eng. J. (August 1974) 347-360 .

[7] Gringarten ,A.C., Ramey ,H.J.Jr. and Raghavan ,R. : *" Unsteady State Pressure Distributions Created by a Well With a Single Horizontal Fracture , Partial Penetration , or Restricted Entry , "* Soc. Pet. Eng. J. (August 1974) 413-422 .

[8] Holditch, S.A, and Morse, R.A : *" The Effects of Non-Darcy Flow on the Behavior of Hydraulically Fractured Gas Wells ,"* J . Pet. Tech. (October 1976) 1169-1179 .

[9] Cinco-L, H., Samaniego-V, F., and Dominguez-A., N. : *" Transient Pressure Behavior for a Well with a Finite-Conductivity Vertical Fracture , "* Soc. Pet. Eng. J. (August 1978) 253-264 .

[10] Agrwal, R.G., Carter, R.D., and Pollock, C.B. : *" Evaluation and Performance Prediction of Low-Permeability Gas Wells Stimulated by Massive Hydraulic Fracturing , "* J . Pet. Tech. (March 1979) 362-372 .

[11] Cinco-L, H., Samaniego-V, F. : *" Transient Pressure Analysis for Fractured Wells ,"* J. Pet. Tech. (September 1981) 1749-1766 .

[12] Evans, R.D., and Caroll, H.B.Jr. : *" Modeling of Hydraulically Fractured Gas Wells Completed in Noncontinuous Lenticular Formations ,"* Journal of Energy Resources Technology (June 1981) 153-158 VOL.103 .

[13] Allam , A.M. : *" Numerical Simulation of Heterogeneous Fractured Gas Reservoir Systems with Turbulence and Closure Stress Effects ,"* Ph.D. Thesis, Norman, Oklahoma (1981) .

[14] AL-Hashim, H.S. : *" The Effect of Finite Conductivity Vertical Fracture and Turbulent Flow on the Transient Pressure Behavior of Fractured Gas Wells ,"* Ph.D. Thesis, Colorado School of Mines . (1982) .

[15] Guppy, K.H., Cinco-L, H., Ramey, H.J.Jr., and Samaniego-V, F. : *" Non-Darcy Flow in Wells with Finite-Conductivity Vertical Fractures ,"* Soc. Pet. Eng. J. (October 1982) 681-698 .

[16] Guppy, K.H., Cinco-L, H., and Ramey, H.J.Jr. : *" Pressure Buildup Analysis of Fractured Wells Producing at High Flow Rates ,"* J. Pet. Tech. (November 1982) 2656-2666 .

[17] Rubin, M.B. : *" Experimental Study of Hydraulic Fracturing in an Impermeable Material ,"* Journal of Energy Resources Technology (June 1983) 116-124 VOL.105 .

[18] Bennett, C.O., Camacho-V, R.G., Reynolds, A.C. and Raghavan, R. : *" Approximate Solutions for Fractured Wells Producing Layered Reservoirs ,"* Soc. Pet. Eng. J. (October 1985) 729-742 .

[19] Bennett, C.O., Reynolds, A.C. and Raghavan, R. and Elbel, J.L. : *" Performance of Finite-Conductivity , Vertically Fractured Wells in Single Layer Reservoirs ,"* SPE Formation Evaluation (August 1986) 399-412 .

[20] Tai Lee, S., and Brockenbrough, J.R. : *" A New Approximate Analytic Solution for*

Finite-Conductivity Vertical Fractures , " SPE Formation Evaluation (February 1986) 75-88 .

[21] Kabir, C.S., and Hasan, A.R. : " *Prefracture Testing in Tight Gas Reservoirs* , " SPE Formation Evaluation (April 1986) 128-138 .

[22] Guppy, K.H. : " *Analysis of Fractured Wells Producing at High Flow Rates Using Late-Time Data* , " SPE Formation Evaluation , (December 1987) 555-559 .

[23] Stanislav, J.F., Easwaran, C.V., and Kokal, S.L. : " *Analytical Solutions for Vertical Fractures in a Composite System* , " The Journal of Canadian Petroleum Technology (September-October 1987) 51-56 .

[24] Holditch, S.A., Robinson, B.M., and Whitehead, W.S. : " *Prefracture and Postfracture Formation Evaluation Necessary to Characterize the Three-Dimensional Shape of a Hydraulic Fracture* , " SPE Formation Evaluation (December 1987) 523-534 .

[25] Guppy, K.H., Kumar, S., and Kagawan, V.D. : " *Pressure Transient Analysis for Fractured Wells Producing at Constant Pressure* , " SPE Formation Evaluation , (March 1988) 169-178 .

[26] Tiab, D., and Puthigai, S.K. : " *Pressure-Derivative Type Curves for Vertically Fractured Wells* , " SPE Formation Evaluation (March 1988) 156-158 .

[27] Overbey, W.K.Jr., Yost ,A.B. and Wilkins, D.A. : " *Inducing Multiple Hydraulic Fractures from* " a Horizontal Wellbore ," SPE Paper 18249 Presented at the 63 rd Annual Technical Conference and Exhibition of the Society of Petroleum Engineers held in Houston , Tx, October 2-5 , 1988 .

[28] Soliman , M.Y. , Hunt Two, J.L. and EL-Rabaa , W. : " *On Fracturing Horizontal wells* , " SPE Paper 18542 Presented at the SPE Eastern Regional Meeting in Charleston , WV , November 1-4 , 1988 .

[29] Wilkinson D.J. : " *New Results for Pressure Transient Behavior of Hydraulically Fractured wells* , " SPE Paper 18950 presented at the SPE Joint Rocky Mountain

Regional/ Low Permeability Reservoirs Symposium and Exhibition held in Denver , Colorado , March 6-8 , 1989 .

[30] Okoye , C.U. , Oshinuga , A.D. and Ghalambor, a. : *" Pressure Transient Behavior in Multilayer Vertically Fractured Gas Reservoir with Finite Conductivity , "* SPE Paper 18960 presented at the SPE Joint Rocky Mountain Regional/ Low Permeability Reservoirs Symposium and Exhibition held in Denver , Colorado , March 6-8 , 1989 .

[31] Hunt Three , W.C. and Shu , W.R. : *" Controlled Pulse Fracturing for Well Stimulation ,"* SPE Paper 18972 presented at the SPE Joint Rocky Mountain Regional/ Low Permeability Reservoirs Symposium and Exhibition held in Denver , Colorado , March 6-8 , 1989 .

[32] Olarewaju , J.S , Holditch , S.A. , and Lee , W.J. : *" A New Analytical Model of Finite Conductivity Hydraulic Fracture in a Finite Reservoir , "* SPE Paper 19093 Presented at the SPE Gas Technology Symposium held in Dallas , Texas , June 7-9 , 1989 .

[33] Acharya, D. : *" Hydraulic Fracture Treatment Design Simulation , "* J. Pet. Tech. (February 1988) 139-142 .

[34] Earlougher ,R.C. : *" Advances in Well Test Analysis "* Monograph Series , SPE , NewYork , Dallas (1977) .

[35] Lee, W.J. ,and Holditch, S.A. : *" Fracture Evaluation with Pressure Transient Testing in Low Permeability Gas Reservoirs , "* J. Pet. Tech. (September 1981) 1776-1792 .

[36] Cuderman, J.F., and Northrop, D.A. : *" A Propellant-Based Technology for Multiple fracturing wellbores to Enhance Gas Recovery : Application and Results in Devonian Shale, "* SPE Production Engineering (March 1986) 97-103 .

[37] Warpanski,.N.R et al. : *" High Energy Gas Frac : Multiple Fracturing in a Wellbore , "* Proc..U. of texas. 20th U.S. Symposium on Rock Mechanics. Austin (1979)

143-152 .

[38] Schmidt,R.A., Warpanski,.N.R.,and Cooper,P.W. : *" In Situ Evaluation of Several Tailored-Pulse Well-Shooting Concepts ,"* Paper SPE 8934 presented at the 1980 SPE California Regional meeting. Los Angeles. April 9-11 .

[39] Swift, R.P. and Kusubov, A.S. : *" Technique for Studying Multiple Fractures Produced at Intermediate Loading Rates ,"* Proc..U. of Missouri-Rolla School of Mines . 21st U.S. Symposium on Rock Mechanics (1980) 682-690 .

[40] Swift, R.P., and Kusubov, A.S. : *" Multiple Fracturing of Boreholes by Using Tailored-Pulse Loading , "* Soc. Pet. Eng. J. (December 1982) 923-932 .

[41] Schmidt, R.A., Warpanski, N.R., and Cooper, P.W. : *" In-Situ Evaluation of Several Tailored-Pulse Well-Shooting Concepts , "* Soc. Pet. Eng. (May 1980) 105-111 .

[42] Veatch, R.W.Jr., and Moschovidis, Z.A. : *" An Overview of Recent Advances in Hydraulic Fracturing Technology , "* Soc. Pet. Eng. (March 1986) 421-454 .

[43] AL-Hussainy ,R., Ramey ,H.J.Jr. And Crawford, P.B. : *" The Flow of Real Gases Through Porous Media ,"* J . Pet. Tech. (May 1966) 624-636 .

[44] AL-Hussainy ,R. and Ramey ,H.J.Jr. : *" Application of Real Gas Flow Theory to Well Testing and Deliverability Forecasting ,"* J . Pet. Tech. (May 1966) 637-642 .

[45] Peceman,D.W : *" Fundamentals of Numerical Reservoir Simulation ,"* Elsevier Scientific Publishing Company, AmsterdamOxford -NewYork (1977) .

[46] Miller, C.C., Dyes, A.B., and Hutchinson, C.A., Jr.: *" The Estimation of Permeability and Reservoir Pressure from Bottom Hole Pressure Build-up Characteristics , "* Trans., AIME (1950) 189-191 .

Appendix-A

APPENDIX A

FLOW DIAGRAM OF NUMERICAL MODEL

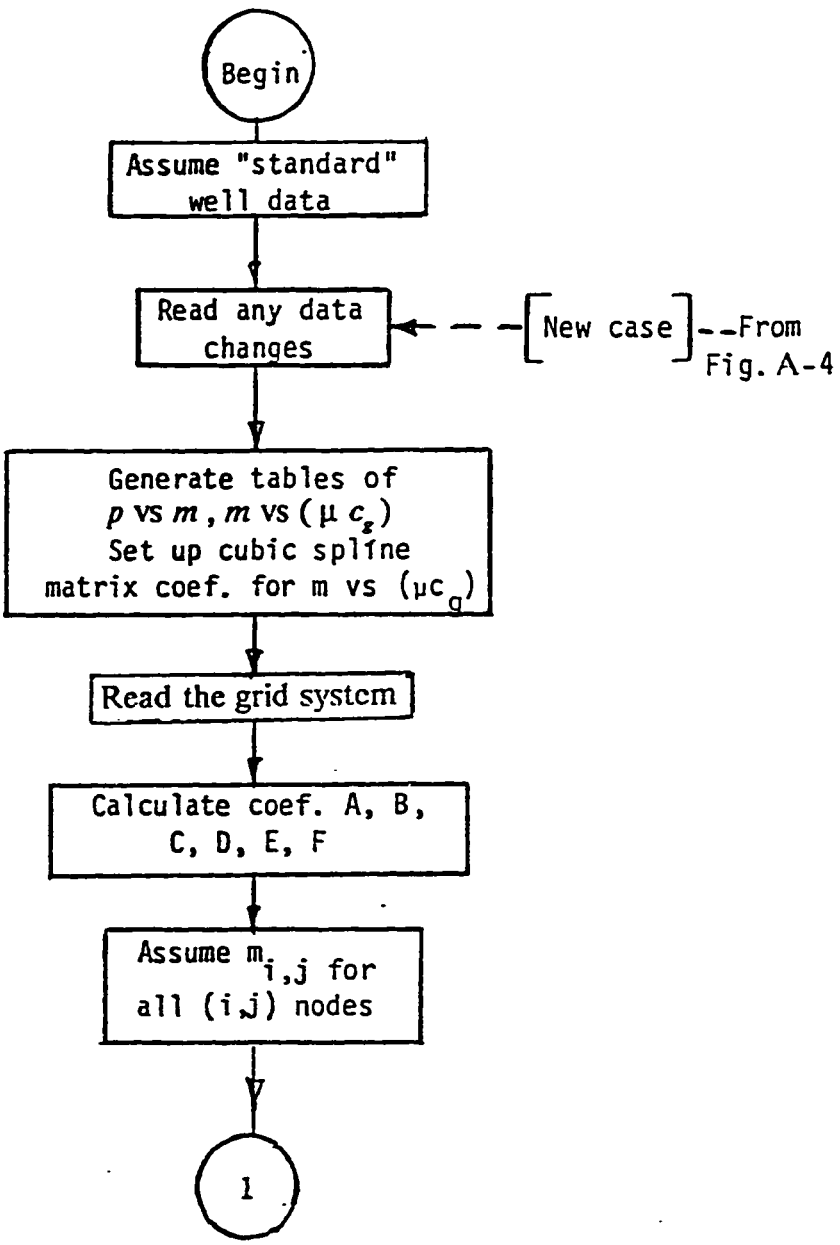

Figure A-1 : Numerical Model Flow Diagram

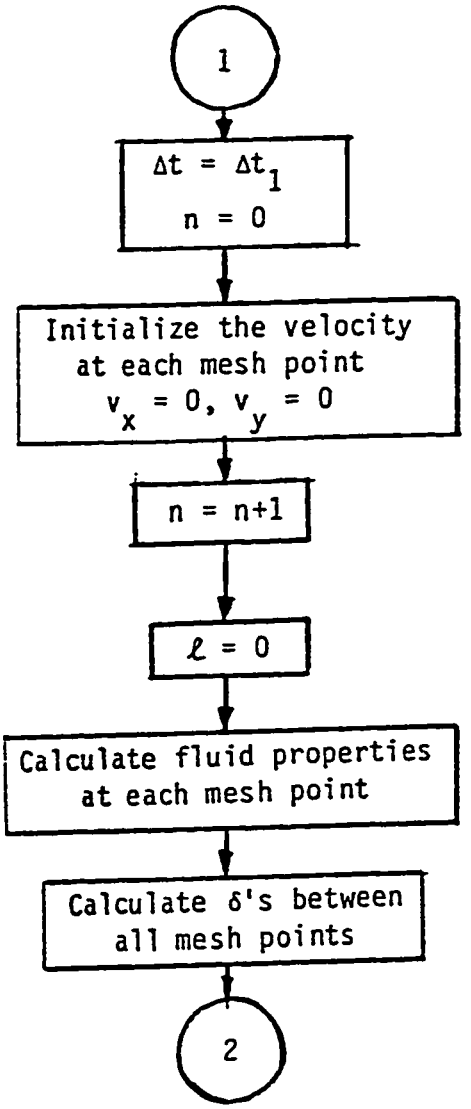

Figure A-2 : Numerical Model Flow Diagram (con't.)

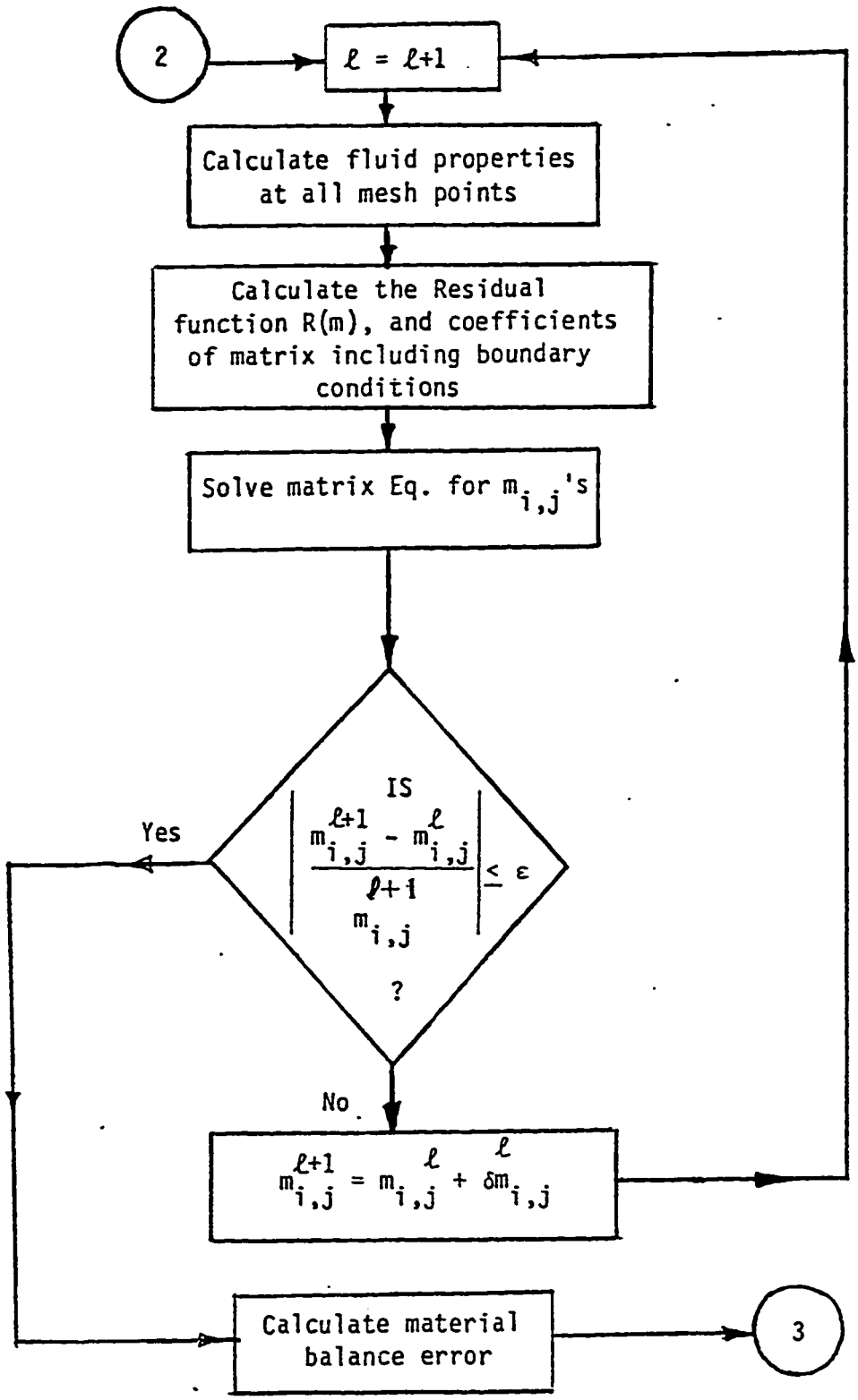

Figure A-3 : Numerical Model Flow Diagram (con't.)

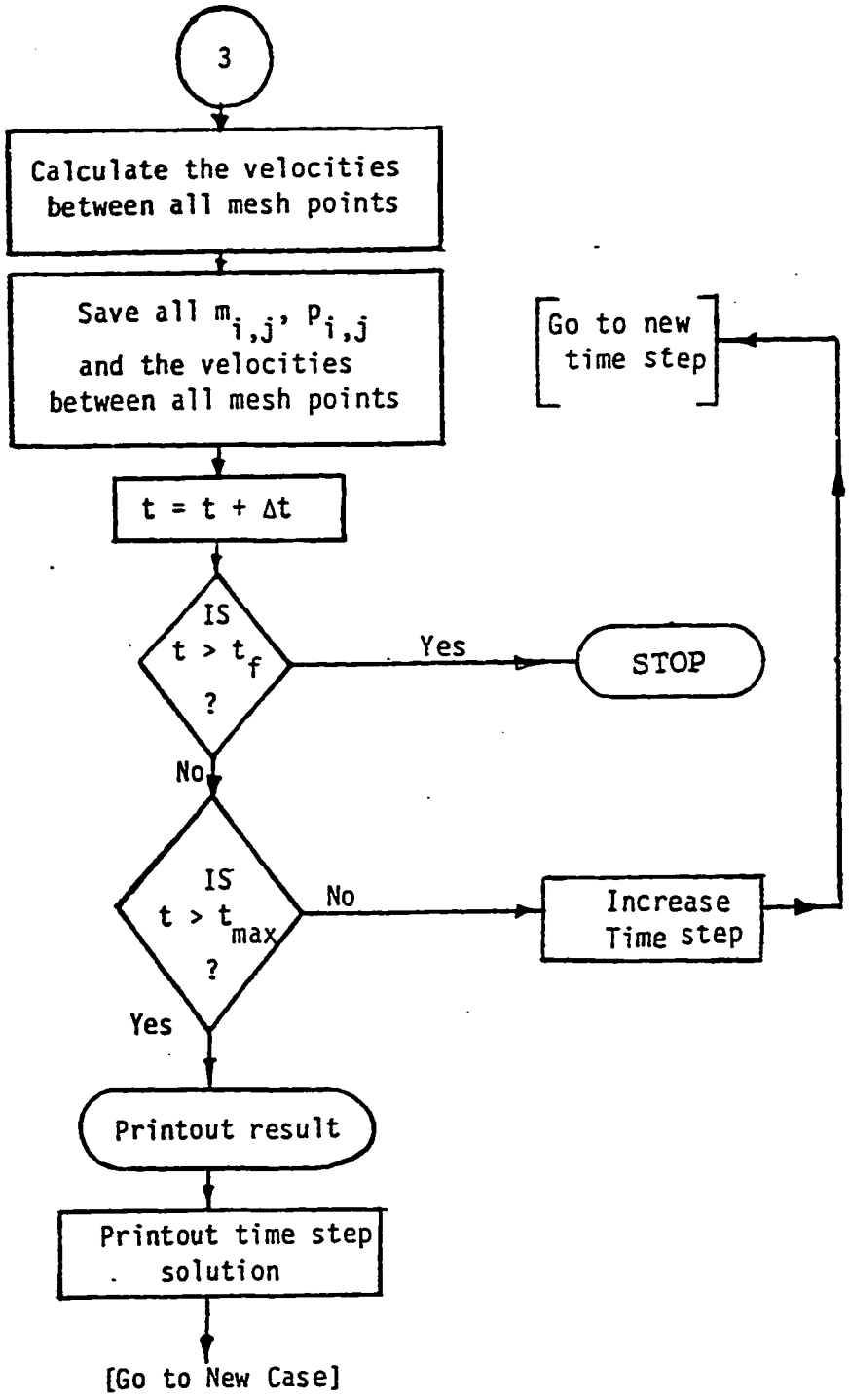

Figure A-4 : Numerical Model Flow Diagram (con't.)